

A Thesis for the Degree of Ph.D. in Engineering

Gel Characteristics and Viscoelasticity
of Semi-crystalline Polymers and Copolymers
for the Fabrications of Nanofibers and Hydrogels

January 2016

Graduate School of Science and Technology
Keio University

Tomoki Maeda

Chapter 1. Introduction.....	1
1.1. Nanofiber-sheets and hydrogels with 3D-network polymer.....	1
1.2. Details on nanofiber-sheets	2
1.3. Details on hydrogels	6
1.4. Purpose of this study.....	8
1.4.1. Purpose of the study on nanofiber-sheets	8
1.4.2. Purpose of the study on hydrogels.....	8
Chapter 2. Fundamentals on nanofiber-sheets and gels	10
2.1. Fundamentals on polymer solution.....	10
2.1.1. Solution in organic solvents and solubility parameter.....	10
2.1.2. Viscosity of polymer solution.....	12
2.2. Fundamentals on electrospinning and the formation of nanofibers	15
2.2.1. Electrospinning.....	15
2.2.2. Process parameters of electrospinning	17
2.2.3. Solution parameters of electrospinning	19
2.3. Fundamentals on gels	21
2.3.1. Classification of gels	21
2.3.2. Physical gels with microcrystalline junctions	21
2.3.3. Physical gels with associating junctions.....	22
Chapter 3. Syndiotactic polypropylene (sPP) electrospun nanofibers	24
3.1. Background on polypropylene (PP) nanofibers.....	24
3.2. Experimental.....	28
3.2.1. Materials	28
3.2.2. Solution preparations	28
3.2.3. Gelation-speed evaluation	28
3.2.4. Fabrication of sPP nanofibers by electrospinning	29
3.2.5. Morphological analysis of electrospun sPP nanofibers.....	29
3.2.6. Characterization of physical properties of solvents.....	29
3.2.7. Rheological analysis of sPP solutions	29

3.3. Results and Discussion	31
3.3.1. Gelation-speed evaluation of sPP solutions.....	31
3.3.2. Morphology of electrospun sPP nanofibers.....	42
3.3.3. Physical properties of solvents: electric property and volatility.....	45
3.3.4. Rheological aspects of sPP solutions.....	48
3.3.5. Conditions for fabricating thinner sPP nanofibers	53
3.4. Summary of this chapter	54
Chapter 4. MPC random-copolymer electrospun nanofibers	55
4.1. Background on MPC	55
4.2. Experimental.....	57
4.2.1. Materials	57
4.2.2. Preparation of the MPC Solution.....	57
4.2.3. MPC nanofiber fabrication by electrospinning	58
4.2.4. Morphological analysis of MPC fibers.....	58
4.2.5. Rheological analysis of MPC solutions.....	59
4.2.6. <i>In vitro</i> drug-release test.....	59
4.3. Results and Discussion	61
4.3.1. Morphologies of electrospun MPC fibers	61
4.3.2. Rheological analysis of MPC solutions.....	63
4.3.3. Function evaluation as a drug delivery system.....	66
4.4. Summary of this chapter	69
Chapter 5. Elastomeric block-copolymer electrospun nanofibers.....	70
5.1. Background on elastomeric block-copolymer nanofibers	70
5.2. Experimental.....	73
5.2.1. Materials	73
5.2.2. Solution preparation	73
5.2.3. Evaluation of sol-gel characteristics.....	73
5.2.4. Fiber fabrication by electrospinning.....	74
5.2.5. Morphological observation of electrospun SIS nanofibers	74

5.2.6. Characterization of physical properties of mixed solvents.....	74
5.2.7. Rheological analysis of SIS solutions	75
5.3. Results and Discussion	76
5.3.1. Sol-gel characteristics of SIS solutions	76
5.3.2. Morphologies of electrospun SIS fibers	79
5.3.3. Physical properties of the mixed solvents	81
5.3.4. Rheological analysis of SIS solutions with DMF/toluene mixed solvents...	84
5.4. Summary of this chapter.....	90
Chapter 6. Clay-sheet/PLGA-PEG-PLGA hydrogels	91
6.1. Background on PLGA-PEG-PLGA hydrogels.....	91
6.2. Experimental.....	95
6.2.1. Materials	95
6.2.2. Synthesis of PLGA-PEG-PLGA	95
6.2.3. Characterization of the synthesized PLGA-PEG-PLGA	95
6.2.4. Aqueous system preparation.....	96
6.2.5. Phase diagram measurement	97
6.2.6. Rheological analysis	97
6.2.7. Cryogenic-transmission electron microscopy (Cryo-TEM).....	98
6.3. Results and Discussion	98
6.3.1. Characterization of PLGA-PEG-PLGA triblock copolymers	98
6.3.2. Thermo-responsive sol-gel transition behavior	104
6.3.3. Rheological properties of laponite/PLGA-PEG-PLGA systems.....	120
6.3.4. Microstructural analysis of laponite/PLGA-PEG-PLGA systems	124
6.4. Summary of this chapter.....	127
Chapter 7. Summary	128
7.1. Summary on nanofiber fabrication.....	128
7.2. Summary on hydrogel fabrication	129
List of publications	130
Acknowledgement.....	132

References 134

List of Figures

Chapter 1.

Figure 1. 1 Typical setup of electrospinning.	3
--	---

Chapter 2.

Figure 2. 1 Physical expression of polymer solutions: (a) dilute solution, (b) semidilute unentangled solution, (c) semidilute entangled solution, and (d) concentrated solution.	13
Figure 2. 2 Charge injection in the electrospinning process.	16
Figure 2. 3 Schematic image of crystalline gels.	22
Figure 2. 4 Schematic images of thermo-responsive gelation of block copolymers.	23

Chapter 3.

Figure 3. 1 Sol-Gel phase change by concentration and time with cyclohexane.	33
Figure 3. 2 Sol-Gel phase change by concentration and time with methyl-cyclohexane.	33
Figure 3. 3 Sol-Gel phase change by concentration and time with ethyl-cyclohexane. ..	34
Figure 3. 4 Sol-Gel phase change by concentration and time with propyl-cyclohexane.	34
Figure 3. 5 Sol-Gel phase change by concentration and time with butyl-cyclohexane. ..	35
Figure 3. 6 Sol-Gel phase change by concentration and time with decalin.	35
Figure 3. 7 Molecular structures of solvents: (a) cyclohexane, (b) methyl-cyclohexane, (c) ethyl-cyclohexane, (d) propyl-cyclohexane, (e) butyl-cyclohexane, and (f) decalin.	41
Figure 3. 8 SEM images of sPP nanofibers fabricated from sPP/methyl-cyclohexane solution at different concentrations: (a) 1wt%, (b) 2wt%, (c) 3wt%, and (d) 4wt%.	42
Figure 3. 9 SEM images of sPP nanofibers fabricated from the solution with different solvents: (a) cyclohexane, (b) methyl-cyclohexane, (c) ethyl-cyclohexane, and (d) decalin.	44

Figure 3. 10 Frequency distributions of the diameter of sPP nanofibers fabricated from the solution with (a) methyl-cyclohexane and (b) cyclohexane..... 44

Figure 3. 11 Evaporation loss against time using different solvents: cyclohexane, methyl-cyclohexane, ethyl-cyclohexane, and decalin. 46

Figure 3. 12 Zero-shear viscosity as a function of concentration by different solvents: (a) cyclohexane with alkyl chains and (b) decalin. 49

Figure 3. 13 Specific viscosity as a function of concentration by different solvents: (a) cyclohexane with alkyl chains and (b) decalin..... 50

Figure 3. 14 Schematic images of evaporation, gelation, and elongation of crystalline polymer solution during electrospinning..... 54

Chapter 4.

Figure 4. 1 Chemical structure of poly (MPC-co-BMA). 57

Figure 4. 2 SEM images of MPC fibers from the solutions with different concentrations: (a) 1wt%, (b) 2wt%, (c) 3wt%, (d) 5wt%, (e) 7.5wt%, and (f) 10wt%..... 62

Figure 4. 3 Zero-shear rate viscosity of MPC solutions with different concentrations.. 64

Figure 4. 4 Specific viscosity of MPC solutions with different concentrations..... 64

Figure 4. 5 Cumulative released amount of curcumin from MPC fibers and film..... 66

Figure 4. 6 Specific surface areas of MPC fibers and film..... 68

Chapter 5.

Figure 5. 1 Phase diagram of SIS solution with different DMF ratios in DMF/toluene mixed solvent..... 78

Figure 5. 2 Solubility parameters of DMF/toluene mixed solvent with different DMF ratios. 78

Figure 5. 3 SEM images of SIS fibers from different solutions: DMF ratio of 0.2 and SIS concentrations of (a) 10wt%, (b) 15wt%, and (c) 17wt%; DMF ratio of 0.4 and SIS concentrations of (d) 10wt%, (e) 15wt%, and (f) 17wt%; DMF ratio of 0.5 and SIS concentration of (g) 10wt%, (h) 15wt%, and (i) 17wt%. 79

Figure 5. 4 Conductivities of DMF/toluene mixed solvents.	81
Figure 5. 5 Dielectric constants of DMF/toluene mixed solvents.	82
Figure 5. 6 Evaporation loss of DMF/toluene mixed solvent as a function of time.....	83
Figure 5. 7 Zero-shear rate viscosity of SIS solutions with different DMF ratios in DMF/toluene mixed solvent.	85
Figure 5. 8 Specific viscosity of SIS solutions with different DMF ratios in DMF/toluene mixed solvent.	85
Figure 5. 9 Specific viscosity of SIS solution with DMF ratio of 0.0 in DMF/toluene mixed solvent (i.e. pure toluene).	86
Figure 5. 10 DMA results for SIS solutions with DMF/toluene mixed solvent at DMF ratio of 0.2.....	88
Figure 5. 11 DMA results for SIS solutions with DMF/toluene mixed solvent at DMF ratio of 0.4.....	89
Figure 5. 12 DMA results for SIS solutions with DMF/toluene mixed solvent at DMF ratio of 0.5.....	89
 Chapter 6.	
Figure 6. 1 ¹ H-NMR spectrum of P1.0-short.....	99
Figure 6. 2 ¹ H-NMR spectrum of P1.0-long.	100
Figure 6. 3 ¹ H-NMR spectrum of P1.5-short.....	100
Figure 6. 4 ¹ H-NMR spectrum of P1.5-long.	101
Figure 6. 5 ¹ H-NMR spectrum of P3.0-short.....	101
Figure 6. 6 ¹ H-NMR spectrum of P3.0-long.	102
Figure 6. 7 GPC curves of PLGA-PEG-PLGA with PEG midblock of Mn=1000.	103
Figure 6. 8 GPC curves of PLGA-PEG-PLGA with PEG midblock of Mn=1500.	103
Figure 6. 9 GPC curves of PLGA-PEG-PLGA with PEG midblock of Mn=3000.	104
Figure 6. 10 Images of tube inverting test for solutions: (a) P1.0-short solution and (b) laponite/P1.0-short system (1.0wt%/5.0wt%).	106
Figure 6. 11 Phase diagrams of laponite/P1.0-short aqueous systems with different	

laponite concentrations: (a) 0.75wt%, (b) 1.0wt%, and (c) 1.5wt%.....	108
Figure 6. 12 Sol-gel transition temperatures of laponite/P1.0-short systems with different laponite concentrations.	109
Figure 6. 13 Temperature range exhibiting gel for laponite/P1.0-short systems with different laponite concentrations.	110
Figure 6. 14 Phase diagrams of laponite/P1.5-short aqueous systems with different laponite concentrations: (a) 0.75wt%, (b) 1.0wt%, and (c) 1.5wt%.....	112
Figure 6. 15 Sol-gel transition temperatures of laponite/P1.5-short systems with different laponite concentrations.	113
Figure 6. 16 Temperature range exhibiting gel for laponite/P1.5-short systems with different laponite concentrations.	113
Figure 6. 17 Phase diagrams of laponite/P3.0-short aqueous systems with different laponite concentrations: (a) 0.75wt%, (b) 1.0wt%, and (c) 1.5wt%.....	115
Figure 6. 18 Sol-gel transition temperatures of laponite/P3.0-short systems with different laponite concentrations.	116
Figure 6. 19 Temperature range exhibiting gel for laponite/P3.0-short systems with different laponite concentrations.	116
Figure 6. 20 Sol-gel transition temperature of laponite/PLGA-PEG-PLGA systems with different molecular weights of PEG midblock.....	117
Figure 6. 21 Phase diagram of PLGA-PEG-PLGA aqueous solutions with long PLGA endblock.....	118
Figure 6. 22 Sol-gel transition temperatures of PLGA-PEG-PLGA aqueous solutions with long PLGA endblock.....	118
Figure 6. 23 DMA results as a function of temperature for laponite/P1.0-short systems (1.0wt%/5.0wt%).....	120
Figure 6. 24 DMA results as a function of temperature for laponite/P1.0-short systems with 1.0wt% of laponite and with different P1.0-short concentrations: (a) G' and (b) G".	122
Figure 6. 25 DMA results as a function of temperature for laponite/P1.5-short systems with 1.0wt% of laponite and with different P1.5-short concentrations:	

solid for G' and hollow for G'' 123

Figure 6. 26 Cryo-TEM images of laponite/P1.0-short system (1wt%/5wt%) in sol state.
..... 124

Figure 6. 27 Cryo-TEM images of laponite/P1.0-short system (1wt%/5wt%) in gel state.
..... 125

Figure 6. 28 Schematic images of gelation for laponite/PLGA-PEG-PLGA systems: (a)
in sol state and (b) in gel state. 126

List of Tables

Chapter 3.

Table 3. 1 Hansen solubility parameters for solvents..... 37

Table 3. 2 Solubility parameters calculated by various methods. 37

Table 3. 3 Conductivities and dielectric constants of solvents..... 45

Chapter 4.

Table 4. 1 Compositions of MPC solutions with curcumin. 58

Chapter 5.

Table 5. 1 Evaporation rate of DMF/toluene mixed solvents..... 83

Chapter 6.

Table 6. 1 Molecular weight and composition of synthesized PLGA-PEG-PLGA. 102

Chapter 1. Introduction

1.1. Nanofiber-sheets and hydrogels with 3D-network polymer

Nanofiber-sheets and hydrogels with different scale of 3D-network polymer have received great attention for developing various applications.¹ Nanofiber-sheets with the nano and submicron scale 3D-network of polymer nanofibers usually possess a high specific surface area and porosity.² Due to the nature of nanofiber-sheets, various applications such as filters, solar cells,³⁻⁴ sensors,⁵⁻⁶ composites,⁷⁻¹¹ and tissue scaffolds¹²⁻¹⁴ are actively studied. On the other hand, hydrogels with the angstrom-scale network of polymer chain possess the capability to contain water and chemicals inside the network, and the high diffusivity of chemicals inward and outward. Due to the nature of hydrogels, the applications such as drug delivery and tissue scaffolds are actively studied.¹⁵⁻²²

In order to develop the functionality of these applications using nanofiber-sheets and hydrogels, the established fabrication method for nanofiber-sheets and the regulation of gel characteristics for hydrogels are required. As for the nanofiber-sheets, nanofibers should be made from the materials adapted for the applications. However, the fabrication method of nanofibers from various polymers has not been comprehensively studied. As for the hydrogels, various kinds of materials forming hydrogels have been synthesized. However, their gel characteristics are not sufficiently controlled considering the practical use. In the following section, the more detailed information on the previous studies, the current situation of nanofiber-sheets and hydrogels are described separately, and the requirements for nanofiber-sheets and hydrogels will be revealed.

1.2. Details on nanofiber-sheets

Nanofiber-sheets are attractive materials for wide range of applications because of its 3D structure and high specific surface area. For example, the 3D structures of nanofiber-sheets turned out to resemble extracellular matrix (ECM) in our body through the studies in the field of tissue engineering.²³ ECM consists of 50 - 500 nm fibrous structure made of protein materials and shows multiple functions such as the framework of tissues, the scaffold for cells to adhere and proliferate, and the material holding and providing growth factors.²⁴ From the bio-mimicry conceptual views, the nanofiber-sheets with the structures resembling ECM are a desired candidate for tissue scaffolds. In terms of the high specific surface area of nanofiber-sheets, the applications using the surface can show the enhanced functionalities. For example, the sensitivity of sensors can be enhanced with the increasing specific surface area working as sensing area. Other than two applications described above, composite materials, drug delivery systems, and filters are proposed for the applications of nanofiber-sheet with the 3D structures and the high specific surface area.

These attractive sheets composed of nanofibers can be feasibly fabricated by electrospinning as compared to other methods. Electrospinning is well known as one of the feasible fabrication methods in the field of polymer science. The feasibility of electrospinning attributes to its simple setup. The typical setup is just composed of a syringe pump, a high voltage supplier, and a metal collector as shown in Figure 1.1. By using the setup, the fabrication process of nanofibers by electrospinning is as follows. First, polymer solutions contained in a syringe are fed to the tip of the syringe needle. Then, the solutions are extracted from the needle tip and elongated by electrostatic force. During the elongation, the solvents are evaporated from the solutions due to the increase of the specific surface area. Thus, continuous ultrafine polymer fibers can be obtained

on the metal collector as a nonwoven fabric (i.e. nanofiber-sheets). The wide range in the diameters from a few micrometers down to tens of nanometers, which is difficult to be realized by the other conventional spinning techniques, is one of the prominent features of electrospinning.

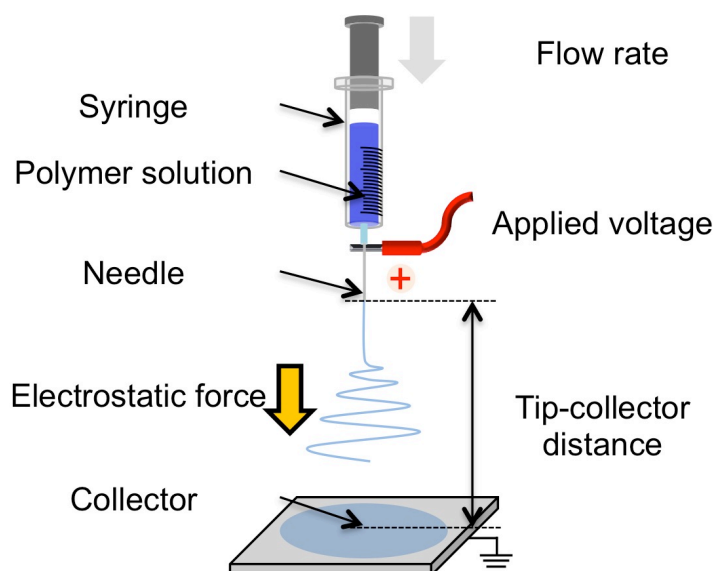


Figure 1. 1 Typical setup of electrospinning.

The controllability of fiber diameter is the most focused point among the various aspects of the electrospun fibers in order to develop the functionalities of applications with nanofiber-sheets. The control of the diameter leads to the control of the morphology of 3D structures and the surface area. For instance, as the fiber diameter significantly decreases, the surface area of nanofiber-sheet becomes extremely high. Actually, various papers have focused their attention on the fabrication of thinner fibers and the development of applications with nanofiber-sheets. As a basic study, Nakano *et al.* reported the fabrication method of thinner fibers based on the solubility parameter.²⁵ As an applied study, Kwon *et al.* reported that the decrease in the fiber diameter down to ~300 nm enhanced the cell adhesion and proliferation on nanofiber-sheets.²⁶

As well as the control of fiber diameter, the control of the nanofiber composition by changing the polymer materials is also the actively studied point. The property of nanofibers basically depends on the material of nanofibers. In fact, nanofibers with various kinds of polymers have been fabricated by electrospinning previously. For example, the natural polymers such as silk, chitosan, collagen, hyaluronic acid, gelatin, and fibrinogen were electrospun into fibers. The synthetic polymers such as poly (glycolide) (PGA)²⁷, poly (ε-caprolactone) (PCL)²⁸, poly (l-lactide)²⁹, polyurethane (PU)³⁰, polystyrene (PS)³¹, poly (vinyl alcohol) (PVA)³², and poly (methyl methacrylate) (PMMA)³³ were also electrospun into fibers.

In order to obtain nanofibers with thinner diameters from various types of polymeric materials, the investigation on parameters during electrospinning has been actively carried out. However, the investigation was mainly limited to the case of amorphous homo-polymers.³⁴ In controlling the diameter of nanofibers, process parameters and solution parameters are known to be important. As for the process parameters, the flow rate, the tip-collector distance, and the applied voltage are known

as parameters. As for the solution parameters, the solution concentration, the conductivity, the dielectric constant, and the volatility are also known as parameters. For determining the effects of parameters, amorphous homo-polymers were selected and used in many reports. Amorphous homo-polymers, polymers composed of one type of monomers and showing an amorphous state, are used as versatile materials but often less functional as compared to the polymers such as copolymers composed of two or more types of monomers and crystalline polymers.

In order to develop nanofiber-sheets with more functional materials, there have been still requirements to provide the proper conditions of electrospinning for various types of materials such as copolymers and crystalline polymers. It has been expected that nanofibers with functional materials would provide us the significantly enhanced functionalities. As functional materials other than amorphous homo-polymers, copolymers and crystalline polymers are good candidates. Copolymers are known as functional materials and actually used as elastomer materials, biomedical coating materials, biodegradable materials, and patterning materials for lithography. Crystalline polymers are also known as functional materials with high Young's modulus and thermal resistivity. Although we have such functional materials, we have not obtained such functional materials in forms of nanofiber-sheets. Therefore, in this study, I systematically investigated the proper conditions of electrospinning for crystalline polymers and copolymers.

1.3. Details on hydrogels

Polymer gels are “soft material” composed of plenty of solvents with low concentration of polymers. In gels, polymers are connected with each other and form 3D networks of molecular chains. Inside the networks, plenty of solvents compared to polymers are contained. From this composition of gels, polymer gels show both liquid-like and solid-like behavior and are recognized as the representative of “soft material.”

Especially, PEG-based gels, one of the water-based gels (i.e. hydrogels), are actively studied because of their great capability in medical applications.^{16, 35} Hydrogels are composed of water-soluble polymers and water. As for the polymers, poly (ethylene glycol) (PEG), a water-soluble polymer possessing excellent biocompatibility, and its derivatives are widely used. Of course, water is also not harmful and rather compatible for lives on the earth. These PEG-based hydrogels tend to be used as biomedical applications such as cell scaffolds and drug delivery systems.^{16, 35}

Among various kinds of PEG-based hydrogels, thermo-responsive gels are suggested as the more practical candidate for medical applications.³⁶ Thermo-responsive gels are defined as the solution exhibiting the sol-gel transition due to the temperature rising. As for the applications of thermo-responsive gels, injectable gels working as cell scaffold matrixes and drug delivery systems are proposed. For example, the use of thermo-responsive gels as injectable gels is as follows: cells or drugs are mixed and dispersed homogeneously in polymer solution *in vitro* at room temperature, and the cell/drug-loaded solution is injected into our body, and eventually the solution becomes gels responding to the physiological temperature.

For obtaining thermo-responsive gels, thermo-responsive copolymers with

PEG block have been widely synthesized and reported. The representative thermo-responsive copolymer is Pluronic[®] composed of PEG and poly (propylene oxide) (PPO). Pluronic[®] is a commercially available thermo-responsive copolymer produced by BASF and sold as materials suitable for cell cultures.³⁷ ReGel[®] is also a commercially available thermo-responsive copolymer composed of poly (D, L-lactic acid-*co*-glycolic acid) (PLGA) and poly (ethylene glycol) (PEG).³⁸ Generally, these copolymers show gel-state over 10wt% at physiological temperature.

In order to enhance the functionalities of thermo-responsive gels, there have been still requirements to tune the sol-gel transition temperature around the physiological temperature and to decrease the solution concentration for containing more cells and drugs.³⁹ Considering the gels as an injectable system, at room temperature (25°C) the solution should be in sol state, and at physiological temperature (37°C) the solution should be in gel state. Therefore, the sol-gel transition temperature should be between 25°C and 37°C. Considering the gels as a carrier of cells and drugs, as the fraction of water increased in gels by decreasing the amount of polymers, more amount of cells and drugs can be loaded into the water-region of gels. So far, although various reports have treated the purpose, we still pursue the optimal thermo-responsive hydrogels with more PEG block and less hydrophobic block showing the sol-gel transition slight below the physiological temperature.

1.4. Purpose of this study

The purpose of this study is divided into two parts: one for nanofiber-sheets and the other for gels.

1.4.1. Purpose of the study on nanofiber-sheets

In order to develop thinner nanofibers from highly functional materials other than amorphous homo-polymers, the fabrication conditions were systematically studied using three different types of polymers. It is syndiotactic polypropylene (sPP), a crystalline polymer with excellent mechanical properties, 2-methacryloyloxyethyl phosphorylcholine (MPC) copolymer, a random copolymer with excellent blood compatibility and biocompatibility, and polystyrene-*b*-polyisoprene-*b*-polystyrene (SIS) triblock copolymer, a triblock copolymer with excellent elastic recovery. In detail, focusing on the interactions among polymers and solvents, the careful selection of solvents was conducted. For the systematical study, the morphology of obtained fibers, the physical properties of solvent, and the rheological properties of solutions were totally examined.

1.4.2. Purpose of the study on hydrogels

In order to develop thermo-responsive gels with low amount of copolymers with high hydrophilicity, the new types of hydrogels made from too hydrophilic copolymers to form hydrogels by themselves and clay sheets were developed and systematically studied. As for thermo-responsive copolymers, poly (D, L-lactic acid-*co*-glycolic acid)-*b*-poly (ethylene glycol)-*b*-poly (D, L-lactic acid-*co*-glycolic acid) (PLGA-PEG-PLGA) triblock copolymer was selected. As for the clay sheets, laponite was selected and mixed into the PLGA-PEG-PLGA aqueous solutions. Focusing on the interactions among copolymers and clay sheets, the ratio of clay sheets to copolymers

and the ratio of hydrophilic PEG block to the hydrophobic PLGA block were changed and totally examined.

Chapter 2. Fundamentals on nanofiber-sheets and gels

2.1. Fundamentals on polymer solution

2.1.1. Solution in organic solvents and solubility parameter

The solubility of polymers into solvents is governed by the thermodynamics equation of the free energy of mixing given as follows:

$$\Delta G_M = \Delta H_M - T\Delta S_M \quad (2-1)$$

where ΔG_M is the Gibbs free energy of mixing, ΔH_M is the heat of mixing, T is the absolute temperature, and ΔS_M is the entropy change in the mixing. In this equation, ΔG_M must be zero or negative in case that the mixing spontaneously occurs, and $T\Delta S_M$ is always positive due to the increase in the entropy on mixing. Therefore, the magnitude of ΔH_M determines the solubility.

The heat of mixing is positive in usual case for relatively non-polar organic compounds. Hildebrand and Scott proposed ΔH_M for regular mixtures as follows:

$$\Delta H_M = V_M \left(\sqrt{\frac{\Delta E_1}{V_1}} - \sqrt{\frac{\Delta E_2}{V_2}} \right)^2 v_1 v_2 \quad (2-2)$$

where V_M is the total volume of the mixture, ΔE_1 and ΔE_2 are the energy of evaporation to become a gas, V_1 and V_2 are the molar volume of each components, and v_1 and v_2 are the volume fraction of each components. $\Delta E/V$ means the vaporization energy per volume and is called the cohesive energy density.⁴⁰

The square root of the cohesive energy density is the first definition of the solubility parameter (SP) by Hildebrand and Scott:

$$\delta = \sqrt{\frac{\Delta E}{V}} \quad (2-3)$$

Thus, by using the solubility parameter, ΔH_M can be rewritten as follows:

$$\Delta H_M = V_M (\delta_1 - \delta_2)^2 v_1 v_2 \quad (2-4)$$

Thus, in polymer solution, when the solubility parameters δ of polymer and solvent are very close, ΔH_M can become smaller than the value of $T\Delta S_M$. Therefore, the polymer can be dissolved into solvents spontaneously. It is known that polymers can be dissolved into solvents with solubility parameters different by $\pm 2.0 \text{ MPa}^{1/2}$ from the solubility parameters of polymers.

The solubility parameters of solvents and polymers can be calculated from the equation as follows:

$$\delta = \frac{\rho \sum G}{M} \quad (2-5)$$

where G is the group molar attraction constants, ρ is the density, and M is the molecular weight. The group molar attraction constants G is derived from the measurement of the heat in evaporation by Small and Hoy.⁴¹

Hansen developed the solubility parameter by introducing the term of polar interactions into the equation as follows:

$$\delta = \sqrt{\frac{\Delta E}{V}} = \sqrt{\frac{\Delta E_d + \Delta E_p + \Delta E_h}{V}} \quad (2-6)$$

where ΔE_d is the dispersion cohesive energy from the nonpolar interactions, ΔE_p is the polar cohesive energy from the permanent dipole-permanent dipole interactions, and

ΔE_h is the cohesive energy from hydrogen bonding.

The equation (2-6) can be rewritten using the Hansen solubility parameters as follows:

$$\delta = \sqrt{\delta_d^2 + \delta_p^2 + \delta_h^2} \quad (2-7)$$

where δ_d is the dispersion solubility parameter based on atomic force, δ_p is the polar solubility parameter based on dipole moment, and δ_h is the hydrogen bonding solubility parameter based on hydrogen bonding. This Hansen solubility parameter is known as the most reliable values among various solubility parameters proposed by many researchers.⁴²

2.1.2. Viscosity of polymer solution

The polymer solutions were classified into four types as a function of the solution concentration: dilute solution, semidilute unentangled solution, semidilute entangled solution, and concentrated solution (Figure 2.1). When the solution concentration is sufficiently low, the solution is defined as dilute solution. As the solution concentration increased, the coils start to overlap at the overlap concentration c^* expressed as follows:

$$c^* = \frac{3M}{4\pi R_g^3 N_{av}} \quad (2-8)$$

where M is the molecular weight, N_{av} is the Avogadro number, and R_g is the radius of gyration. The solution at the concentration over c^* is defined as semidilute solution. As the solution concentration further increased, the chains start to entangle at the entanglement concentration c_e . When the solution concentration is exceedingly high, the solution is defined as concentrated solution.

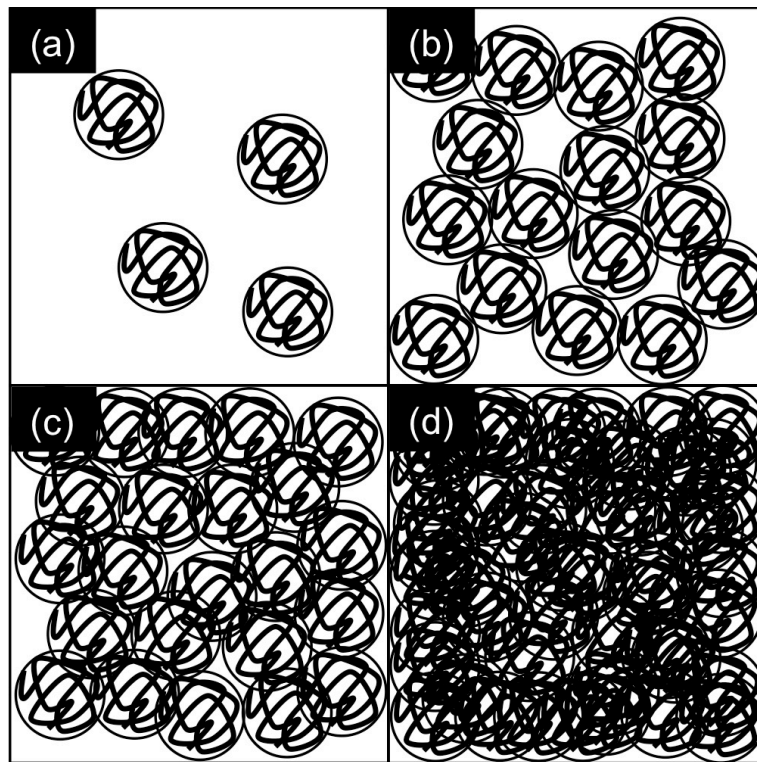


Figure 2. 1 Physical expression of polymer solutions: (a) dilute solution, (b) semidilute unentangled solution, (c) semidilute entangled solution, and (d) concentrated solution.

In the dilute solution with good solvents, the viscosity η of polymer solution was experimentally known to be proportional to the concentration as follows:

$$\eta \sim c \quad (2-9)$$

In the semidilute solution with good solvents, the power law for the viscosity of the solution can be predicted firstly based on the reptation model by de Gennes. The power law dependence for the viscosity is described as follows:

$$\eta = \eta_s \left(\frac{c}{c^*} \right)^{3/(3\nu-1)} \quad (2-10)$$

where η_s is the viscosity of solvents and ν is the Flory exponent. As for the good solvent, ν is 0.6 and eq. (2-10) become simple as follows:

$$\eta = \eta_s \left(\frac{c}{c^*} \right)^{3.75} \quad (2-11)$$

Colby *et al.* then provided the alternative power law for semidilute solution and divided the semidilute solution into the semidilute unentangled solution and the semidilute entangled solution. In the semidilute unentangled solution, the viscosity dependence on concentration can be predicted as follows:

$$\eta \sim c^{1.25} \quad (2-12)$$

In the semidilute entangled solution, the viscosity dependence on concentration can be predicted as follows:

$$\eta \sim c^{4.5} \quad (2-13)$$

2.2. Fundamentals on electrospinning and the formation of nanofibers

2.2.1. Electrospinning

Electrospinning is the process based on electrohydrodynamics. Basically, in electrospinning process, charges generate the stress inducing the motion of polymer solution in the electric fields. In more detail, the process can be divided into four stages: charge generation, jet initiation, elongation/splitting, and solidification.

The charge generation is the first step and is induced by field emission. The field emission is the injection process of electrons from the electrode surface into the surrounding medium. Basically, the process is induced under the influence of locally high electric field. The locally high electric field necessary for emission is achieved typically by using the syringe needle and metal-plate collector in electrospinning. Especially, the configuration of the needle electrode and the opposite plate electrode is known as point-plane geometry suitable for charge injection from a needle into a liquid medium (Figure 2.2). In fact, by using the geometry in electrospinning, as the applied voltage increased over 8–10 kV, charges are injected from a syringe needle to the polymer solution.

The jet initiation is the second step and is induced by the electric field. The charged solution experiences the stress induced by the electric field and form a cone-like shape at the needle tip. This is known as the Taylor cone. As the strength of electric field increased, the stress overcomes the surface tension and the jet of polymer solution is ejected from the top of the Taylor cone.

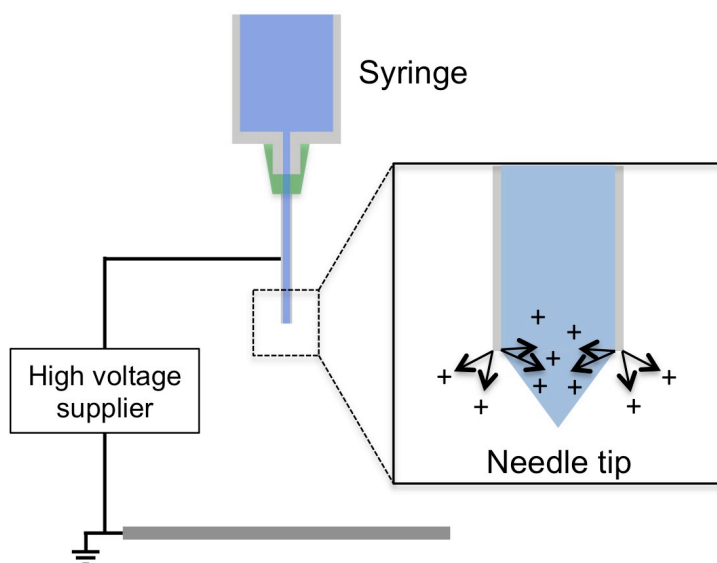


Figure 2. 2 Charge injection in the electrospinning process.

The elongation is the third step and is driven electrically by bending stability. During the travel from needle tip to the collector, the jet experiences the bending instabilities. The bending instabilities are believed to be an important factor in the formation of thinner fibers during electrospinning by Shin *et al.*⁴³ Other than the bending instabilities, Reneker *et al.* reported that the splitting of the jet due to the charge repulsion in radial direction also attributes to the reduction in the diameter of fibers.⁴⁴

The solidification is the final step and is due to the evaporation loss of solvents from the polymer solution. During the travel from needle tip to the collector, the jet of polymer solution experiences the evaporation loss of solvents basically due to the low partial pressure of solvents in air. As the diameter of jet decreased and the surface area of jet drastically increased by elongation and splitting, the evaporation of solvents is enhanced and the jet become a solid fiber before getting to the collector. Thus microfibers or nanofibers are obtained by electrospinning.

According to the mechanisms of fiber formation during electrospinning, various kinds of experimental parameters are suggested and divided into two major categories: process parameters and polymer solution parameters. Process parameters include the applied voltage, the feeding rate of polymer solution to the needle tip, and the tip-collector distance. Polymer solution parameters include the solution concentration, the volatility, the conductivity, and the dielectric constant.⁴⁵ In the following section, I would like to introduce the detailed information on process parameters and solution parameters, respectively.

2.2.2. Process parameters of electrospinning

Process parameters including the applied voltage, the feeding rate of polymer solution to the needle tip, and the tip-collector distance should be set at an appropriate value, although they possess less significant effects on the fiber formation than the polymer solution parameters.

Applied voltage is the parameter on the formation of the jet. As mentioned above, as the applied voltage become high enough to overcome the surface tension, the jet is ejected from the Taylor cone at the needle tip. Deitzel *et al.* reported the effects of the applied voltage on the fiber morphology using poly (ethylene oxide) (PEO)/water solutions.⁴⁶ In their report, as the applied voltage was increased, the Taylor cone receded and the jet originated from the nearly flat liquid surface around the needle tip. The nanofiber-sheets produced at this conditions showed increasing number of bead defects. As the applied voltage further was increased, the jet originated directly from the needle tip and the jet was found to move around the edge of needle tip. The nanofiber-sheets produced at this conditions showed higher degrees of bead defects. This phenomenon is considered to be due to the fluctuation in charge density according to the dissipation of charges into the atmosphere. Other researchers also reported this

tendency using other materials such as chitosan and gelatin.⁴⁷⁻⁴⁸ On the other hand, Zhang *et al.* reported that the diameter of fibers slightly increased as the applied voltage was increased.⁴⁹ Therefore, it can be concluded that in order to obtain nanofiber-sheets with uniform and thinner fibers, the applied voltage should be over the critical voltage necessary to overcome the surface tension but should not be increased exceedingly.

Feeding rate of polymer solution is also the parameter on the formation of the jet. Zong *et al.* reported the effects of feeding rate of polymer solution on the fiber morphology using poly (α -lactic acid) (PDLA)/dimethyl formamide (DMF) solutions.⁵⁰ In their report, the uniform fibers with smaller diameter were obtained at the slow feeding rate. However, as the feeding rate of polymer solution was increased, the fibers with larger diameter and beads were obtained. This was considered to be because as the feeding rate was increased, the velocity of the jet became large leading to the insufficient solidification before reaching the collector. Yuan *et al.* also reported this tendency using polysulfone.⁵¹ Wannatong *et al.* also reported this tendency but different attribution of feeding rate to the morphology using polystyrene/DMF solution. They considered that the solution forming Taylor cone at the needle tip became too large to be suspended at the tip leading to the drop from the tip.⁵² Therefore, it was concluded that in order to obtain the uniform fibers with smaller diameters, the feeding rate should be set at an appropriate rate to form the appropriate size of Taylor cone at the needle tip.

Tip-collector distance is the parameter on the solidification during the travel from the needle tip to the collector. Zhao *et al.* reported the effects of tip-collector distance on the fiber morphology using poly (vinylidene fluoride) (PVDF) solutions.⁵³ In their report, there was no significant effect on the fiber morphology. They concluded that as the tip-collector distance was increased, an opportunity to be elongated before reaching the collector was given to the jet, but at the same time the electric force

became too weak to elongate the jet sufficiently. It is also known that the distance required for the sufficient solidification during the travel should be kept between the needle tip and the collector.⁴⁷

2.2.3. Solution parameters of electrospinning

Solution parameters including the polymer concentration, the volatility, the conductivity, and the dielectric constant have more significant influence on the morphology of electrospun fibers. Among the solution parameters, the polymer concentration has a substantial influence on the morphology of electrospun products. To begin with, when the solution for jet is composed of pure solvent or solute with low molecular weight and the viscosity of the solution is not substantially high, the jet experiences the Plateau-Rayleigh instability and break up into the spherical droplets to minimize the total surface energy.⁵⁴ This process is called electrospaying. On the other hand, when the solution for jet is composed of solute with high molecular weight (i.e. polymer) and the viscosity of the solution is substantially high, the jet become to overcome the Plateau-Rayleigh instability. Eventually the fiber-like structures are remained after the process. This process is the electrospinning.

In order to make the solution viscosity substantially high, the polymer concentration should be increased to develop the entanglement of polymer molecules. When the polymer concentration is too low, a spray will be formed as well as electrospaying and the electrospun products become particles often called beads. As the concentration is increased, polymer molecules started to entangle with each other in solution, and the electrospun products become fibers with beads. As the concentration is further increased, polymer molecules are sufficiently entangled and the electrospun products finally become uniform fibers. However, when the concentration becomes exceedingly high, the process is disrupted due to the exceedingly high viscosity or the

fast solidification at the tip before the initiation of jet.³⁴ Within the optimal concentration range of the solutions, the diameters of uniform fibers gradually increase as the polymer concentration increased.

The volatility is the parameter on the solidification during the travel of jet. In order to determine the volatility, the boiling point of solvent can be used. When the solvent with high boiling point is used for the preparation of solution for electrospinning, the sufficient solidification of jet cannot be achieved before reaching the collector. On the other hand, the solvent with low boiling point is used for the preparation of solution for electrospinning, the solution solidifies at the tip before the initiation of jet. In many cases, in using the solvents with relatively low boiling point such as tetrahydrofuran (THF) and chloroform, a small amount of solvent with relatively high boiling point are added to adjust the volatility. For example, N, N-dimethylformamide (DMF) with high permittivity was frequently used for this purpose.

The conductivity and the dielectric constant are the parameters on the charge injection and the elongation in the electric field. Many researchers reported that the uniform and thinner nanofibers were obtained by increasing the conductivities using a solvent with high permittivity and a salt. By using solvents with high conductivities, the charge-carrying capacities are introduced to the solution and the solution can be sufficiently elongated in the electric field. Barber *et al.* reported the fabrication of chitin nanofibers using chitin/ionic liquid solution.⁵⁵ Ionic liquid is a liquid-state salt and works as an attractive solvent with high conductivities. Luo *et al.* reported the effect of dielectric constant on the fiber morphology. They fabricated poly (ϵ -caprolactone) nanofibers by mixing acetic acid and formic acid with significantly different dielectric constants but the same functional group and comparable physical properties other than

dielectric constants. According to their report, as the dielectric constant increased and approached to 19 and above, PCL nanofibers were obtained.⁵⁶

2.3. Fundamentals on gels

2.3.1. Classification of gels

Polymer gels are classified into chemical gels and physical gels by the type of cross-link point. As for chemical gels, covalent bonds work as the cross-link points, therefore, the cross-link points cannot be broken by heat. On the other hand, as for the physical gels, physical bonds relatively weaker than covalent bonds work as the cross-link points. Due to the nature of physical bonds, the cross-link point is reversibly formed and detached by heat. This thermo-reversibility is one of the great characteristics of physical gels.

2.3.2. Physical gels with microcrystalline junctions

The solution of crystalline polymers forms physical gels with crystalline junctions. The crystalline polymers with stereoregularity in their molecular chains can be dissolved into organic solvents at high temperature around the melting point of crystalline polymers. When the solution is cooled down to room temperature, the chains of crystalline polymer were folded together and the microcrystals working as cross-link point were formed as shown in Figure 2.3.

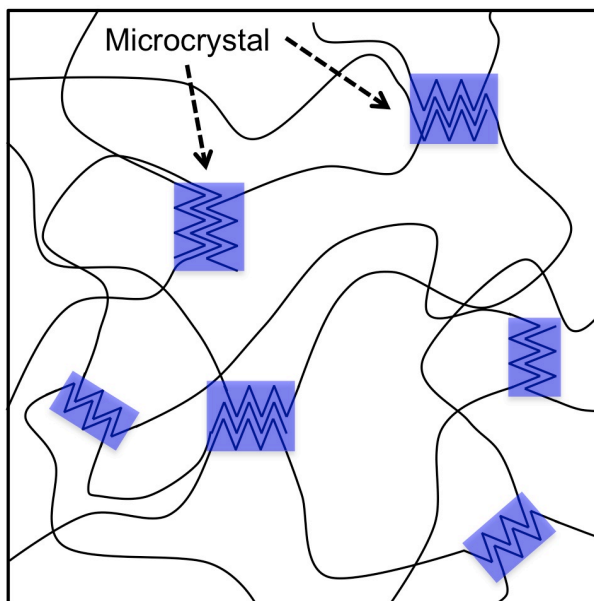


Figure 2. 3 Schematic image of crystalline gels.

2.3.3. Physical gels with associating junctions

The solution of block copolymers forms physical gels with associating junctions. The amphiphilic block copolymers carrying both hydrophilic and hydrophobic group are well known materials forming gel with associating junctions. When the amphiphilic block copolymers are dissolved into water, they form micelles due to hydrophobic association. As the concentration increased, the micelles serve as cross-link points and the amphiphile solution form gels.

Thermo-responsive hydrogel is the aqueous solution with thermo-responsive block copolymers such as PPO-PEG-PPO and PLGA-PEG-PLGA. The mechanisms of thermo-responsive gelation were explained by Jeong *et al.* as follows. As shown in Figure 2.4 (a), the polymer chains not forming micelles, micelles, and networked micelles coexist in the solution. As the temperature increased, the number of micelles

increased by the decrease in the number of polymer chains not forming micelles. At the same time, the micelles percolate and the size of aggregated micelles increased (Figure 2.4 (b)). Eventually, a large part of micelles are connected each other and the network leading to gelation is formed in the solution as shown in Figure 2.4 (c). As the temperature is further increased, the hydrophobic PLGA chains shrink and the hydrophilic PEG chains dehydrate, and eventually the precipitation of polymer is observed (Figure 2.4 (d)).

The block copolymers without water-soluble blocks also form self-assembly structures in organic solvents as well as the amphiphiles. Recently, the ionic gel with triblock polymer and ionic liquid has been focused on as a new conductive material.⁵⁷

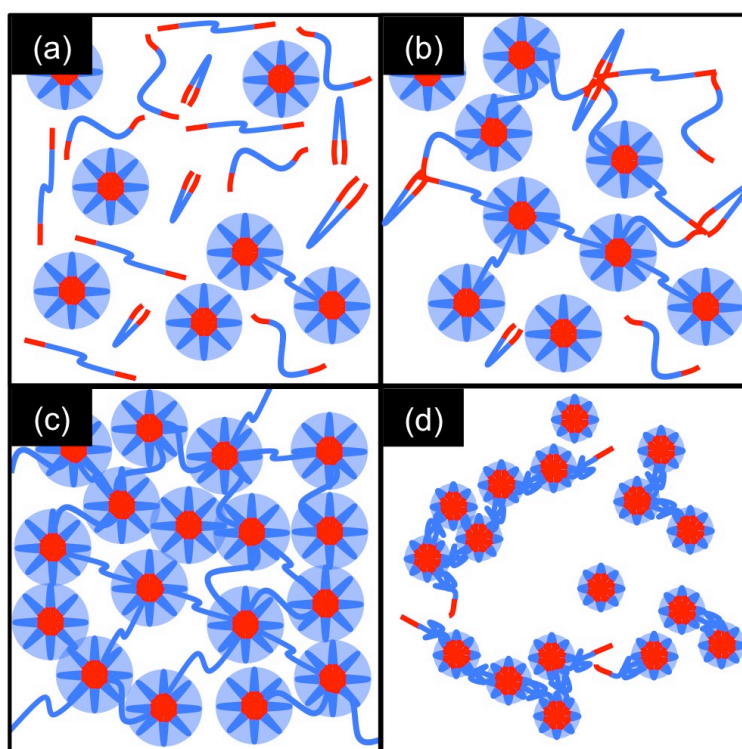


Figure 2. 4 Schematic images of thermo-responsive gelation of block copolymers.

Chapter 3. Syndiotactic polypropylene (sPP) electrospun nanofibers

3.1. Background on polypropylene (PP) nanofibers

Polypropylene (PP) is one of semi-crystalline polymers that have unique properties with outstanding mechanical features and excellent chemical resistance as well as polyethylene (PE). The chemical resistance, however, causes major difficulty in dissolving semi-crystalline polymers into common solvents at ambient temperature due to their chemical stability, which would, therefore, inhibit creating the nanofibers of semi-crystalline polymers by electrospinning using polymer solutions.

In order to solve the problem, since electrospinning process can only be carried out using liquid-state polymer solutions, the dissolution of semi-crystalline polymers into the limited number of good solvents has generally been attempted at substantially elevated temperature.⁵⁸⁻⁵⁹ The polyolefin solutions, however, when they are cooled to ambient temperature, occasionally form thermo-reversible physical gels due to the nature of their semi-crystallinity that could work as physical cross-links.⁶⁰ As such the polymer specimens are no more in the liquid state, once the solutions transform into gels, which would obviously prevent the synthesis of fine fibers by electrospinning.⁶¹

Because of such difficulties in the solution electrospinning of the semi-crystalline polymers, the semi-crystalline polymers were normally spun into fibers through different and sometimes rather complex.⁶² As for isotactic polypropylene (iPP), Wang *et al.* reported the fabrication of iPP nanofibers via high-temperature solution electrospinning. In the high-temperature solution electrospinning, the jacket-type heating system with heated oil was attached to the syringe containing the iPP solution. In addition to the heating system for syringe, high-energy laser light was also used to

heat the needle spinneret locally. This local heating of spinneret prevented from the temperature drop along the needle spinneret due to the use of long and thin needle. Furthermore, an infrared (IR) emitter was used to control the environmental temperature during the electrospinning. This environmental control was required to evaporate rapidly the solvents used for polymer solution because the solvent for iPP solutions usually possess high boiling point. For example, in the work, *o*-dichlorobenzene (*o*-DCB) with boiling point of 180.5°C was used. By using the apparatus with precisely controlled heating systems and by adding Bu₄NClO₄ salts to enhance the solution conductivity, the thinnest iPP nanofibers with the diameter of 286 nm was obtained.⁶³ Cho *et al.* also reported the elevated temperature electrospinning for iPP nanofibers. Their setup possesses four temperature zones: the reservoir of solution, the nozzle, the region of spinning, and the collector. In the article, it was mentioned that the temperature of reservoir was controlled to maintain the solution, temperature of nozzle was adjusted to control the viscosity, the temperature of spinning region was adjusted to control the solvent evaporation and the gelation during the elongation of fibers, and the temperature of collector was controlled to regulate the crystallinity of obtained nanofibers. By using the setup, they eventually obtained iPP fibers with the diameter of 800 nm.⁶⁴

As for syndiotactic polypropylene (sPP), Lee *et al.* reported the preparation of sPP fibers with the diameter of 650 ± 50 nm at slightly elevated temperature (35°C). They used a multi-component solvent system of cyclohexane, acetone, and DMF (80/10/10, cyclohexane/acetone/DMF). Acetone and DMF, non-solvents for sPP, were added to cyclohexane in order to introduce the polarity and volatility. They also tried to fabricate sPP fibers at a lower temperature (25°C) and obtained heterogeneous fibers with two different diameters. For the mechanisms, it was considered that the rapid

gelation from the heterogeneity of solution led to the formation of non-uniform fibers.⁶⁵ Watanabe *et al.* also reported the fabrication of sPP fibers with the average diameter of 530 ± 130 nm using decahydronaphthalene (decalin)-base solvents and sPP fibers with the average diameter of 760 ± 370 nm using cyclohexane-base solvent. The decalin-base solvent was composed of decalin, acetone, and DMF (80/10/10 by weight ratio, decalin/acetone/DMF) and the cyclohexane-base solvent was composed of cyclohexane, acetone, and DMF (80/10/10 by weight ratio, cyclohexane/acetone/DMF). The sPP solution with decalin-base solution was kept at 40°C and used for electrospinning, while the sPP solution with cyclohexane-base solution was used at 25°C for electrospinning. It was also found that the surface of obtained fibers from the sPP solution with decalin-base solvent was smoother than that from the solution with cyclohexane-base solvent. They considered the roughened surface was from the rapid gelation in a heterogeneous solution system.⁶⁶ Jao *et al.* also reported the fabrication of sPP nanofibers using high-temperature electrospinning.⁶⁷ They used sPP/*o*-DCB solution with a salt of tetra-*n*-butyl ammonium. The solution in a syringe was maintained at 80°C during electrospinning. In the study, the sPP nanofibers with the diameter of 137 ± 76 nm were obtained from the 5wt% solution. It was also mentioned that the sPP fibers were more uniform than the fibers obtained by Lee *et al.*⁶⁷

Other than electrospinning, Suzuki *et al.* proposed and developed a new method called CO₂ laser supersonic multi-drawing (CLSMD) for the nanofiber production. The apparatus for CLSMD is basically composed of a CO₂ laser, an acrylic vacuum chamber, and preformed-fiber injection orifices. In CLSMD, the preformed fibers were irradiated by CO₂ laser and drawn by a supersonic airflow from the pressure difference between inside and outside of chamber. By setting the laser power at 35 W and the chamber pressure at 8 kPa, iPP nanofibers with the average

diameter of 350 nm were eventually obtained. This is, at the moment, the minimum diameter of iPP fibers fabricated at room temperature.⁶⁸

Even after the various studies to fabricate finer and more uniform PP nanofibers as shown above, the solution electrospinning for crystalline polymers including PP has not been systematically studied. In the previous studies, the apparatus was mainly developed and the number of parameters required to precisely control increased. Even though there were some trials to fabricate PP nanofibers at milder conditions, the goal has not been achieved so far. Therefore, it can be expected that the systematical study on the fabrication process could realize the mild fabrication process of nanofibers.

In this study, in order to achieve the fabrication of crystalline-polymer nanofibers at milder condition, the fabrication process of sPP nanofibers was systematically studied. For the simplicity, a single solvent system was used to achieve a homogenous solution system (in contrast to the multi-component solvent system as mentioned above) at ambient temperature (25°C). As the solvent, cyclohexane, methyl-cyclohexane, ethyl-cyclohexane, propyl-cyclohexane, butyl-cyclohexane, and decalin were separately examined. These solvents possessed similar chemical structures with close solubility parameters. The selection of the solvents was carefully conducted by primarily considering the gelation behavior and the viscosity of sPP solutions and the solvent properties including conductivity, dielectric constant, and evaporation rate.

3.2. Experimental

3.2.1. Materials

Syndiotactic polypropylene (sPP) was purchased from Sigma-Aldrich Co. LLC. The weight average molecular weight (M_w) and the number average molecular weight (M_n) were 174,000 g/mol and 75,000 g/mol, respectively. The melting point was 127°C measured by differential scanning calorimetry (DSC) (Mettler Toledo International Inc.). Cyclohexane, methyl-cyclohexane, and decahydronaphthalene (mixture of cis- and trans-) (decalin) were purchased from Wako Pure Chemical Industries, Ltd. Ethyl-cyclohexane, and propyl-cyclohexane, and butyl-cyclohexane were purchased from Tokyo Chemical Industry Co., Ltd.

3.2.2. Solution preparations

sPP was dissolved into cyclohexane, methyl-cyclohexane, ethyl-cyclohexane, propyl-cyclohexane, butyl-cyclohexane, and decalin, separately, and stirred at 80°C for overnight. Then, the heated solutions were cooled down to 25°C in 30 min. The concentration of sPP in the solution was changed from 1wt% to 5wt%.

3.2.3. Gelation-speed evaluation

The gelation characteristics of sPP largely depended on the concentrations of the solution and the duration of the cooling process from the heated solution. To confirm the sol state of the solution during electrospinning, we performed gelation tests for sPP solutions by a tube testing method. sPP solutions in glass tube were kept stationary under the controlled environment at 25°C up to 5 days. The tubes were reversed every 24 hours and check whether the solutions were sol state or gel state. We defined the solution as gel state when the flow of solutions was not observed.

3.2.4. Fabrication of sPP nanofibers by electrospinning

sPP nanofibers were fabricated using an electrospinning apparatus (1639, Imoto Co.). Each solution was poured into a syringe (1005LT, Hamilton) with a capillary tip whose inner diameter was 0.53 mm. The needle tip was connected to a high voltage supply and the positive voltage of 10 kV was applied to the polymer solutions. The grounded metal collector was placed 13 cm off the needle tip. The flow rates of the solution were controlled by syringe pump at 0.20 mL/h.

3.2.5. Morphological analysis of electrospun sPP nanofibers

Electrospun sPP fibers were characterized by the field emission scanning electron microscopy (FE-SEM, S-4700, Hitachi High-technology Co.). Before SEM observation, all specimens were coated with osmium to prevent electrostatic charge. For each sample, the diameters of the fabricated fibers were measured at 100 different points on each SEM micrograph selected randomly for the calculation of the average diameter of the fibers.

3.2.6. Characterization of physical properties of solvents

To evaluate characteristic features of the used solvents, the conductivity, the dielectric constant, and the evaporation rate of the solvents were individually measured. The conductivity of the solvents was measured using a non-aqueous conductivity meter (DT700, Dispersion Technology, Inc.) at room temperature (25°C). The dielectric constant of the solvent was also measured using a liquid permittivity meter (Model 871, Nihon Rufuto Co., Ltd.). Furthermore, the evaporation loss was measured by weighing the mass change of each solvent at 25°C. Each solvent was poured into a ϕ 36 mm glass tube and the tube was left at 25°C under the stable airflow.

3.2.7. Rheological analysis of sPP solutions

The zero-shear rate viscosity (η_0) data were obtained by a strain-controlled

rheometer (ARES-G2, TA Instruments) in the cone-plate geometry (50.0 mm in diameter and 0.0192 rad in its cone angle). All viscosity data were measured at 25°C. The shear rate was changed from 0.1 s⁻¹ to 100 s⁻¹ at 25°C. To evaluate the physical properties of the solution, the specific viscosity (η_{sp}) of the sPP solutions in each solvent was calculated by estimating the zero-shear rate viscosity, analyzed by measured experimental viscosity data. η_{sp} was calculated using the zero-shear rate viscosity (η_0) defined as follows:

$$\eta_{sp} = (\eta_0 - \eta_s) / \eta_s \quad (3-1)$$

where η_s is the solvent viscosity. η_{sp} represents the rate of increase in solvent viscosity by mixing polymeric solute.

3.3. Results and Discussion

3.3.1. Gelation-speed evaluation of sPP solutions

Before considering the solvent properties and the viscosity of polymer solutions, the gelation speed of polymer solutions should be checked for crystalline polymers. In general, for non-crystalline polymer, the solvent properties such as conductivity, dielectric constant, and volatility are known as important parameters for electrospinning. The viscosity of polymer solution is also adjusted by changing the solution concentration in various studies. Additionally, for crystalline polymer, the solution tends to form gel at different gelation rate depending on the types of solvents and the solution concentration.⁶⁹⁻⁷⁰ As mentioned before, since the solution for electrospinning should not form gel, first of all, the gelation rate of sPP solutions with various types of solvents was checked.

The gelation speed of sPP solutions at the concentration from 1wt% to 5wt% is shown in Figure 3.1–Figure 3.6. Circle of gray color represents the sol state, square of gray color represents soft gel state, and square of black color represents gel state. Soft gel is defined as the gel state showing the change of form. As shown in Figure 3.1, as for the sPP/cyclohexane solution, all 1–5wt% solutions were in sol states even after 5 days. Among the solvents used in this study, the sPP solution with cyclohexane showed the widest region of sol-state. As for the sPP/methyl-cyclohexane solution shown in Figure 3.2, the 1–2wt% solutions were in sol states even after 5 days, however, the 3wt% solution changed from sol to gel states after 4 days and the 4–5wt% solutions changed from sol to gel states in a few days. As for the sPP/ethyl-cyclohexane solutions shown in Figure 3.3, the 1wt% solution changed from sol to gel states after 4 days, however, the 2–5wt% solutions changed from sol to gel states in a day. As for the sPP/propyl-cyclohexane solutions shown in Figure 3.4 and the sPP/butyl-cyclohexane

solutions shown in Figure 3.5, all 1–5wt% solutions changed from sol to gel states relatively fast in a day and, in other words, all 1–5wt% solutions were in gel states. It was found that the gelation speed got faster as the length of alkyl group bonded to cyclohexane increased.

Additionally, decalin, one of the bicycloalkane with six-membered ring like cyclohexane was also examined. As shown in Figure 3.6, as for the sPP/decalin solution, the 1wt% solution changed from sol to gel states after 4 days and the 2wt% solution after 3 days, while the 3–5wt% solutions changed from sol to gel states in a day. It was found that the gelation speed of sPP/decalin solution was faster than that of sPP/methyl-cyclohexane solution and slower than that of sPP/ethyl-cyclohexane solution. The results indicated that the gelation strongly depended on the types of solvents, the concentrations of the solution, and time. Therefore, it could be concluded that the sol-state solution with cyclohexane and cyclohexane with shorter alkyl chain of methyl-cyclohexane and ethyl-cyclohexane were suitable candidates for the solution electrospinning.

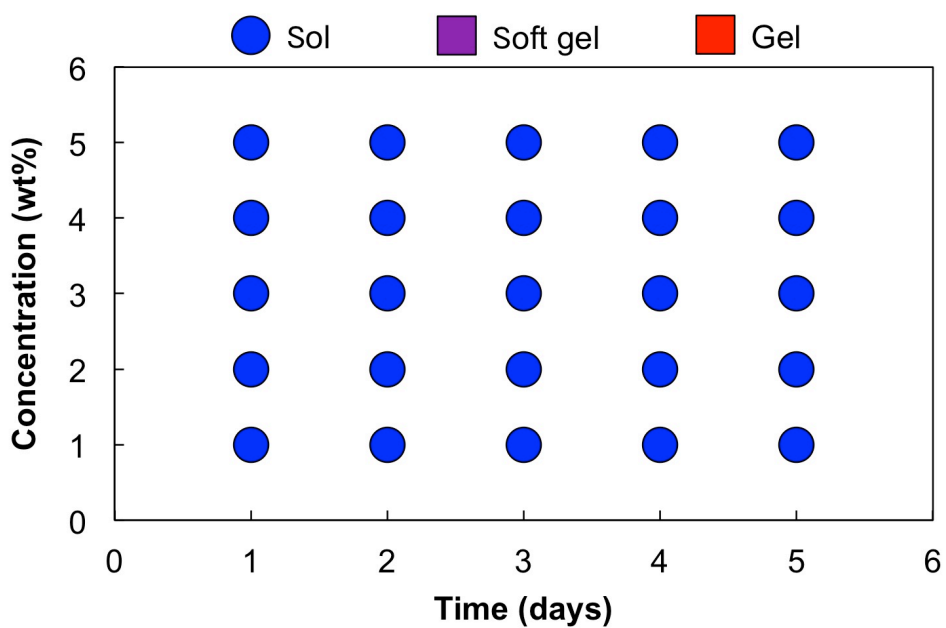


Figure 3. 1 Sol-Gel phase change by concentration and time with cyclohexane.

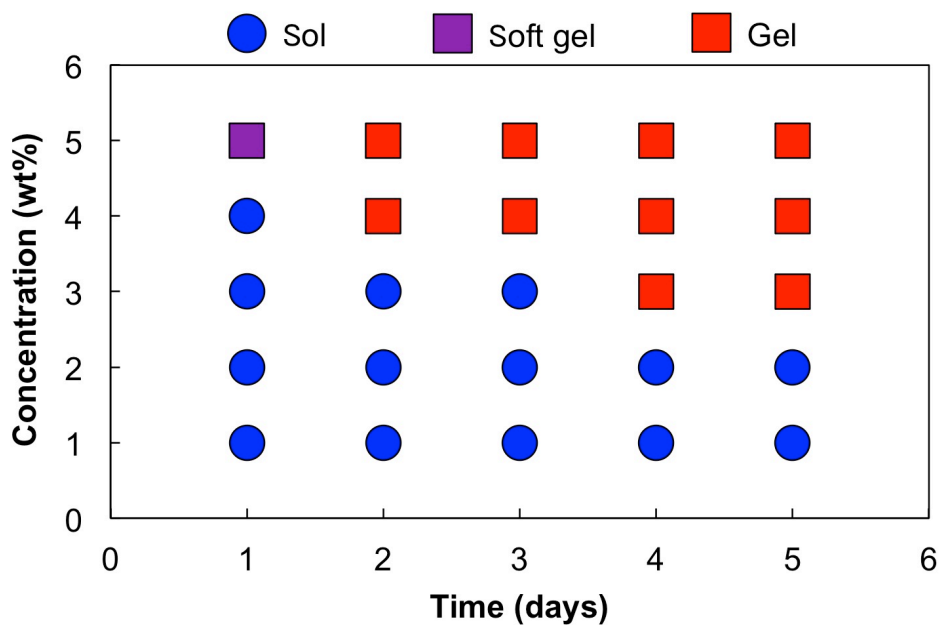


Figure 3. 2 Sol-Gel phase change by concentration and time with methyl-cyclohexane.

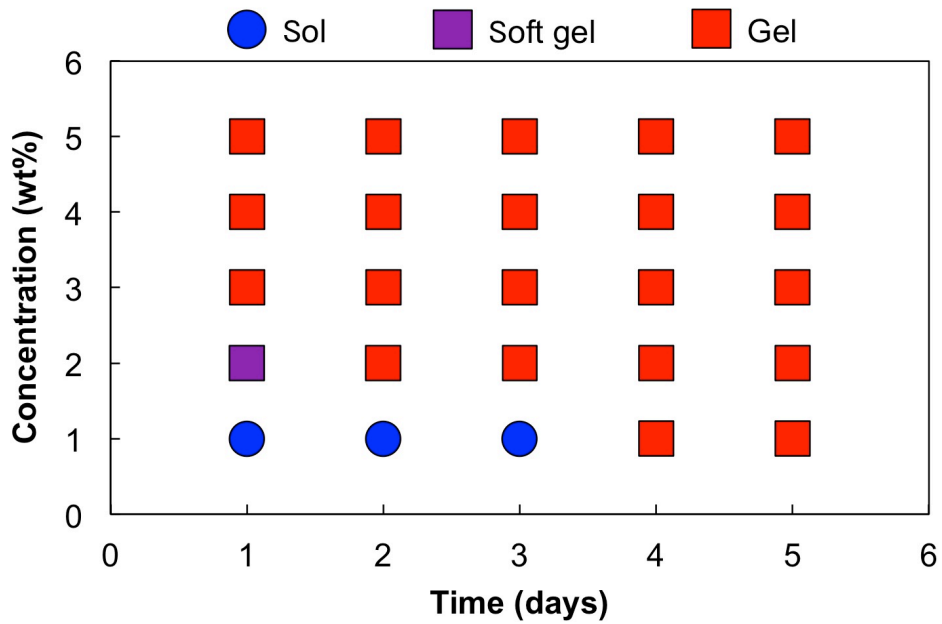


Figure 3. 3 Sol-Gel phase change by concentration and time with ethyl-cyclohexane.

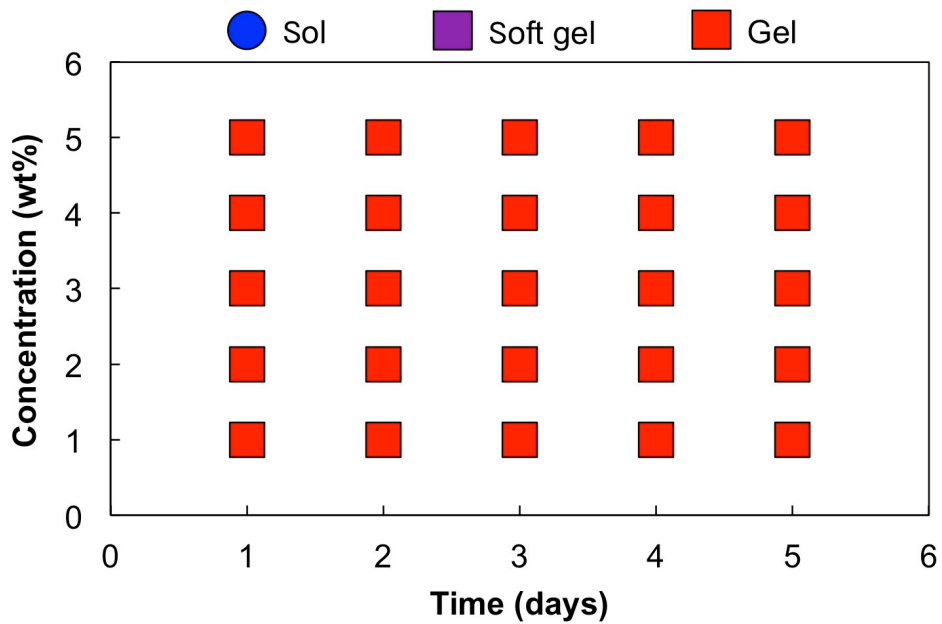


Figure 3. 4 Sol-Gel phase change by concentration and time with propyl-cyclohexane.

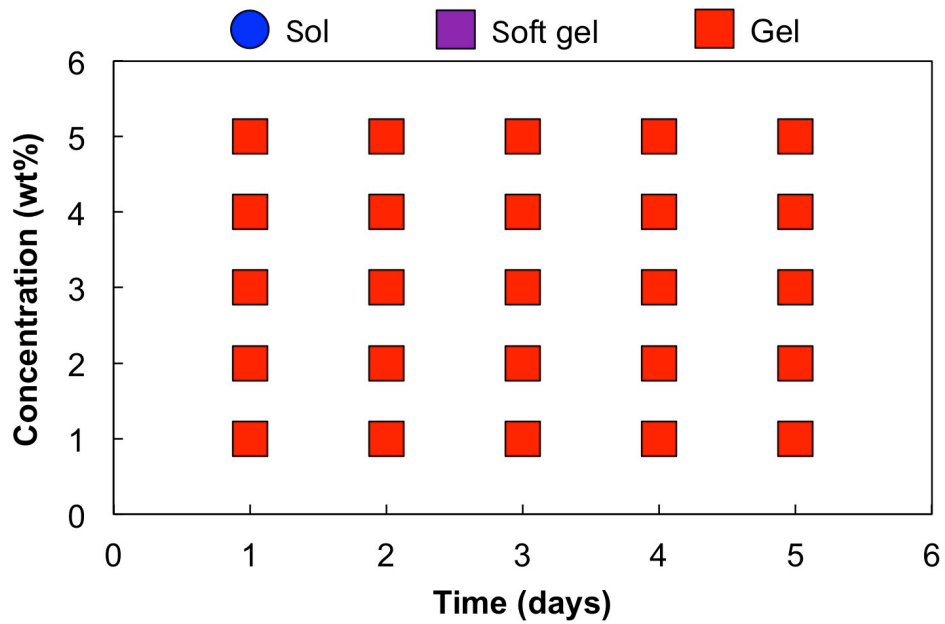


Figure 3. 5 Sol-Gel phase change by concentration and time with butyl-cyclohexane.

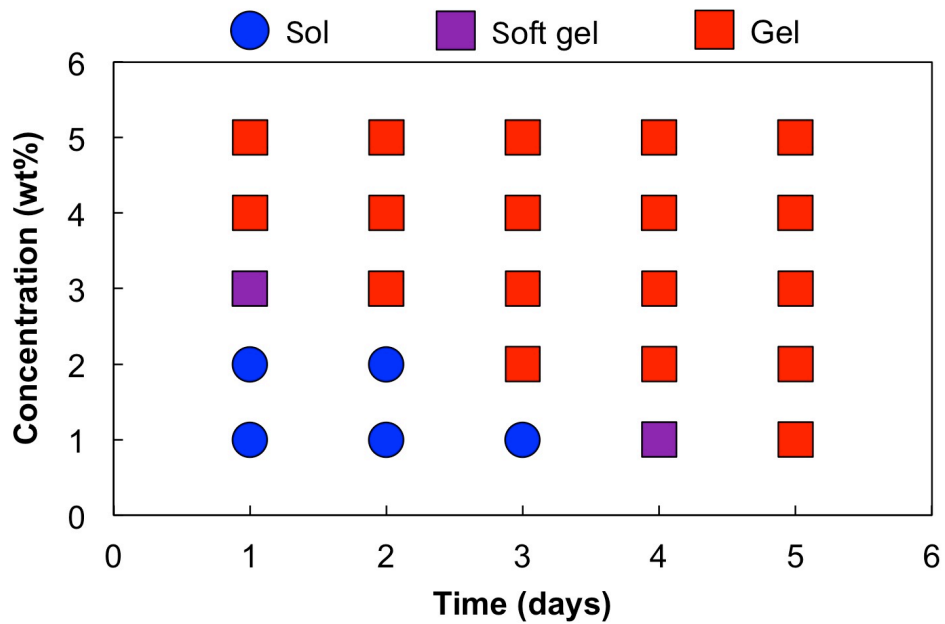


Figure 3. 6 Sol-Gel phase change by concentration and time with decalin.

In order to discuss the difference in the gelation speeds of sPP solution with various types of solvents, the solubility parameters and the size of molecules are introduced here. It is known that the solubility parameter and the molecular size affect the gelation of crystalline polymer solution.⁷¹

Solubility parameters of solvents used in this study were summarized in Table 3.1 and Table 3.2. The solubility parameters listed in Table 3.1 were the experimental values determined by Hansen *et al.* and the solubility parameters listed in Table 3.2 were the theoretically calculated values using the method proposed by Small *et al.*, Fedors *et al.*, and Burrell *et al.*, respectively.⁴¹⁻⁴² The solubility parameters by Hansen *et al.* were not provided for ethyl-cyclohexane and propyl-cyclohexane as shown in Table 3.1. Therefore, the solubility parameters were calculated using various methods as shown in Table 3.2. Among the solubility parameters listed in Table 3.2, since the solubility parameters calculated by Burrell's method were in good agreement with the solubility parameters determined by Hansen *et al.*, the solubility parameters calculated using the method by Burrell *et al.* were mainly taken into consideration.

The solubility parameter affects the interactions between polymers in solution. The solubility parameters on PP and solvents were reported and could be calculated according to their chemical structures, and there are slight differences depending on the calculation methods. Especially for PP, since the solubility parameter depends on the types and the degree of stereo-regularity, it is hard to determine the accurate solubility parameter. According to the literature⁷², the solubility of PP is estimated to be within 16.0–18.0 MPa^{1/2}. When the solubility parameter of PP used in this study is assumed to be 17.0 MPa^{1/2}, the solubility of cyclohexane is the closest and the solubility of methyl-cyclohexane is the most distant. It was found that the solubility parameter could not be used for the explanation of the difference in the gelation rate in our study.

Table 3. 1 Hansen solubility parameters for solvents.

Name	δ_D (MPa ^{1/2})	δ_P (MPa ^{1/2})	δ_H (MPa ^{1/2})	δ (MPa ^{1/2})
Cyclohexane	16.8	0.0	0.2	16.8
Methyl-cyclohexane	16.0	0.0	1.0	16.0
Ethyl-cyclohexane	-	-	-	-
Propyl-cyclohexane	-	-	-	-
Butyl-cyclohexane	16.2	0.0	0.6	16.2
Decalin	cis-	18.8	0.0	18.8
	trans-	18.0	0.0	18.0

Table 3. 2 Solubility parameters calculated by various methods.

Name	δ^a (MPa ^{1/2})	δ^b (MPa ^{1/2})	δ^c (MPa ^{1/2})
Cyclohexane	16.9	17.6	16.9
Methyl-cyclohexane	15.2	17.1	16.3
Ethyl-cyclohexane	14.6	17.1	16.6
Propyl-cyclohexane	13.9	17.2	16.5
Butyl-cyclohexane	13.7	17.2	16.6
Decalin	cis-	-	19.2
	trans-	-	17.7

^a δ was calculated using the method proposed by Small *et al.*

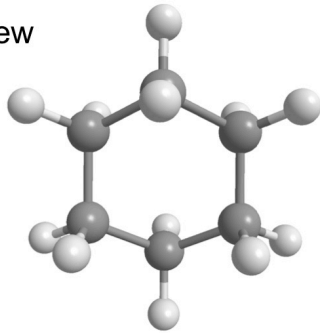
^b δ was calculated using the method proposed by Fedors *et al.*

^c δ was calculated using the method proposed by Burrell *et al.*

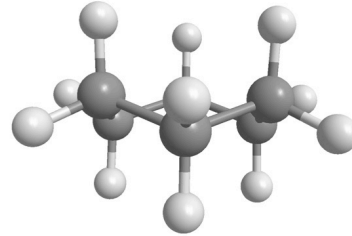
The size of molecules affecting the intermolecular distance of polymers in solution was also examined. Figure 3.7 shows the molecular models of solvents used in this study. As shown in Figure 3.7, the size of molecules basically increases as the molecular weight increases. The size of molecules could also depend on their conformation. According to the literature by Hansen *et al.*, the molar volume was 108.7 cc/mol for cyclohexane, 128.3 cc/mol for methyl-cyclohexane, 156.9 cc/mol for *cis*-decalin and *trans*-decalin, and 176.7 cc/mol for butyl-cyclohexane.⁴² The increase in molar volume was consistent with the increase in gelation speed. Therefore, it was indicated that the difference in the gelation rate of sPP solution could be due to the difference in the molecular size rather than the difference in the solubility parameter.

(a)

Top view

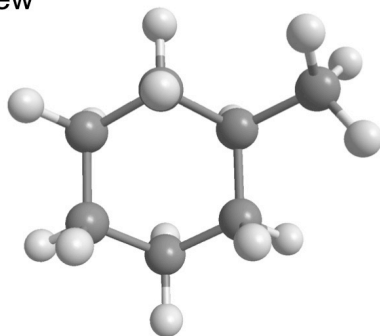


Side view

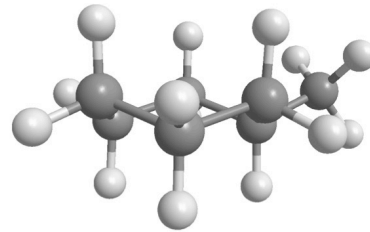


(b)

Top view

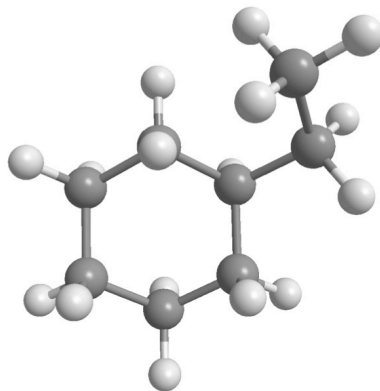


Side view

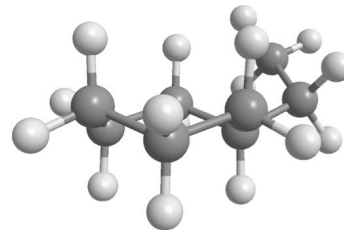


(c)

Top view

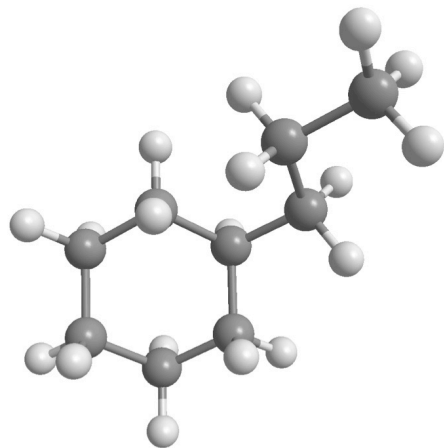


Side view

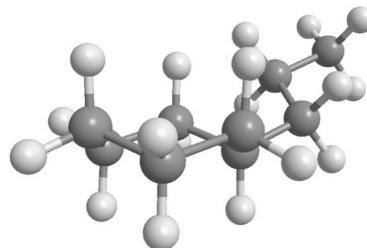


(d)

Top view

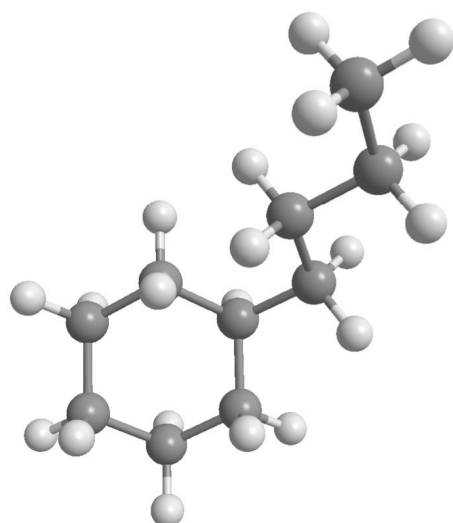


Side view

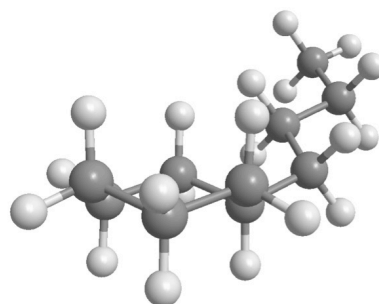


(e)

Top view



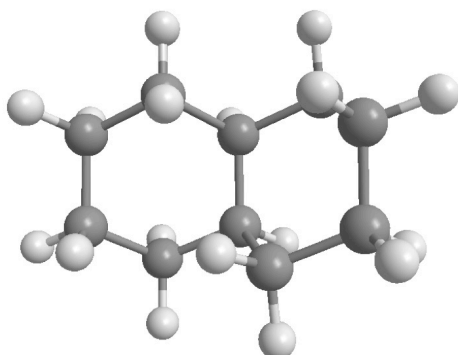
Side view



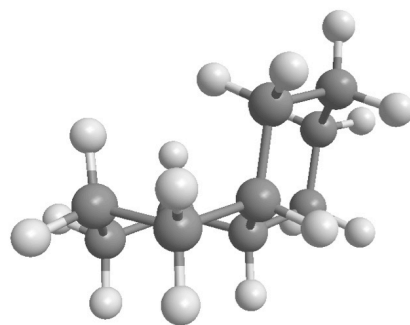
(f)

cis-

Top view

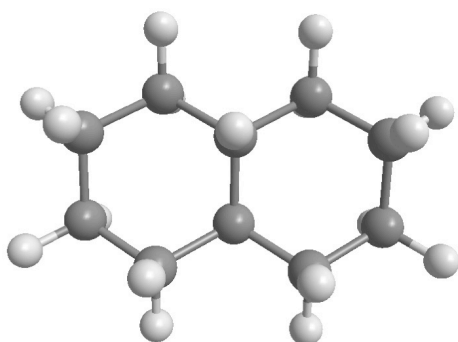


Side view



trans-

Top view



Side view

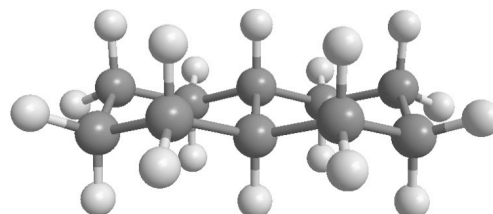


Figure 3. 7 Molecular structures of solvents: (a) cyclohexane, (b) methyl-cyclohexane, (c) ethyl-cyclohexane, (d) propyl-cyclohexane, (e) butyl-cyclohexane, and (f) decalin.

3.3.2. Morphology of electrospun sPP nanofibers

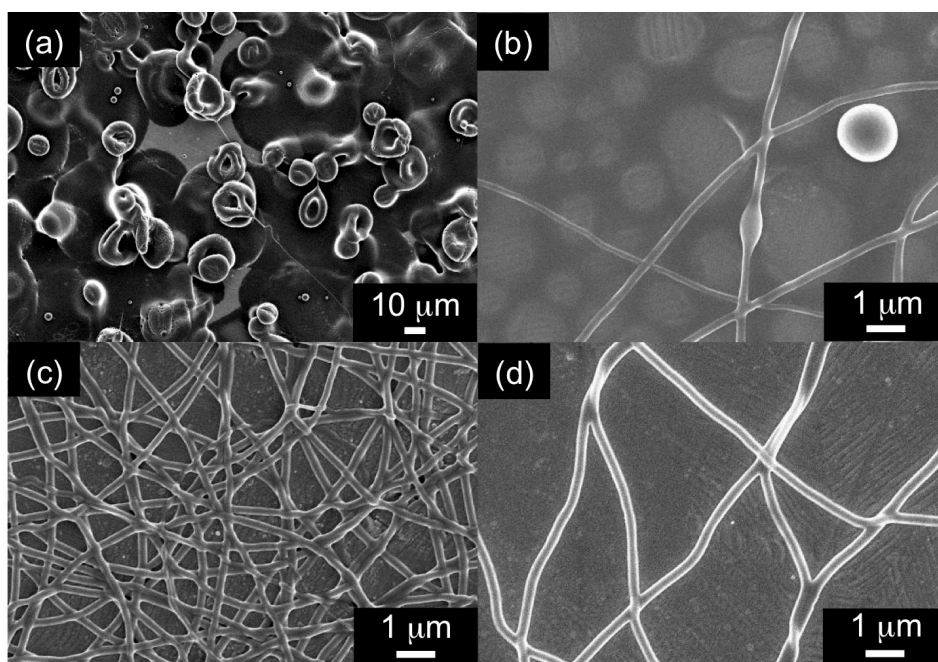


Figure 3. 8 SEM images of sPP nanofibers fabricated from sPP/methyl-cyclohexane solution at different concentrations: (a) 1wt%, (b) 2wt%, (c) 3wt%, and (d) 4wt%.

Figure 3.8 shows the SEM images of sPP nanofibers from the sPP/methyl-cyclohexane solution with different concentrations. As shown in Figure 3.8 (a), from 1wt% solution, beads were obtained. As shown in Figure 3.8 (b), from 2wt% solution, beaded nanofibers were obtained. When the solution concentration was increased to 3wt%, uniform nanofibers were fabricated as shown in Figure 3.8 (c), and above 4wt%, uniform nanofibers with larger diameter were fabricated (Figure 3.8 (d)). The morphological change from beads to uniform nanofibers consisted with the formation of electrospun nanofibers with other polymers in the previous studies.⁷³ From the change, it was also found that the entanglement concentration C_e was between 2wt%

and 3wt%. This is because of the knowledge that the entanglement of polymer chains is required to obtain the bead-free fibers. According to the theoretical calculation, the entanglement concentration C_e can be also estimated by $C_e=2M_e/M_w$.⁷⁴ The entangled molecular weight M_e for molten sPP reported by Liu *et al.* was 3,370 g/mol.⁷⁵ Therefore, the C_e for sPP used in this study with molecular weight M_w of 174,000 g/mol was calculated as 2.7wt%.⁶⁷ This theoretical consideration is in good agreement with the experimental estimation.

Figure 3.9 shows the SEM images of sPP fibers prepared from 3wt% polymer solutions with different solvents via solution electrospinning at 25°C. Figure 3.9 (a) showed the sPP nanofibers from sPP/cyclohexane solution. The average diameter of sPP nanofibers by cyclohexane was 720 ± 154 nm. As demonstrated in Figure 3.9 (b), the finest sPP nanofibers with the average diameter of 230 ± 57 nm were obtained from sPP/methyl-cyclohexane solution. Figure 3.9 (c) showed the sPP nanofibers from sPP/ethyl-cyclohexane solution. The average diameter of sPP nanofibers by ethyl-cyclohexane was 380 ± 130 nm. As for the sPP/decalin solution forming soft-gel in a day, no fibers but micro-beads were obtained as shown in Figure 3.9 (d). As for the sPP/propyl-hexane solution and sPP/butyl-hexane solution, as mentioned before, since the solutions formed brittle gel relatively fast after cooling down to 25°C in a day, the solution electrospinning could not be carried out.

Figure 3.10 shows the frequency distributions of sPP nanofibers from sPP/cyclohexane solution and sPP/methyl-cyclohexane solution. As shown in Figure 3.10 (a), the sPP nanofibers from sPP/methyl-cyclohexane solution showed relatively narrower frequency distribution than the sPP nanofibers from sPP/cyclohexane solution shown in Figure 3.10 (b). The non-uniformity is possibly due to the rapid gelation of sPP solution caused by rapid evaporation of solvents during electrospinning.

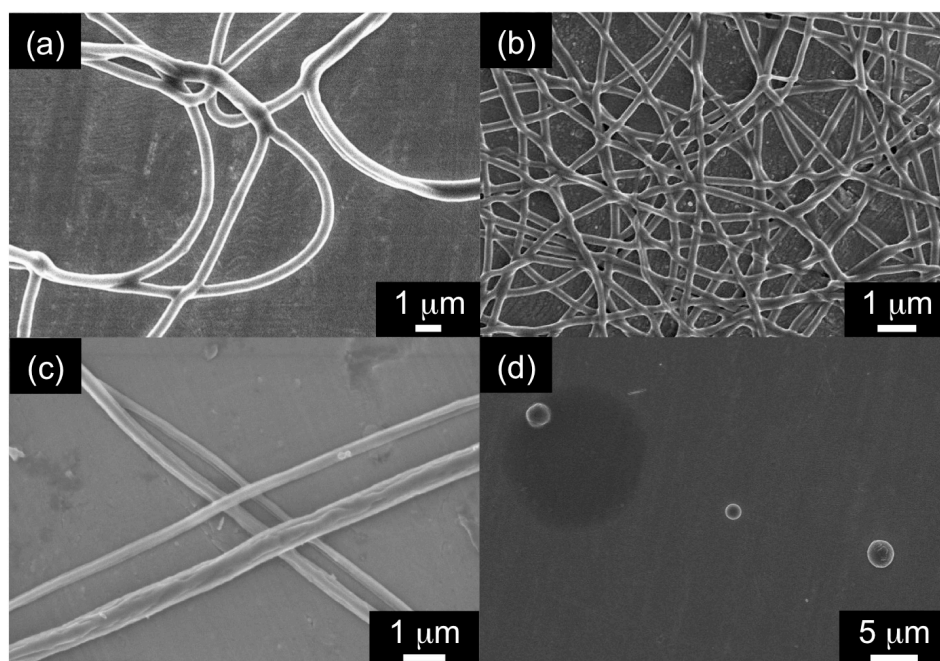


Figure 3. 9 SEM images of sPP nanofibers fabricated from the solution with different solvents: (a) cyclohexane, (b) methyl-cyclohexane, (c) ethyl-cyclohexane, and (d) decalin.

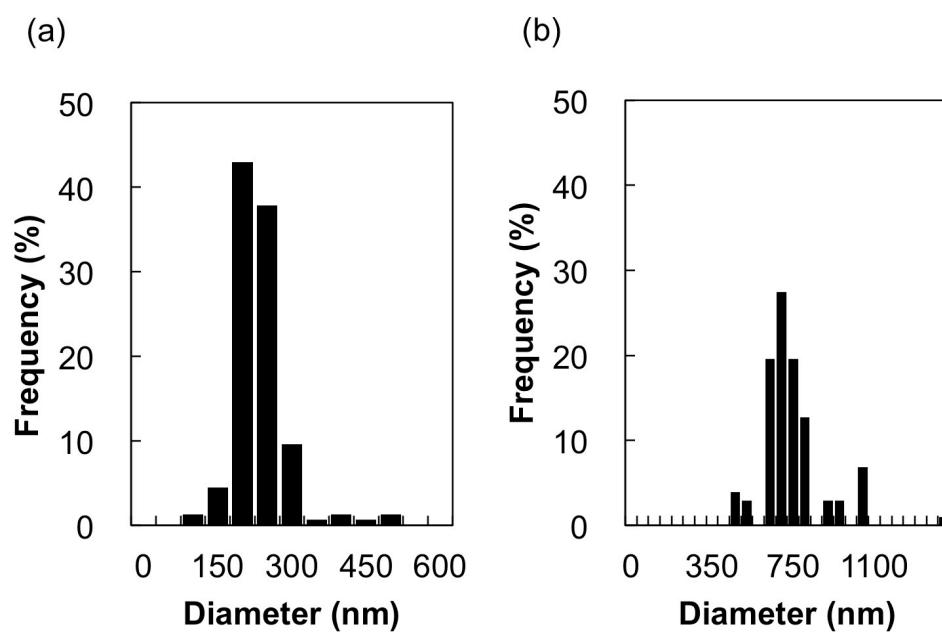


Figure 3. 10 Frequency distributions of the diameter of sPP nanofibers fabricated from the solution with (a) methyl-cyclohexane and (b) cyclohexane.

To summarize the tendency observed in morphological analysis, it was revealed that a slight difference in the chemical structures of solvents could strongly affect the morphology of the resulting electrospun nanofibers. All solvents used in this study were classified as alicyclic hydrocarbons with resembling cyclic chemical structures. For instance, the structural difference among cyclohexane, methyl-cyclohexane, ethyl-cyclohexane, propyl-cyclohexane, and butyl-cyclohexane, can only be seen in their chemical structures without or with a different length of alkyl group as their side chains. Nevertheless, the obtained nanofibers from the solution with these solvents were morphologically quite different. Hence, the selection of solvents was highly significant for the fabrication of thinner nanofibers by electrospinning.

3.3.3. Physical properties of solvents: electric property and volatility

In order to evaluate the effects of physical properties of solvents with slight different structures on the fiber morphology, the conductivity, the dielectric constant, and the evaporation rate of the solvents were measured.

Table 3. 3 Conductivities and dielectric constants of solvents.

Name	Boiling point* (°C)	Conductivity (pS)	Dielectric constant (-)
Cyclohexane	81	6.62	2.04
Methyl-cyclohexane	100	5.20	2.04
Ethyl-cyclohexane	132	10.4	2.04
Propyl-cyclohexane	157	12.2	2.05
Butyl-cyclohexane	180	11.8	2.06
Decalin	cis- 185	5.77	2.19
	trans- 193		

* the data from SDS data sheet provided by the manufacturer

Conductivities and dielectric constants of solvents were summarized in Table 3.3. The conductivities of cyclohexane, methyl-cyclohexane, ethyl-cyclohexane, propyl-cyclohexane, butyl-cyclohexane, and decalin were found to be fairly close to each other at 6.62 pS/cm, 5.20 pS/cm, 10.4 pS/cm, 12.2 pS/cm, 11.8 pS/cm, and 5.77 pS/cm, respectively. The dielectric constants of cyclohexane, methyl-cyclohexane, ethyl-cyclohexane, propyl-cyclohexane, butyl-cyclohexane, and decalin were also very close at 2.04, 2.04, 2.04, 2.05, 2.06, and 2.19, respectively. Considering the trial using the salts such as Bu_4NClO_4 ⁶³ and tetra-n-butyl ammonium perchlorate⁶⁷ or the high-permittivity solvent like DMF⁶⁵⁻⁶⁶ in the previous studies, it could be mentioned that in terms of the electric properties there was not much difference between the solvents. Therefore, it was also concluded that the electric properties could hardly affect the morphology of the fibers in our experiments.

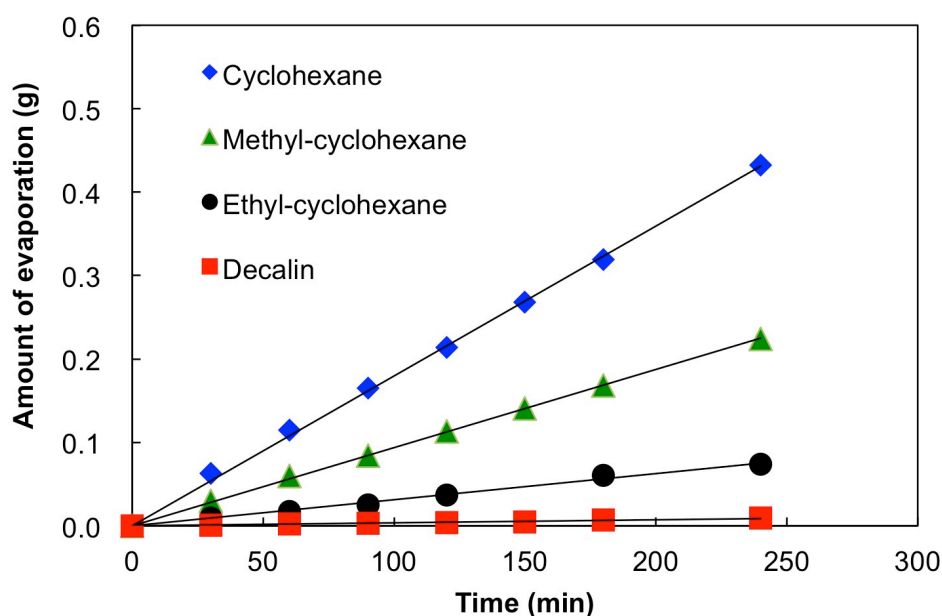


Figure 3. 11 Evaporation loss against time using different solvents: cyclohexane, methyl-cyclohexane, ethyl-cyclohexane, and decalin.

Figure 3.11 shows the evaporation loss of the solvents against time. The evaporation rates of cyclohexane, methyl-cyclohexane, ethyl-cyclohexane, and decalin were calculated as 1.80 mg/min, 0.94 mg/min, 0.30 mg/min, and 0.04 mg/min, respectively. The decrease in evaporation rates was in good agreement with the increase in boiling point (Table 3.3).

According to the morphological analysis of obtained sPP nanofibers, the thinnest nanofibers were obtained from the solution with methyl-cyclohexane, the medium-volatility solvent. Generally for the non-crystalline polymers, it is reported that thinner nanofibers could be obtained from the solvent possessing low volatility.⁷⁶ This is because the elongation by electrostatic force can be sufficiently applied to fiber-like polymer solution before the solidification by the solvent evaporation. Considering the results on evaporation rates, the thinnest fibers should be obtained from the lower-volatility solvent such as butyl-cyclohexane with longer alkyl group and decalin. However, fibers were not obtained from the solution with butyl-cyclohexane and decalin. Therefore, it can be considered that the solvent with too low volatility is not suitable for electrospinning because a sufficient solidification to become solid fibers cannot be achieved before getting to the metal collector.

Especially the solvent for semi-crystalline polymers possesses high boiling point, in other words, too low volatility as compared to the solvents for non-crystalline polymer. This is because in the solution preparation of crystalline polymers, it is required to heat around the temperature equal to the melting point of crystalline polymers. For example, *o*-DCB with boiling point of 180.5°C and decalin with boiling point of ~190°C are frequently used for the preparation. However, for non-crystalline polymer, the heating process is not generally required for the solution preparation. For example, tetrahydrofuran (THF) with boiling point of 66°C and chloroform with boiling

point of 61.2°C are frequently used. Therefore, it could be mentioned that the quantitative evaluation of evaporation is important for selecting solvents used for electrospinning.

To summarize the evaluation of physical properties, in electrospinning for crystalline polymer, it was revealed that the enhancement of electrical properties is not necessarily required and that the proper volatility is required in the selection of solvents. Of course the enhancement of electrical properties by adding salts is an effective way to fabricate thinner nanofibers, however, adding high-permittivity solvents like DMF sometimes make the solution heterogeneous leading to the thicker and non-uniform fiber formation. As for the volatility, since the solvents used for the solution preparation of crystalline polymer possess the lower volatility than the solvent used for the preparation of non-crystalline polymer solution, the solvents with proper degree of evaporation should be chosen.

3.3.4. Rheological aspects of sPP solutions

The viscous behavior depends on the solution concentration and the type of solvent. As discussed before, as the concentration increased, the solutions of crystalline polymer tend to form gel. When the types of solvent were changed for the solution preparation, the gelation speed was totally different. Other than the gelation phenomena, the viscosity of liquid-state polymer solution can be controlled finely by changing the solution concentration and the type of solvent, and is known as an important key parameter for electrospinning. Therefore, the viscosity of liquid-state sPP solutions was evaluated and the combinational effects sPP and solvents on the morphology of sPP nanofibers were examined.

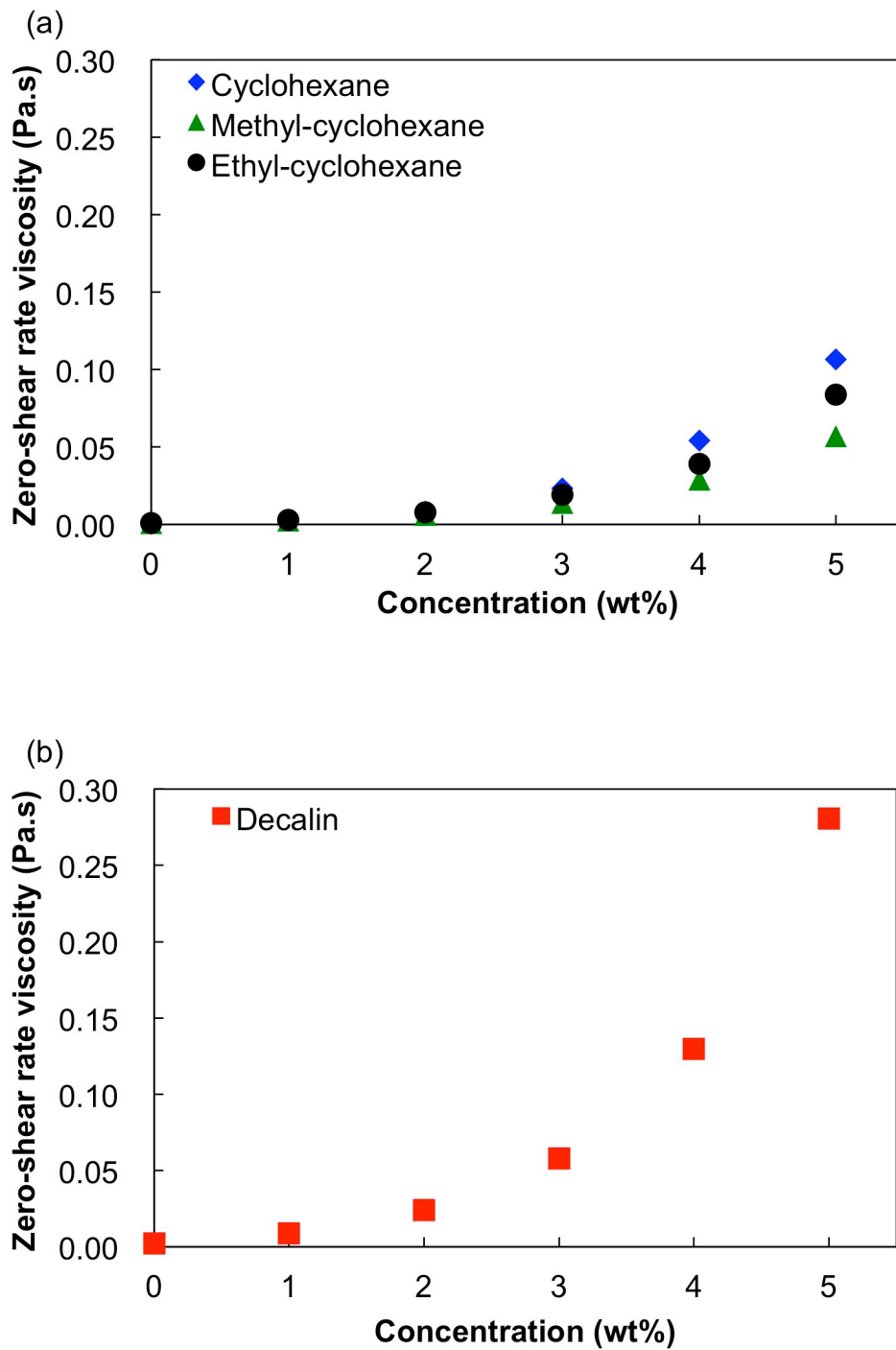


Figure 3. 12 Zero-shear viscosity as a function of concentration by different solvents: (a) cyclohexane with alkyl chains and (b) decalin.

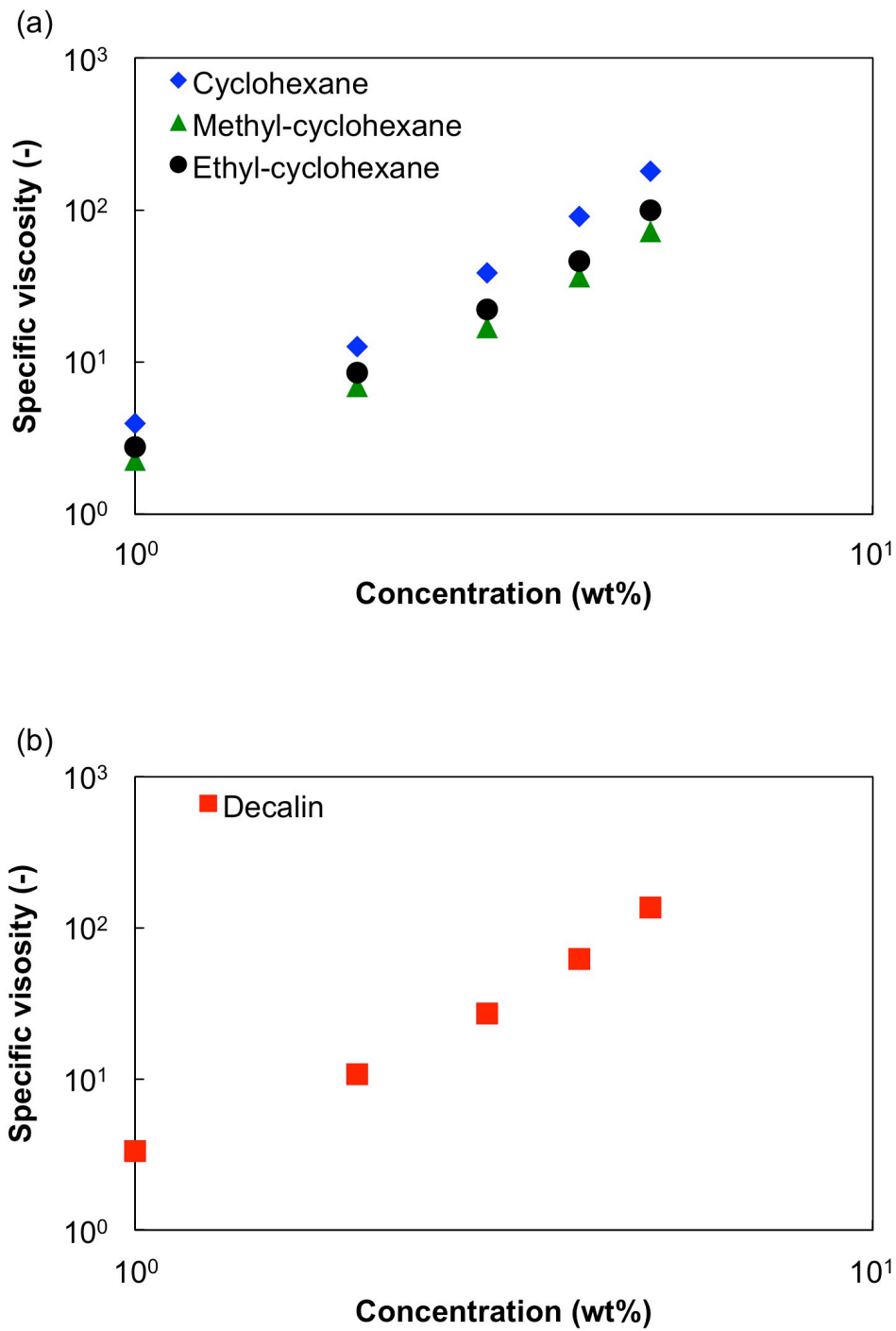


Figure 3. 13 Specific viscosity as a function of concentration by different solvents: (a) cyclohexane with alkyl chains and (b) decalin.

Figure 3.12 shows the zero-shear rate viscosity (η_0) as a function of concentration. η_0 gradually increased as the concentration increased from 1wt% to 5wt%. It was found that as for η_0 , the sPP/decalin solution showed the highest η_0 . It was also found that η_0 of sPP solution with methyl-cyclohexane was lowest and that η_0 of sPP solution didn't depend on the length of alkyl chain attached to cyclohexane.

Figure 3.13 shows the specific viscosity (η_{sp}) as a function of concentration. η_{sp} of sPP solution with cyclohexane was the highest, η_{sp} of sPP solution with methyl-cyclohexane was the lowest, and η_{sp} of sPP solution with ethyl-cyclohexane was middle at every concentration. It was also found that η_{sp} of sPP solution with decalin was lower than that of sPP solution with cyclohexane, while η_0 of sPP solution with decalin was the highest. This could be due to the high viscosity of decalin by itself.

According to the morphological analysis of obtained sPP nanofibers, the thinnest nanofibers were obtained from the sPP/methyl-cyclohexane solution with the lowest η_{sp} . According to the previous studies on intrinsic viscosity for the nanofiber fabrication of non-crystalline polymers²⁵, the sPP/cyclohexane solution with highest viscosity should be the best for the thinnest fiber fabrication. However, sPP nanofibers prepared from the sPP/cyclohexane solution were thicker than the nanofibers prepared from the sPP/methyl-cyclohexane solution. Therefore, it was indicated that the knowledge on intrinsic viscosity could not be applied to our experiments.

To discuss the deviation from the other preceding results, the molecular entanglements are taken into consideration. In fact, it is known that the molecular entanglements took an important role in constructing fibers. Colby *et al.* defined the entanglement concentration C_e at the slope change of η_{sp} .⁷⁷ C_e was also the exact boundary between the semidilute-unentangled and semidilute-entangled regimes. At the concentration of C_e , a significant overlap of polymer chains began to constrain the

molecular chain motion. Considering the fiber formation process during electrospinning from the viewpoint of C_e , no morphology or just beads should be observed when the solution concentration was below C_e i.e. without entanglements. As the concentration increased and became $\sim C_e$, beads or beaded-nanofibers could be obtained. Here, the slightly entangled-polymer jet could not still withstand the excessive force of electrostatic field. Therefore, the jet often tends to break up into droplets or become non-uniform. As the concentration further increased and became kC_e , uniform and defect-free fibers could generally be obtained. The constant k was ~ 2 according to the paper by McKee *et al.*⁷³ Above the concentration of kC_e , the fiber diameter simply became larger due to the abundant entanglements. Thus the favorable concentration for the fabrication of the thinnest fibers may be obtained at $k_f C_e$ (where k_f is constant and $1 < k_f < k$), which is between C_e and kC_e for electrospinning.

According to the morphological analysis as a function of concentration, the favorable concentration of $k_f C_e$ was found to be almost constant at 2–3wt% for each solution in our sPP solution. This was also supported by the theoretical estimation discussed before. Furthermore, it could also be considered that the entanglement concentration kC_e was substantially similar to each other among different solvents because C_e depends on the chemical structure and the molecular weight of polymers.

Considering the η_{sp} of the solution with different solvents at the same $k_f C_e$ in Figure 3.13, the η_{sp} of sPP/methyl-cyclohexane solution was the lowest throughout the whole range of concentrations. In fact, the thinnest sPP nanofibers were fabricated from the sPP/methyl-cyclohexane solution. Therefore, the solution with the lowest viscosity would be the prospective candidate for the fabrication of thinnest nanofibers. This is since the higher mobility of molecules with the same number of entanglements could produce higher extension of polymers for the synthesis of thinner fibers.

3.3.5. Conditions for fabricating thinner sPP nanofibers

The sPP/decalin solution with relatively faster gelation speed, highest viscosity, and lowest volatility did not produce thinner sPP fibers as was presented above. In fact, it was unsuccessful to fabricate sPP nanofibers from the sPP/decalin solution by electrospinning. It was found that the gelation speed of sPP/decalin solution was substantially higher than those of the solution with cyclohexane and cyclohexane with shorter alkyl chain such as methyl-cyclohexane and ethyl-cyclohexane. Among the solvents used in this study, decalin possessed the highest viscosity and relatively lower evaporation rate. This should normally be a good condition to fabricate fine fibers.

Considering the process using the crystalline polymer solution, the evaporation of the solvent directly led to a higher solution concentration, which raised the viscosity and hence caused the gelation of the solution. The gelation eventually hindered the extension of polymers caused by the loss of mobility of the molecules due to the solidification of the electrospun solution during electrospinning. However, the solvent with too low volatility is not suitable for electrospinning because the solidification become insufficient before getting to the metal collector. Therefore, it is expected that by balancing the evaporation rate and the gelation speed and by lowering η_{sp} , the thinner sPP nanofibers could be effectively produced for our sPP solution as shown in Figure 3.14.

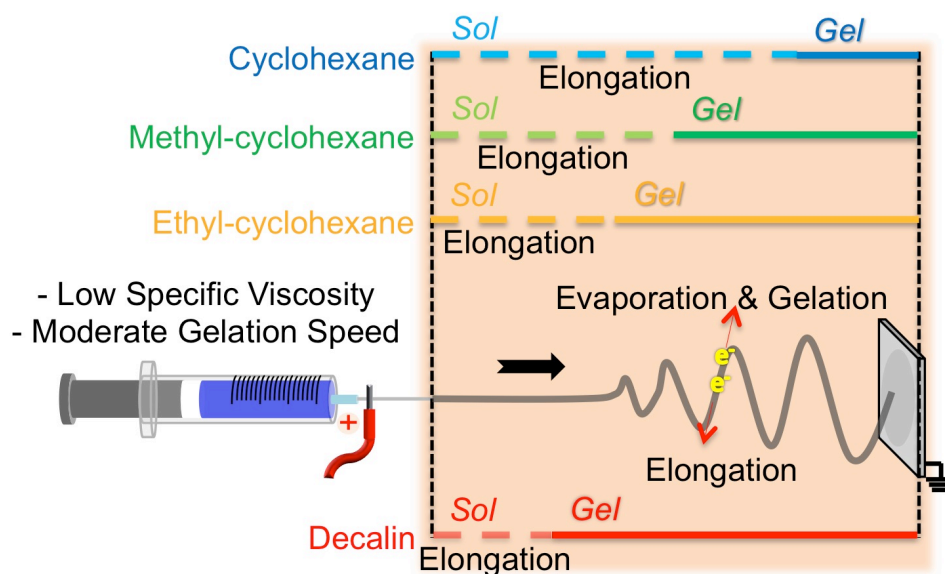


Figure 3. 14 Schematic images of evaporation, gelation, and elongation of crystalline polymer solution during electrospinning.

3.4. Summary of this chapter

Fabrication of sPP nanofibers by solution electrospinning using single solvent at room temperature (25°C) was examined. sPP nanofibers with the average diameter of 230 nm were successfully fabricated by using methyl-cyclohexane for the solvent. The obtained diameter was significantly thinner than the minimum diameter of 350 nm of polypropylene fibers reported previously. Just by selecting lower volatility and higher viscosity, as was suggested by non-crystalline polymer experiments, thinner semi-crystalline sPP fibers could not be synthesized, which was highly due to the gelation caused by the crystallinity of sPP. For the fabrication of nanofibers of semi-crystalline polymers, it is crucial to consider the entanglement of the molecules and hence to choose the moderate gelation speed and the lower specific viscosity of the semi-crystalline solution at $\sim k_f C_e$.

Chapter 4. MPC random-copolymer electrospun nanofibers

4.1. Background on MPC

Phospholipid polymers showing the excellent biocompatibility are attractive materials in a biomedical field. Phospholipid is a major component of cell membrane in our body. Due to the nature of phospholipid, polymers with phospholipid group show excellent biocompatibility as compared to other polymers.

As a representative of phospholipid polymer, 2-methacryloyloxyethyl phosphorylcholine (MPC) has been actively studied over the last two decades. As a pioneer, Nakai *et al.* synthesized polymerizable chemicals with phospholipid group in 1977.⁷⁸ Following the achievement, Kadoma *et al.* synthesized 2-methacryloyloxyethyl phosphorylcholine, a methacrylate with phosphorylcholine group in 1978.⁷⁹ Furthermore, Ishihara *et al.* improved the preparation method of MPC in 1990.⁸⁰

The copolymerization ability of MPC was also evaluated and various kinds of MPC-based copolymers were developed. Kadoma *et al.* evaluated the copolymerization ability of MPC with methyl methacrylate and eventually synthesized poly (MPC-*co*-MMA).⁷⁹ Ishihara *et al.* copolymerized MPC with n-butyl methacrylate and obtained poly (MPC-*co*-BMA).⁸⁰ Ueda *et al.* copolymerized MPC with various alkyl methacrylates: methacrylates with n-butyl, tert-butyl, n-hexyl, n-dodecyl, and n-stearyl groups, respectively.⁸¹ Kojima *et al.* copolymerized MPC with styrene.⁸² For these copolymers, the blood compatibility was also investigated.⁸¹⁻⁸³

Among these MPC copolymers, poly (MPC-*co*-BMA) was found to show the excellent blood compatibility and non-thrombogenicity and became commercially available. Ishihara *et al.* reported that as the mole fraction of MPC increased up to ~0.3 in poly (MPC-*co*-BMA), the activation of platelets and the fibrin formation were

completely suppressed.⁸⁴ Ishihara *et al.* also evaluated the protein adsorption from human plasma to the surface of material and found that the protein adsorption was suppressed by increasing the MPC fraction in poly (MPC-*co*-BMA).⁸⁵ Furthermore, Ishihara *et al.* evaluated the hemocompatibility using human whole blood. In the study, it was found that as the MPC fraction increased in poly (MPC-*co*-BMA), the amount of proteins adsorbed to the surface decreased, while the amount of phospholipids increased.⁸⁶ According to the previous studies introduced above, MPC copolymer was revealed to possess the excellent hemocompatibility and non-thrombogenicity and became a commercially available phospholipid polymer. Now, MPC copolymers named as LIPIDURE are sold by NOI Co.

In this work, we focused on the nanofiber fabrication of poly (MPC-*co*-BMA) with excellent hemocompatibility. This copolymer is one of the most frequently studied phospholipid polymers and also commercially available. The fabrication of MPC nanofibers by electrospinning has not been reported yet. Therefore, the fabrication procedures of MPC fibers were thoroughly investigated in this research. Additionally, the capability of MPC nanofibers as a drug delivery system was examined. In detail, the capability of controlling the drug-release rate by varying the diameter of MPC fibers was explored. For this test, curcumin, known as an antithrombogenic, antioxidant, and antiproliferating agent, was used as a model drug.

4.2. Experimental

4.2.1. Materials

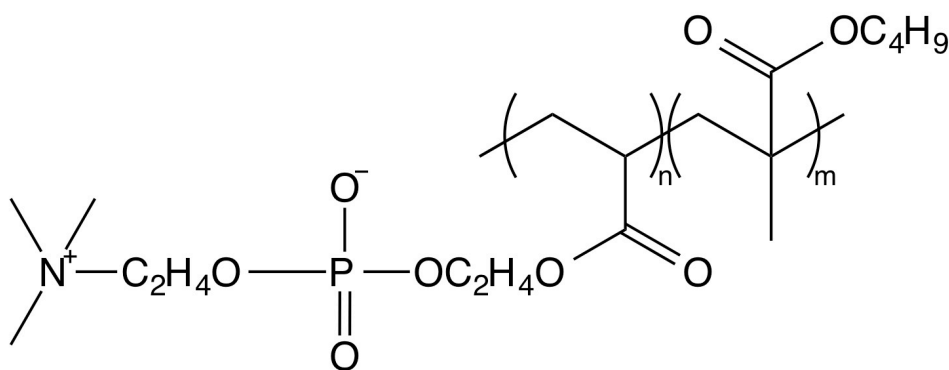


Figure 4. 1 Chemical structure of poly (MPC-*co*-BMA).

Poly (MPC-*co*-BMA) copolymer was supplied from Terumo Clinical Supply Co., Ltd. The chemical structure of MPC copolymer was presented in Figure 4.1. The average molecular weight was 500,000 g/mol and the block ratio of MPC/BMA in MPC copolymer was 3/7 (w/w). Curcumin was selected as an eluted drug and purchased from Sigma-Aldrich Co., Ltd. Ethanol was used as a solvent for MPC copolymer and curcumin and purchased from Wako Pure Chemical Industries, Ltd.

4.2.2. Preparation of the MPC Solution

The solutions of MPC copolymer were prepared by dissolving the copolymer into ethanol at room temperature (25°C). Then, curcumin was added to the poly (MPC-*co*-BMA)/ethanol solution. The mixture was stirred for 24 h at room temperature to ensure a complete dissolution of MPC copolymer and curcumin. The concentration of MPC copolymer in the solution was set at 1, 2, 3, 5, 7.5, and 10wt%. The mass ratio

of curcumin to MPC copolymer was also fixed at 0.04wt%. The composition of the solution was summarized in Table 4.1.

Table 4. 1 Compositions of MPC solutions with curcumin.

Solution	Ethanol	MPC	Curcumin
1.0wt% for fiber	99.0	1.0	0.04
2.0wt% for fiber	98.0	2.0	0.08
3.0wt% for fiber	97.0	3.0	0.12
4.0wt% for fiber	96.0	4.0	0.16
5.0wt% for fiber	95.0	5.0	0.20
7.5wt% for fiber	92.5	7.5	0.30
10wt% for fiber	90.0	10	0.40
5.0wt% for film	95.0	5.0	0.20

4.2.3. MPC nanofiber fabrication by electrospinning

After the preparation of homogeneous composite solution, MPC nanofibers were fabricated by solution electrospinning. The setup of electrospinning was same as the one used in other chapter. A high voltage of 12.5 kV was applied between the syringe needle (i.e., the polymer solution) and aluminum collector grounded on the earth. The voltage was found to be the minimum voltage required to fabricate fibers stably. The collector was horizontally separated from the needle and the needle-collector distance was set at 10 cm. The flow rate of MPC solution through the syringe needle was set at 0.5 mL/h. The electrospun MPC fibers were dried in a vacuum oven (VOS-201SD, EYELA Co., Ltd.) at 25°C for 24 h to remove the residual solvent.

4.2.4. Morphological analysis of MPC fibers

The morphology of MPC fibers was observed by scanning electron microscopy (SEM) (S-2380N, Hitachi Co., Ltd.). Before SEM observation, according to the general procedure of preventing electrostatic charges against the polymers, MPC

fiber-sheets cut into a sheet of 20-mm square were coated with osmium for 15 s using an ion osmium coater (HPC-1 SW, Vacuum Device, Inc.). The thickness of osmium was approximately 5 nm. After the pretreatment by osmium, SEM observation was carried out at an accelerating voltage of 5 kV. The diameters of MPC fibers were calculated by the free image processing software called Image J (ver. 1.47).

4.2.5. Rheological analysis of MPC solutions

The zero-shear viscosity (η_0) was obtained by a strain-controlled rheometer (ARES-G2, TA Instruments) in the cone-plate geometry (50.0 mm in diameter and 0.0192 rad in its cone angle). All viscosity data were measured at 25°C. The shear rate was changed from 0.1 to 100 s⁻¹. To evaluate the physical properties of the solution, the specific viscosity (η_{sp}) of the sPP solutions in each solvent was calculated by estimating the zero-shear rate viscosity, analyzed by measured experimental viscosity data. η_{sp} was calculated using the zero-shear rate viscosity (η_0) defined as follows:

$$\eta_{sp} = (\eta_0 - \eta_s) / \eta_s \quad (4-1)$$

where η_s is the solvent viscosity. η_{sp} represents the rate of increase in solvent viscosity by mixing polymeric solute.

4.2.6. *In vitro* drug-release test

MPC fiber-sheets with different diameters were soaked in phosphate buffered saline (PBS) medium (pH=7.4) of 2 mL at 37°C. The PBS medium was removed and collected every 24 h to measure the concentration of the released-drug from MPC fibers into PBS medium. After removing the PBS medium for the concentration experiments, new fresh PBS medium was added in order to examine the drug-release continuously. The drug-release/elution time was defined as the immersion time of the samples in PBS

medium. The 0 days of drug-release/elution time was the time when we started the drug-release testing.

The concentration of released drug i.e. curcumin in PBS medium was measured by ultraviolet-visible spectroscopy (UV-vis) (U-2810, Hitachi, Co., Ltd.). The wavelength used for the test ranged from 400 to 500 nm. The concentration of released drug i.e. curcumin was calculated with the Lambert-Beer equation as follows:

$$A = \epsilon cl \quad (4-2)$$

where A is the absorbance, ϵ is the molar absorbance coefficient, c is the concentration, and l is the length of the light path. The concentration of released drug was eventually converted to the weight of released drug. In our experiments, ϵ was found to be 49.1×10^4 (L/mol cm) from the analysis of the UV absorbance of curcumin/PBS solution with different concentrations of curcumin. l was 1 cm from the size of cell containing the solution during the test. The results were plotted as cumulative micrograms of released drug as a function of the drug releasing/elution time.

As a reference for comparison, a solvent-cast MPC film with curcumin was also prepared. The procedure of the preparation is as follows: MPC copolymers were dissolved in ethanol at 5wt%. Then, curcumin was added to the MPC solution at 4wt% against the mass of MPC copolymer. The solution was coated onto an aluminum plate and dried slowly in air to evaporate the solvent. Finally, the dried substrates were kept in vacuum oven for more than 24 h to remove any residual solvent completely.

4.3. Results and Discussion

4.3.1. Morphologies of electrospun MPC fibers

Since the morphology of electrospun fibers is mainly influenced by the solution properties strongly dependent on the polymer concentration, the MPC concentration was varied from 1 to 10wt%, whereas the process parameters were fixed. Before the electrospinning, it was confirmed that the MPC copolymer/ethanol solution with different MPC concentration was in sol-state.

Figure 4.2 shows the SEM images of MPC fibers with curcumin fabricated by electrospinning. As shown in Figure 4.2 (a), (b), and (c), beads or beaded-fibers were obtained from the solution at the concentration lower than 5wt%. With the increase in the concentration, the thinnest and uniform nanofibers were obtained at the concentration of 5wt% (Figure 4.2 (d)). As the concentration further increased, the fiber diameter gradually increased as shown in Figure 4.2 (e) and at the concentration of 10wt% ribbon-like fibers were obtained (Figure 4.2 (f)). As a result, different diameters of MPC fibers could be obtained from the solution at different MPC concentrations. In detail, the average diameter of MPC fibers from the 5wt% MPC solution was 164 ± 73 nm, from the 7.5wt% MPC solution was 637 ± 198 nm, and from the 10wt% MPC solution was 1265 ± 451 nm. This trend is in good agreement with the knowledge that the increase in viscosity from the increased concentration resulted in the increase in the fiber diameter. It is also estimated that the ribbon-like fibers were attributed to the difference in solidification speed inside and outside of the fibers caused by the increase in diameter. Koombhongs *et al.* reported that the jet with a solid skin was deformed by mutual electric forces between the segments of jet and ribbon-like fibers were eventually obtained.⁸⁷

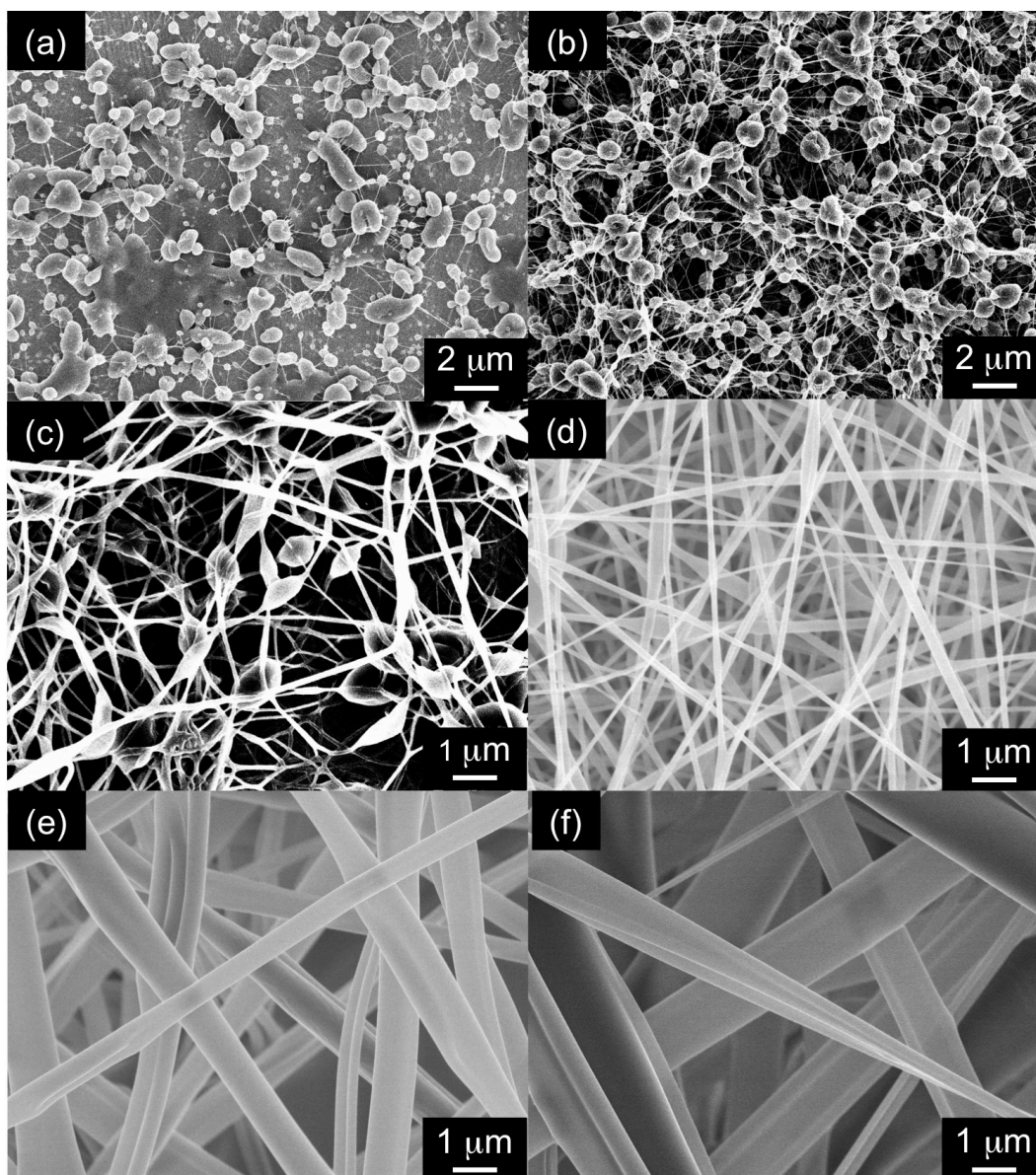


Figure 4. 2 SEM images of MPC fibers from the solutions with different concentrations: (a) 1wt%, (b) 2wt%, (c) 3wt%, (d) 5wt%, (e) 7.5wt%, and (f) 10wt%.

From the morphological change from beads to beaded fibers, it was also found that the entanglement concentration c_e was around 1wt% and 2wt%. According to the fact that the uniform MPC nanofibers were obtained from 5wt% (equal to $2c_e$) solution in this study, the determined c_e was confirmed to be reasonable. It was reported by McKee *et al.* that c_e was the minimum concentration required for the formation of beaded fibers, while $2c_e$ was the minimum concentration required for the formation of uniform fibers.⁷³ In order to determine c_e by the quantitative approach, rheological analysis was carried out as described in the following section.

4.3.2. Rheological analysis of MPC solutions

Figure 4.3 shows the zero-shear rate viscosity (η_0) of MPC/ethanol solution as a function of MPC concentration. As the concentration increased from 1 to 10wt%, η_0 gradually increased. It was also found that the viscosity of MPC/ethanol solution didn't depend on the shear rate. In other words, the MPC/ethanol solution behaved as Newtonian solution. Therefore, the MPC solution was confirmed to be in sol state.

Figure 4.4 shows the specific viscosity (η_{sp}) calculated from η_0 . From the slope change of η_{sp} , c_e was estimated to be 2.5wt%. This is close to c_e determined from the morphological analysis of the obtained MPC fibers. Therefore, it could be concluded that the knowledge from the fiber fabrication of amorphous polymers in the previous reports could be applied to the fiber fabrication of random copolymers.

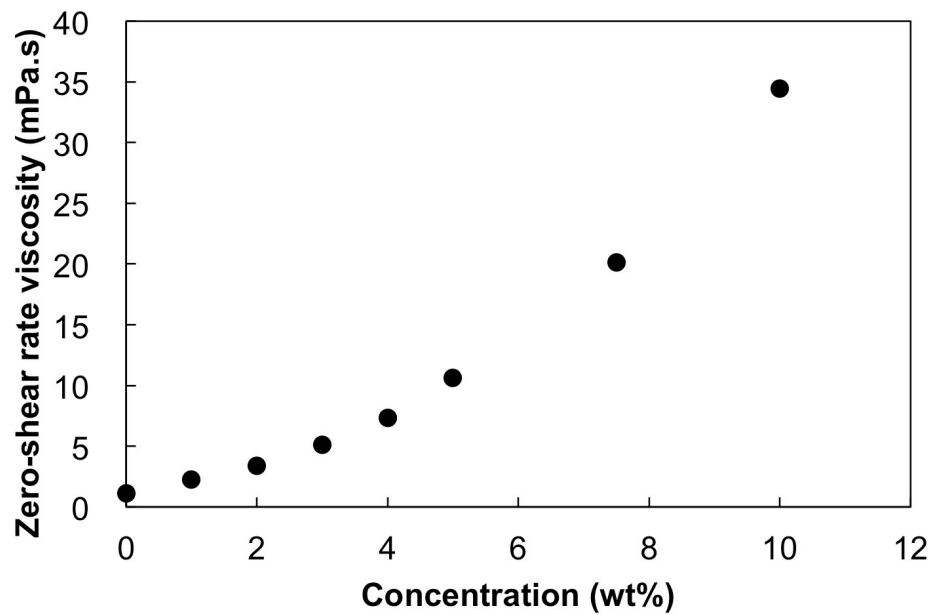


Figure 4. 3 Zero-shear rate viscosity of MPC solutions with different concentrations.

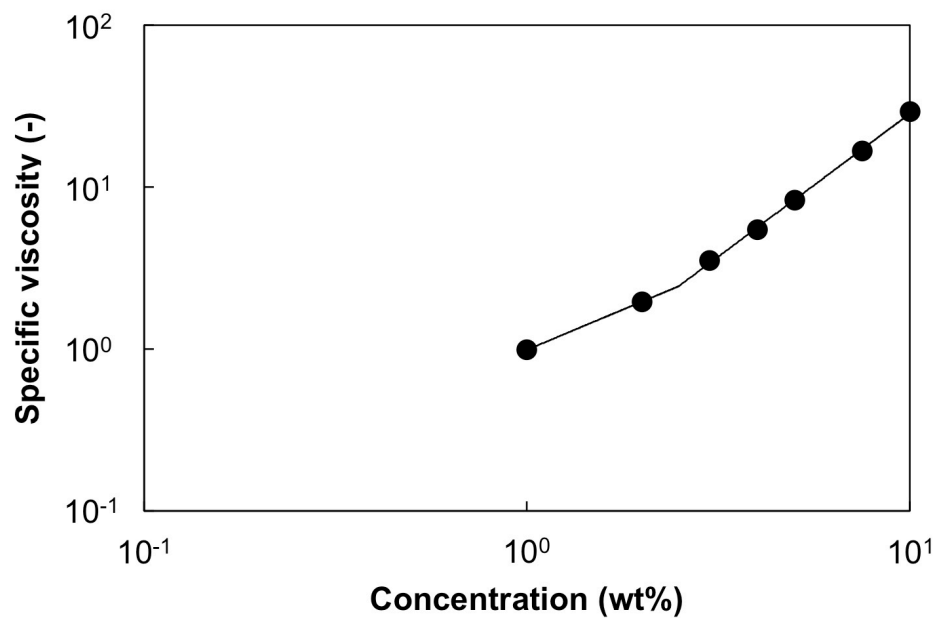


Figure 4. 4 Specific viscosity of MPC solutions with different concentrations.

According to the theoretical calculation, the entanglement concentration can be also estimated by the equation $c_e = 2M_e/M_w$. Here, since the entangled molecular weight M_e for MPC copolymer is not experimentally determined, M_e for poly (butyl methacrylate) (PBMA) calculated at $\sim 10,800$ g/mol was alternatively used.⁸⁸ Therefore, the c_e for MPC copolymer with 70% PBMA in the molecular chain was roughly estimated at ~ 5.7 wt%. This theoretically estimated concentration wasn't close to the concentration estimated from the morphology. This difference could attribute to the MPC units in the MPC copolymer.

Considering the solubility parameter, the effect of MPC units in the copolymer could be revealed. According to the report by Hansen *et al.*, the solubility parameter of ethanol is $26.5 \text{ MPa}^{1/2}$. On the other hand, the solubility parameter of poly (butyl methacrylate) was calculated to be $20.0 \text{ MPa}^{1/2}$. In order to dissolve MPC copolymers into ethanol, the solubility parameter of MPC should be from ~ 35.0 to $\sim 48.3 \text{ MPa}^{1/2}$. These values are reasonable because MPC is soluble to water with the solubility parameter of $48.0 \text{ MPa}^{1/2}$. Therefore, it can be concluded that the MPC copolymer was composed of two units with significantly different solubility parameters and this led to the disagreement between the experimental and theoretical estimation of c_e .

4.3.3. Function evaluation as a drug delivery system

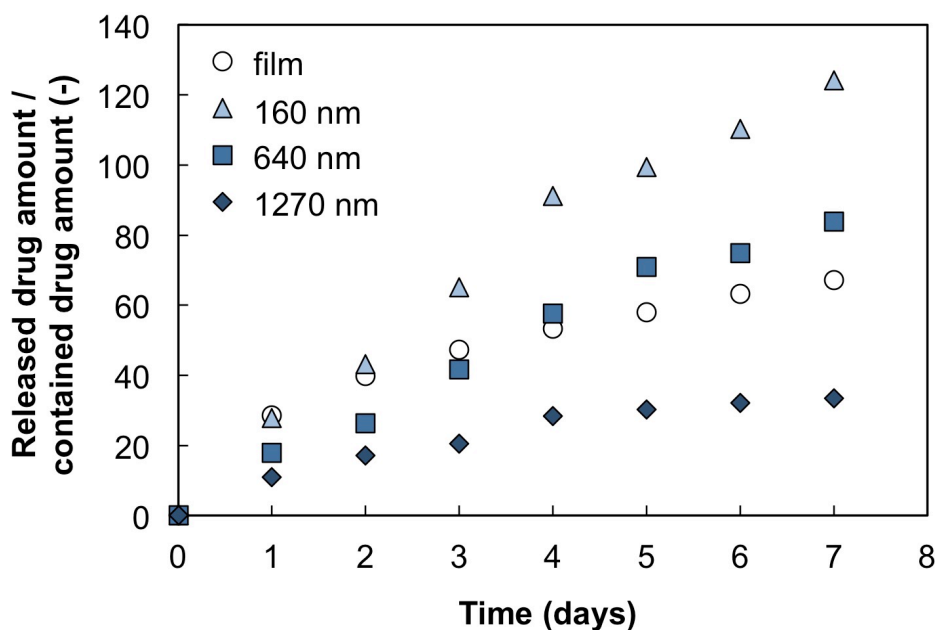


Figure 4. 5 Cumulative released amount of curcumin from MPC fibers and film.

Figure 4.5 shows the cumulative released amount of curcumin from the MPC fibers to PBS medium as a function of time. The triangles, crosses, and squares in the graph represent the drug-release behaviors of the MPC fibers with the diameter of ~160, ~640, and ~1270 nm (i.e. the MPC fibers electrospun from 5, 7.5, and 10wt% MPC solutions), respectively. The drug-release behavior of the MPC film as a control is shown using the circles in Figure 4.5. The released amount per the contained amount became larger with the decrease in the diameter of fibers. The drug-release rate was also well controlled by the decrease in the diameter of the MPC nanofibers. In detail, the MPC nanofibers with diameters of ~160 and ~640 nm possessed the enhanced drug-release features without an initial burst release observed in the MPC film in the early stage of the drug-release/elution time. On the other hand, the MPC microfibers with the diameter of ~1270 nm also did not present such an initial burst release

observed in the MPC film. However, the released amount was less than that of the film in the experimental time frame.

This tendency could be due to the increase of the surface area caused by the reduction of the fiber diameter according to the Higuchi model. Higuchi *et al.* reported the mathematical equation describing the release rate of drugs from matrix systems.⁸⁹ The Higuchi model is widely used to describe the drug-release phenomenon and the basic equation is as follows:

$$M_t = A\sqrt{D(2c_0 - c_s)c_s t} \quad (4-3)$$

where M_t is the cumulative absolute amount of released drug at time t , A is the surface area of drug-release device exposed to the medium, D is the diffusivity of drug in the polymer, c_0 is the initial concentration of drug, and c_s is the soluble concentration of drug into polymer, respectively. For this equation, c_0 should be larger than c_s .

In this study, D was determined from the result of released amount for film by curve fitting and c_0 was experimentally kept at constant. Therefore, D , c_0 , and c_s in the equation (4-3) were constant because the samples were all composed of MPC copolymer and curcumin. Eventually, the equation could be simplified as follows:

$$M_t = KA\sqrt{t} \quad (4-4)$$

where K is constant. In other words, the surface area directly affects the cumulative amount of released drug. In order to confirm this, the surface area of each sample was examined.

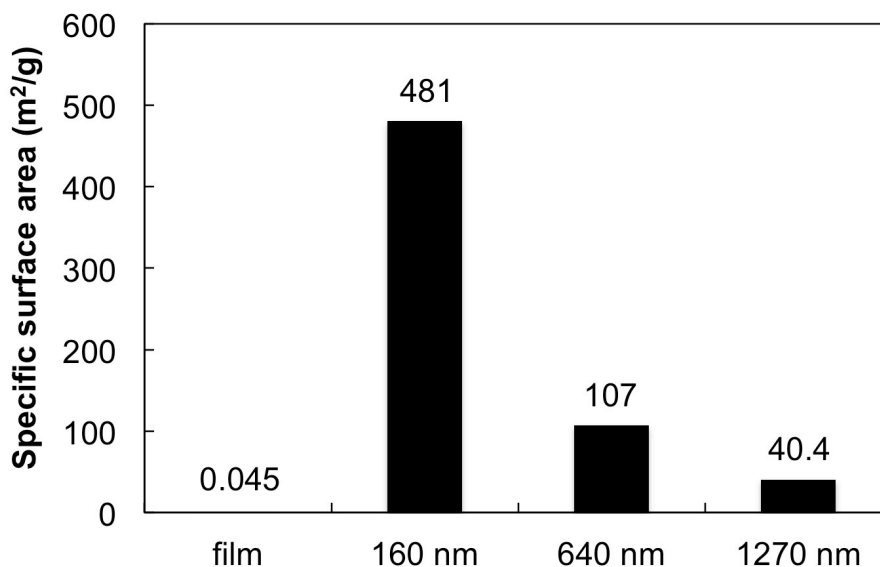


Figure 4. 6 Specific surface areas of MPC fibers and film.

Figure 4.6 shows the surface area calculated mathematically from the configuration of the samples. In detail, for simplification, the obtained fiber was considered to be cylinder. For example, the area of the fibers was calculated from the diameter of the fibers and the area of the film was calculated from the surface contacting the medium. The MPC nanofibers with the diameter of ~160 nm showed the highest surface area, and the surface area gradually decreased as the diameter of the MPC fibers increased. As was expected, the film showed the lowest surface area. Therefore, it can be concluded that the drug-release rate from MPC could be controlled by changing the surface area of the MPC fibers according to the diameter of the MPC fibers.

4.4. Summary of this chapter

MPC nanofibers and microfibers were successfully produced by electrospinning and their drug-release characteristics were investigated. According to the morphological analysis of electrospun MPC fibers by SEM, it was found that the increase in MPC concentration brought about an increase in the diameter of the MPC fibers. As for the functionalities as drug-delivery system, the drug-release rate from the electrospun MPC fibers was well controlled and enhanced by the decrease in the diameter of the MPC fibers. The preliminary experimental results may be highly applicable to next-generation vascular grafts that possess both biocompatibility and well-controlled drug-release characteristics to prevent thrombosis.

Chapter 5. Elastomeric block-copolymer electrospun nanofibers

5.1. Background on elastomeric block-copolymer nanofibers

Polystyrene-*b*-polyisoprene-*b*-polystyrene triblock copolymer (SIS) is a thermoplastic elastomer manufactured widely by industrial companies. Rubbers used for vehicle tires are generally cross-linked chemically by sulfur and behave as a thermoset. On the other hand, elastomers based on block copolymers are cross-linked physically by a glass-state region composed of a block of copolymers. As for SIS, polystyrene has its glass transition point at $\sim 110^{\circ}\text{C}$ and forms a glass-state region working as a cross-link point in SIS at ambient temperature.

SIS can also be in liquid state by dissolving SIS into organic solvents due to the nature of the cross-link point. When cross-linked rubbers are put into organic solvents, the rubbers just swell by the diffusion of solvents into the rubber and keep their shape by the existence of the chemical cross-link point. On the other hand, when elastomers such as SIS are put into organic solvents, especially good solvents for the cross-link region, the elastomers lose their shape and behave as liquid. This is because the physical cross-link points are deformed by increasing the chain mobility of polymers in the cross-link region due to the existence of good solvents.

Elastomeric block copolymers capable of dissolving into organic solvents and basically behave as a liquid-state solution enabled us to fabricate elastomeric nanofibers by solution electrospinning. In the previous study, as for SIS, Chuangchote *et al.* reported the fabrication of SIS microfibers with the average diameter from $4.2\ \mu\text{m}$ to $9.3\ \mu\text{m}$ using 1, 2-dichloroethane as a solvent. In their report, it was mentioned that the enlargement of electrospun fibers may be due to the strong molecular recoiling derived from the nature of thermoplastic elastomers.⁹⁰ Feng *et al.* also reported the fabrication

of submicron SIS fibers by electrospinning and evaluated the mechanical properties of SIS fibers. They fabricated SIS fibers using a pure solvent of tetrahydrofuran (THF) and a mixed solvent of THF and N, N-dimethylformamide (DMF). It was mentioned that the addition of DMF enhanced the spinnability during electrospinning and that the solution concentration from 8 to 15wt% was suitable for the fabrication of SIS fibers.⁹¹ Furthermore, Feng *et al.* reported the fabrication of SIS fibers with polystyrene (i.e. PS/SIS blend fibers) using THF/DMF mixed solvent (80/20, w/w). In their report, it was found that the increase of SIS in PS/SIS blend resulted in the formation of thicker and more non-uniform fiber.⁹²

Other than SIS, styrene-based elastomeric block copolymers were electrospun into nanofibers. As for polystyrene-*b*-polybutadiene-*b*-polystyrene triblock copolymer (SBS), Fong *et al.* reported the fabrication of SBS nanofibers with the diameter of ~100 nm using THF/DMF mixed solvent (75/25, w/w).⁹³ Feng *et al.* reported the fabrication of SBS fibers with polystyrene (i.e. PS/SBS blend fibers) using THF/DMF mixed solvent (80/20, w/w).⁹⁴ As for polystyrene-*b*-polyisobutylene-*b*-polystyrene (SIBS), Liu *et al.* reported the disability of SIBS to be modified into fibers by electrospinning due to the low conductivity of SIBS solutions. They also reported that the addition of single wall carbon nanotubes and iron (III) p-toluenesulfonate enabled us to enhance the conductivity of solutions leading to the fabrication of SIBS fibers. Lim *et al.* also reported the fabrication of SIBS nanofibers with the average diameter of 540 ± 60 nm using THF/toluene mixed solvent (95/5, w/w).⁹⁵ Although the fabrication of nanofibers with elastomeric block copolymer was reported in many papers, the viscoelastic study of block-copolymer solutions for electrospinning has not systematically been conducted.

In case that the solvent is block selective, tri-block copolymer solutions form

gels and the gelation could disable us to fabricate nanofibers by solution electrospinning. Dürschmidt *et al.* reported that tri-block copolymer of polystyrene-*b*-poly(ethylene/butylene)-*b*-polystyrene (SEBS) formed highly elastic gels around 10wt% in paraffin oil, a solvent incompatible for polystyrene (PS) endblock but compatible for poly(ethylene/butylene) (PEB) midblock. In the system, PS endblocks aggregated and micelles were formed, and PEB midblocks formed loops or bridges between micelles. Monge *et al.* also reported that tri-block copolymer of polystyrene-*b*-poly(2-ethylhexanyl acrylate)-*b*-polystyrene formed elastic gels around 20wt% in paraffin oil. In this case, poly(2-ethylhexanyl acrylate) was soluble and PS was insoluble in paraffin oil. These gels are highly elastic and not suitable for the solution used for electrospinning as repeatedly mentioned in the previous sections.

In this study, the sol-gel characteristics of SIS solution were controlled and the SIS solution with different viscoelastic features was used for electrospinning. In order to control the characteristics, toluene was mixed with DMF at various DMF/toluene ratios and the mixture was used as a solvent for the preparation of SIS solutions. By varying the DMF ratio in DMF/toluene mixed solvent, the effects of mixing solvents on the fabrication of fibers, the physical properties of solvents, and the rheological properties of SIS tri-block copolymer solution were systematically investigated.

5.2. Experimental

5.2.1. Materials

Polystyrene-*b*-polyisoprene-*b*-polystyrene tri-block copolymer (SIS) containing 22wt% styrene was purchased from Sigma-Aldrich Co. N, N-dimethylformamide (DMF) and toluene were purchased from Wako Pure Chemical Industries, Ltd.

5.2.2. Solution preparation

SIS was firstly dissolved into toluene, a solvent compatible for both polystyrene block and polyisoprene block. Then DMF, a solvent incompatible for polyisoprene block, was added to the SIS/toluene solution and stirred at 60°C overnight. Finally, the SIS solution with DMF/toluene mixed solvent was obtained. The ratio of DMF in the DMF/toluene mixed solvent was varied from 0 to 0.5. The SIS concentration in the solution was varied from 5 to 25wt%.

5.2.3. Evaluation of sol-gel characteristics

The gelation characteristics of solutions with tri-block copolymers largely depended on the concentration of the solution and the solubility of solvents.⁹⁶ To confirm the state of the solution, we performed gelation tests for SIS solutions by tube testing method. After the stirring in a glass tube at 60°C overnight in order to prepare a homogeneous solution, SIS solution was kept stationary under the controlled environment at 25°C. The tube was inclined and checked whether the solutions were sol-state or gel-state. We defined the solution as gel state when the flow of the solutions was not observed.

5.2.4. Fiber fabrication by electrospinning

SIS fibers were fabricated using an electrospinning apparatus (1639, Imoto Co.). The SIS solution with DMF/toluene mixed solvent was sealed into a syringe (1005LT, Hamilton) with a 21G needle whose inner diameter was 0.53 mm. The needle was connected to a high voltage supply and the positive voltage of 12.5 kV was applied to the polymer solution. The grounded metal collector was placed 10 cm off the needle tip. The flow rate of the solution was controlled by syringe pump at 0.40 mL/h.

5.2.5. Morphological observation of electrospun SIS nanofibers

SIS fibers fabricated by electrospinning were characterized by the field emission scanning electron microscopy (FE-SEM, S-4700, Hitachi High-technology Co.). Before SEM observation, all specimens were coated with osmium to prevent electrostatic charge. For each sample, the diameters of the fabricated fibers were measured at 100 different points on each SEM micrograph selected randomly for the calculation of the average diameter of the fibers.

5.2.6. Characterization of physical properties of mixed solvents

To evaluate characteristic features of the used solvents, the conductivity, the dielectric constant, and the evaporation rate of the solvents were individually measured. The conductivity of the solvent was measured using a non-aqueous conductivity meter (DT700, Dispersion Technology, Inc.) at room temperature (25°C). The dielectric constant of the solvent was also measured using a liquid permittivity meter (Model 871, Nihon Rufuto Co., Ltd.) at 25°C. Furthermore, the evaporation loss was measured by weighing the mass change of each solvent at 25°C. Each solvent was poured into a ϕ 36 mm glass tube and the tube was kept under the stable airflow.

5.2.7. Rheological analysis of SIS solutions

The zero-shear rate viscosity (η_0) data were obtained by a strain-controlled rheometer (ARES-G2, TA Instruments) in the cone-plate geometry (50.0 mm in diameter and 0.0192 rad in its cone angle). All viscosity data were measured at 25°C. The shear rate was changed from 0.1 to 100 s⁻¹. To evaluate the physical properties of solutions, the specific viscosity (η_{sp}) of SIS solutions in DMF/toluene mixed solvent was calculated by estimating the zero-shear rate viscosity from the measured experimental viscosity data. The equation for calculation using the zero-shear rate viscosity (η_0) was as follows:

$$\eta_{sp} = (\eta_0 - \eta_s) / \eta_s \quad (5-1)$$

where η_s is the solvent viscosity. η_{sp} represents the rate of increase in solvent viscosity by mixing polymeric solute.

The storage modulus (G') and the loss modulus (G'') were also measured by dynamic mechanical analysis (DMA) using a stress-controlled rheometer (ARES-G2, TA Instruments) in the cone-plate geometry (50.0 mm in diameter and 0.0192 rad in its cone angle). All data were measured at 25°C. The angular frequency was changed from 0.1 to 100 rad/s. Before the DMA measurement, the strain sweep test was carried out in order to determine the linear region. According to the results, the strain for measurement was determined to set at 3%.

5.3. Results and Discussion

5.3.1. Sol-gel characteristics of SIS solutions

The solution of block copolymers forms gel depending on the types of solvents, while the solution for electrospinning should be in a liquid state. Therefore, the sol-gel characteristics of SIS solutions with mixed solvents were firstly examined. Figure 5.1 shows the sol-gel phase change of SIS solutions. The SIS solutions with DMF/toluene mixed solvents showed liquid sol-state up to 0.3 of DMF ratio in DMF/toluene mixed solvent. This was regardless of the concentrations up to 25wt%. At the DMF ratio higher than 0.3, the SIS solutions at the concentration equal to or higher than 15wt% showed gel-state, while the SIS solution showed sol-state at the concentration below 15wt%. In terms of the gel region, the concentration required for gelation became lower as the DMF ratio in DMF/toluene mixed solvent increased up to 0.4. At the DMF ratio of 0.5, the gelation concentration became slightly high. Further increase of DMF in DMF/toluene mixed solvents caused the polymer-solvent phase separation in SIS solutions.

This sol-gel change of SIS solutions could be explained by the change in solubility parameters. Figure 5.2 shows the calculated solubility parameters of DMF/toluene mixed solvent. The solubility parameters of mixed solvents were calculated using the equation as follows:

$$\delta_{mix} = \delta_1\phi_1 + \delta_2(1 - \phi_1) \quad (5-2)$$

where δ_{mix} is the solubility parameter of mixed solvent, δ_1 and δ_2 are the solubility parameters of pure solvent 1 and solvent 2, ϕ_1 is the volume fraction of solvent 1.⁹⁷ The solubility parameter of pure toluene was 18.2 MPa^{1/2}. As the DMF ratio in DMF/toluene mixed solvent increased, the solubility parameter of DMF/toluene mixed solvent

gradually increased and approached to that of pure DMF ($24.7 \text{ MPa}^{1/2}$). As for the copolymer, the solubility parameter of polystyrene is $18.8 \text{ MPa}^{1/2}$ and the solubility parameter of polyisoprene is $16.6 \text{ MPa}^{1/2}$.

The solubility parameter of toluene was first between the solubility parameters of polystyrene and polyisoprene. In other words, the solubility parameter of toluene was close to those of both polystyrene and polyisoprene. Therefore, it was concluded that toluene is compatible for both polystyrene block and polyisoprene block in SIS. As the DMF ratio in DMF/toluene mixed solvent increased, the solubility parameter of the mixed solvent became closer to that of polystyrene. At the DMF ratio of 0.1, the mixed solvent was well compatible for polystyrene and slightly incompatible for polyisoprene. As the DMF ratio in DMF/toluene mixed solvent further increased, the solubility parameter of the mixed solvent also increased and the compatibility of mixed solvent for polystyrene block and polyisoprene block gradually decreased. Especially, polyisoprene block became insoluble to the mixed solvent. Around the DMF ratio of 0.35, SIS formed micelles with a shell of polystyrene and a core of polyisoprene. These cores from aggregated polymers work as cross-link points. As a result, the solutions with micelles tend to form gels. As the DMF ratio in DMF/toluene mixed solvent further increased, both polystyrene and polyisoprene became insoluble to the mixed solvent. Around the DMF ratio of 0.6, the micelles of SIS strongly aggregated and eventually the solution showed precipitation due to poor solubility. Therefore, it was concluded that the sol-gel change of the SIS solution as a function of DMF ratio in DMF/toluene mixed solvent could be due to the change in solubility parameter. It was also found that the sol-gel change of the tri-block copolymer could be controlled by the ratio of two solvents with different solubility parameters.

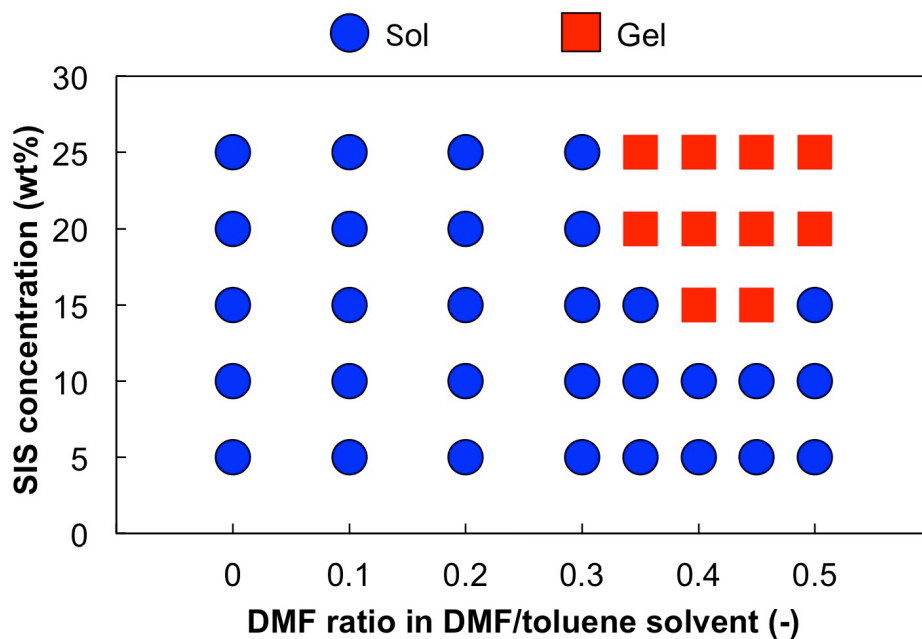


Figure 5. 1 Phase diagram of SIS solution with different DMF ratios in DMF/toluene mixed solvent.

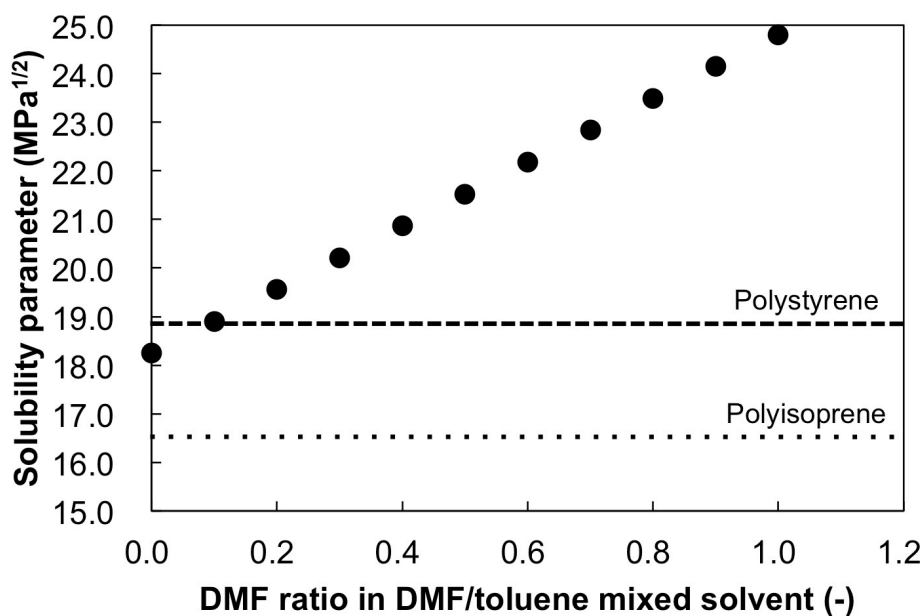


Figure 5. 2 Solubility parameters of DMF/toluene mixed solvent with different DMF ratios.

5.3.2. Morphologies of electrospun SIS fibers

Figure 5.3 showed the SEM images of SIS fibers fabricated by electrospinning using the solutions with various DMF ratios in DMF/toluene mixed solvent. At the DMF ratio of 0.2 in DMF/toluene mixed solvent, microbeads and beaded nanofibers were obtained at the SIS concentration of 17wt%. At the DMF ratio of 0.4 in DMF/toluene mixed solvent, the beaded nanofibers were also obtained from at the concentration of 17wt%. On the other hand, at the DMF ratio of 0.5 in DMF/toluene mixed solvent, the uniform nanofibers were obtained from the solution with relatively low SIS concentration of 10-17wt%.

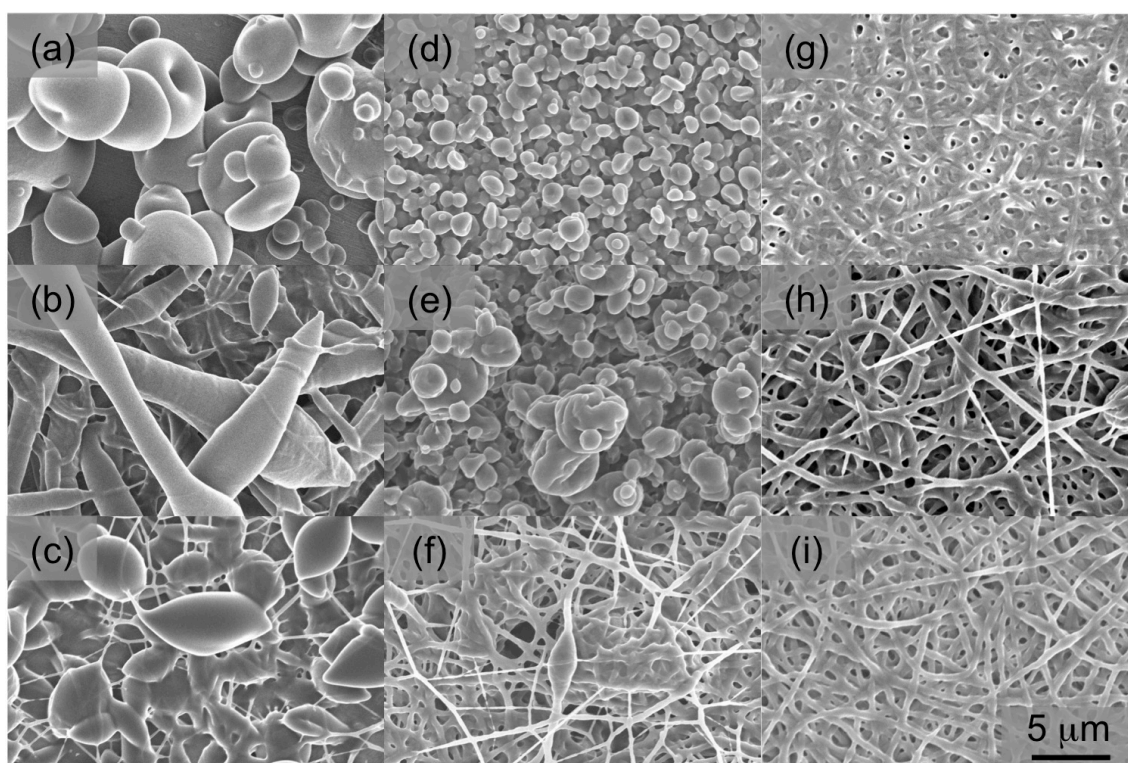


Figure 5. 3 SEM images of SIS fibers from different solutions: DMF ratio of 0.2 and SIS concentrations of (a) 10wt%, (b) 15wt%, and (c) 17wt%; DMF ratio of 0.4 and SIS concentrations of (d) 10wt%, (e) 15wt%, and (f) 17wt%; DMF ratio of 0.5 and SIS concentration of (g) 10wt%, (h) 15wt%, and (i) 17wt%.

Considering the results of sol-gel characteristics of SIS solutions, the SIS solutions at low DMF ratio showed sol-state known to be suitable for electrospinning. However, the electrospun products from the solutions were beads or beaded fibers with micron diameters at the concentration ranged from 10 to 17wt%. It was also confirmed that uniform microfibers were obtained from the SIS solution at the concentration over 25wt%. On the other hand, the solution at DMF ratio of 0.4 and 0.5 showed gel-state unsuitable for electrospinning. However, the electrospun products were beaded fibers or nanofibers. It was also confirmed that uniform nanofibers were obtained from the solution at DMF ratio of 0.5 in DMF/toluene mixed solvent and at the SIS concentration of 17wt%. From the results, it was concluded that for SIS tri-block copolymers the sol-state solution was not necessarily suitable for the fabrication of nanofibers, while the gel-state solution was rather suitable for the fabrication of nanofibers. It is known that, as for amorphous homo-polymers, uniform fibers could not be obtained from the high concentration solution with a characteristic like a weak gel.⁴⁶ It is also known that, as for crystalline polymers, the gelation prevent us from the fabrication by electrospinning.⁶¹ In order to confirm the clue of nanofiber fabrication using the gel-state solution of tri-block copolymer, the systematical investigation on physical properties of mixed solvents and rheological properties of SIS solutions with DMF/toluene mixed solvents was carried out as described in the following section.

5.3.3. Physical properties of the mixed solvents

In order to evaluate the effects of mixing solvents on the physical properties of solvents, the properties leading to the fiber morphology such as the conductivity, the dielectric constant, and the evaporation rate of the mixed solvents were measured.

Figure 5.4 showed the conductivities of DMF/toluene mixed solvents as a function of the DMF ratio in DMF/toluene mixed solvent. The conductivity of pure toluene was 16.9 pS/cm. As the DMF ratio in DMF/toluene mixed solvent increased, the conductivity of DMF/toluene mixed solvent rapidly increased within low DMF ratio in DMF/toluene mixed solvent and approached asymptotically to that of pure DMF (97.4 μ S/cm). In detail, the conductivities of mixed solvents were 0.079 μ S/cm at DMF ratio of 0.1, 3.01 μ S/cm at DMF ratio of 0.2, 15.0 μ S/cm at DMF ratio of 0.3, 27.8 μ S/cm at DMF ratio of 0.4, and 39.0 μ S/cm at DMF ratio of 0.5.

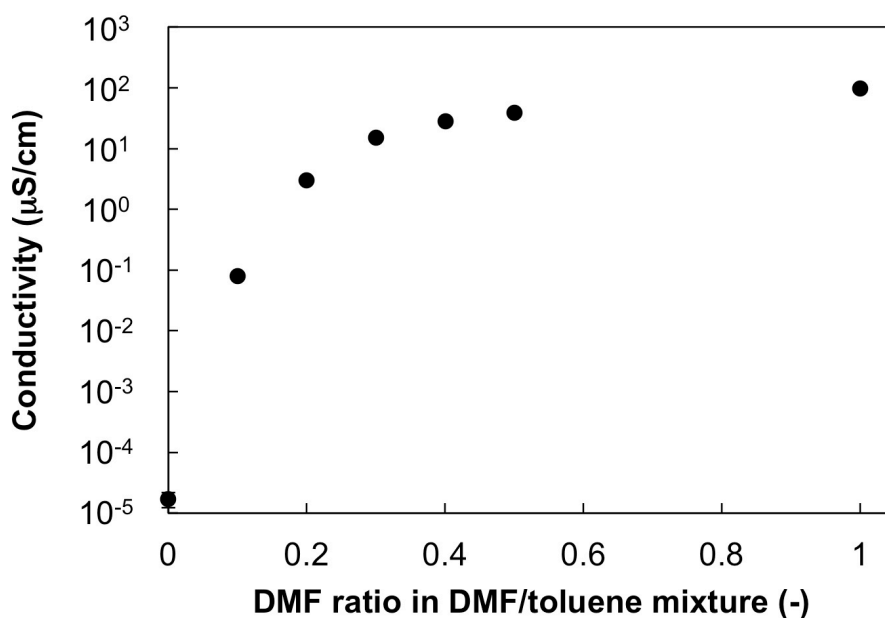


Figure 5. 4 Conductivities of DMF/toluene mixed solvents.

Figure 5.5 showed the dielectric constants of DMF/toluene mixed solvents as a function of the DMF ratio in DMF/toluene mixed solvent. The dielectric constant of pure toluene was 2.53. As the DMF ratio in DMF/toluene mixed solvent increased, the dielectric constant of DMF/toluene mixed solvent linearly increased and finally reached to that of pure DMF (39.0). In detail, the dielectric constants were 4.77 at DMF ratio of 0.1, 7.42 at DMF ratio of 0.2, 10.4 at DMF ratio of 0.3, 13.8 at DMF ratio of 0.4, and 17.4 at DMF ratio of 0.5.

Figure 5.6 showed the evaporation loss against time. From the slope, the evaporation rates were calculated and summarized in Table 5.1. The evaporation rate of pure toluene was 0.5176 mg/min. As the DMF ratio in DMF/toluene mixed solvent increased, the evaporation ratio gradually decreased and reached to that of pure DMF (15.9 $\mu\text{g}/\text{min}$).

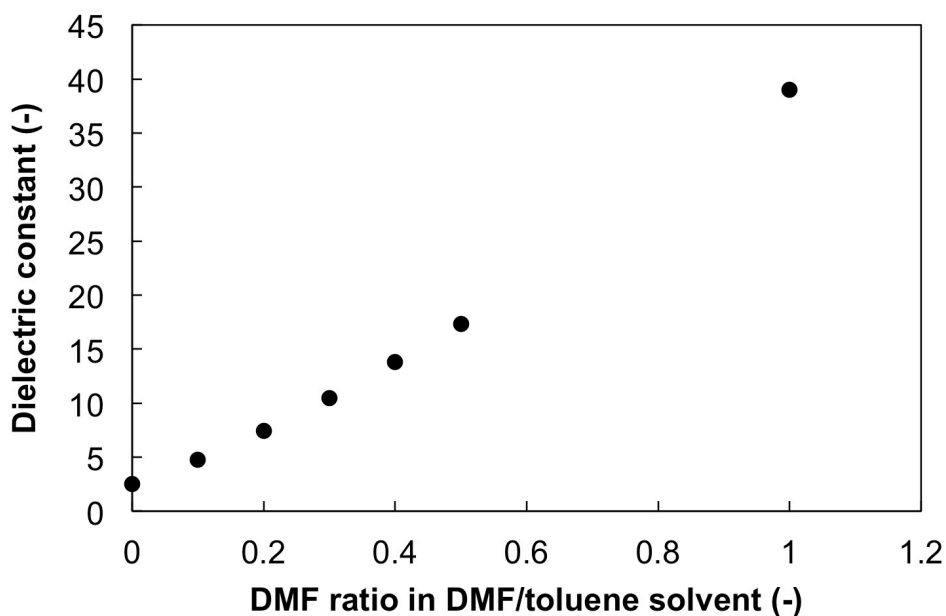


Figure 5. 5 Dielectric constants of DMF/toluene mixed solvents.

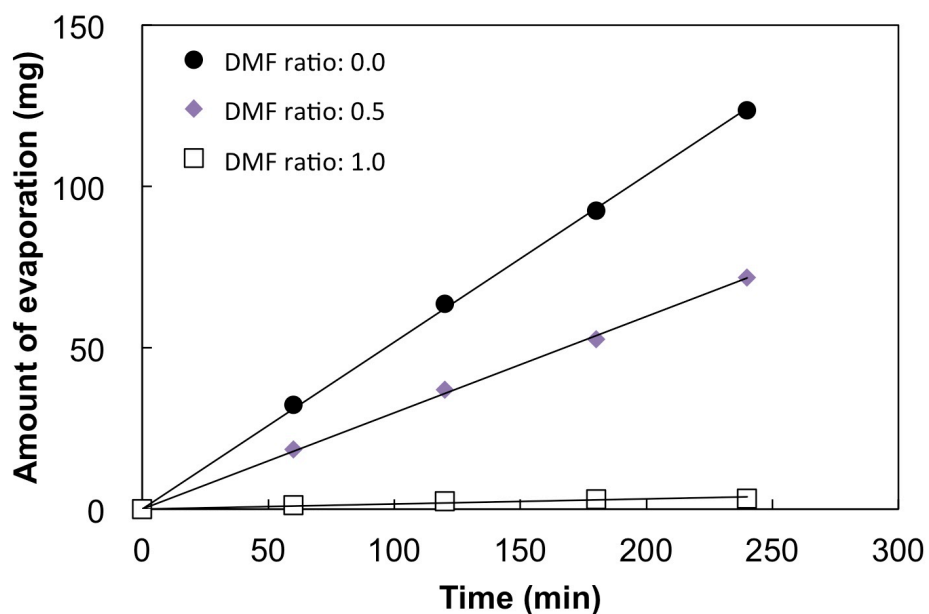


Figure 5. 6 Evaporation loss of DMF/toluene mixed solvent as a function of time.

Table 5. 1 Evaporation rate of DMF/toluene mixed solvents.

DMF ratio in DMF/toluene mixed solvent (-)	Evaporation rate (mg/min)
0.0	0.52
0.2	-
0.4	-
0.5	0.30
1.0	0.016

From the results on physical properties of solvents, by the addition of DMF to toluene, the DMF/toluene mixed solvent got the increased conductivity and dielectric constant and the decreased evaporation rate and became a more suitable solvent for electrospinning. The solvent with higher conductivity and dielectric constant and with lower volatility is known as a suitable solvent for electrospinning. This is because the coulomb repulsion between charged species in a jet responsible for the elongation during electrospinning was enhanced and the elongation could be sufficiently applied to the jet before the solidification of the jet due to the evaporation of solvents.⁴⁴

5.3.4. Rheological analysis of SIS solutions with DMF/toluene mixed solvents

The viscous behavior depends on the solution concentration and the type of solvent as mentioned repeatedly in this work. As discussed before, when the DMF ratio in DMF/toluene mixed solvent was changed, the sol-gel change of SIS solutions was totally different. Other than the gelation phenomenon, the viscosity of liquid-state polymer solution can be controlled finely by changing the solution concentration and the type of solvent, and is known as an important key parameter for electrospinning. Therefore, the modulus of gel-state SIS solutions and the viscosity of liquid-state SIS solutions were evaluated and the combinational effects of SIS and mixed solvents on the morphology of SIS fibers were examined.

Figure 5.7 shows the zero-shear rate viscosity (η_0) as a function of solution concentration. η_0 gradually increased as the concentration increased from 1wt% to 10wt%. Figure 5.8 shows the specific viscosity (η_{sp}) as a function of solution concentration. η_{sp} also gradually increased as the concentration increased from 1wt% to 10wt%. It was found that as the DMF ratio in DMF/toluene mixed solvent increased, η_{sp} became lower regardless of solution concentration below 10wt%.

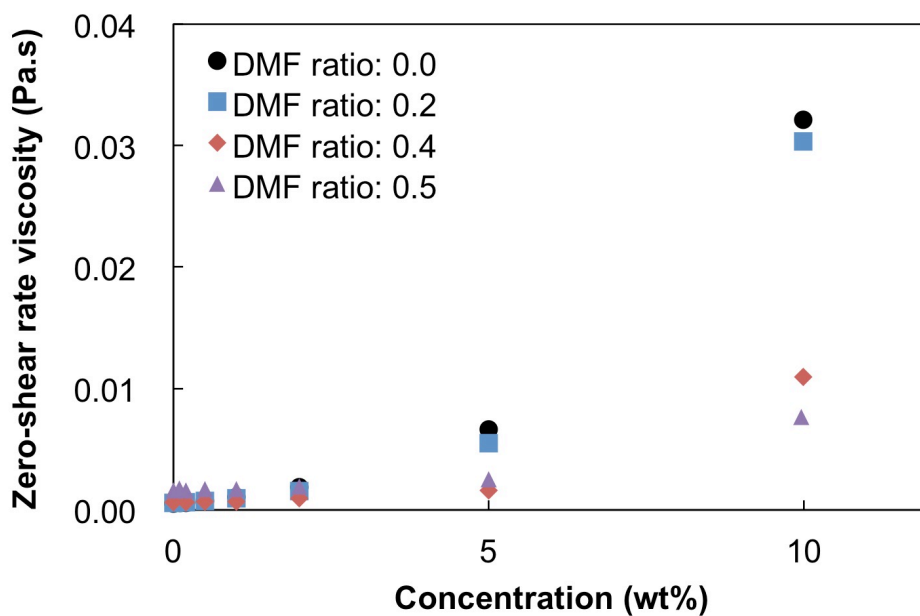


Figure 5. 7 Zero-shear rate viscosity of SIS solutions with different DMF ratios in DMF/toluene mixed solvent.

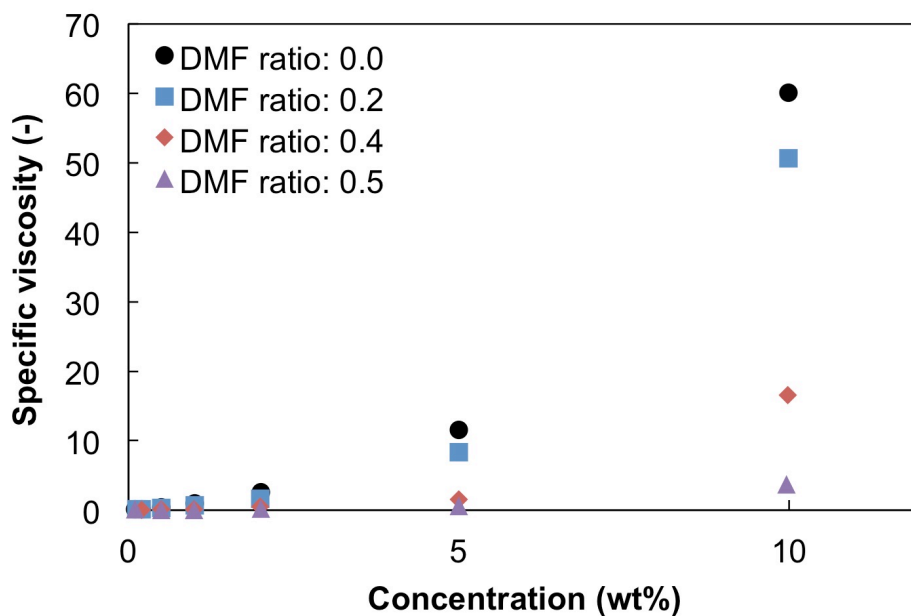


Figure 5. 8 Specific viscosity of SIS solutions with different DMF ratios in DMF/toluene mixed solvent.

In order to determine the entanglement concentration c_e , the specific viscosity of SIS solution with DMF/toluene mixed solvent at DMF ratio of 0.0 (i.e. pure toluene) was further analyzed (Figure 5.9). At the concentration below 6wt%, η_{sp} was proportional to $c^{1.28}$. This dependence is close to the theoretical prediction for the semidilute unentangled solution with linear polymer and good solvent ($\eta_{sp} \sim c^{1.25}$). At the concentration higher than 6wt%, η_{sp} was proportional to $c^{3.26}$. This dependence is not close to the theoretical prediction for the semidilute entangled solution with linear polymer and good solvent ($\eta_{sp} \sim c^{4.8}$). Kong *et al.* and McKee *et al.* also reported the low dependence.^{73, 98} Therefore, it was confirmed that c_e for SIS was $\sim 6\text{wt}\%$. From the determined c_e , it was also estimated that the concentration required for the fabrication of uniform fibers was 12–15wt%. However, the concentration is not consistent with the results from the morphological analysis. This difference could attribute to the weak interaction of polyisoprene indicated from the low concentration dependence of η_{sp} .⁹⁸

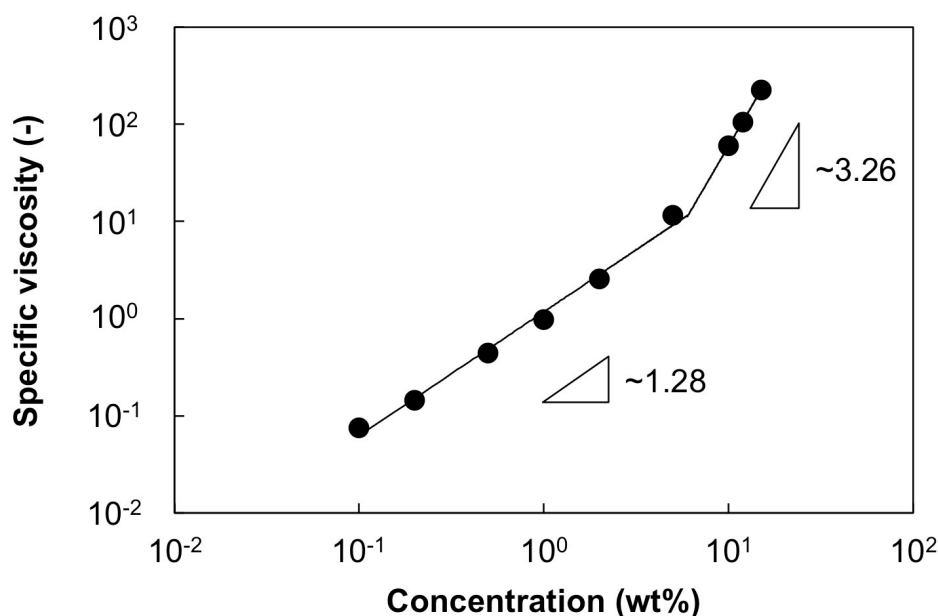


Figure 5. 9 Specific viscosity of SIS solution with DMF ratio of 0.0 in DMF/toluene mixed solvent (i.e. pure toluene).

As for the SIS solution with the concentration higher than 10wt%, since the solution behaved as the non-Newtonian fluid, the rheological properties were evaluated using DMA. Figure 5.10–Figure 5.12 shows the G' and G'' of SIS solutions with different DMF ratios in DMF/toluene mixed solvent. As for the SIS solution with DMF/toluene mixed solvent at DMF ratio of 0.2 (Figure 5.10), G' gradually increased as the SIS concentration increased. However, G' was lower than G'' . In other words, the interaction between polymer chains was too weak to store the energy applied by external force. As for the SIS solution with DMF/toluene mixed solvent at DMF ratio of 0.4 (Figure 5.11), at the SIS concentration of 10wt%, the solution represented the characters of viscoelastic liquid according to the law of $G' \approx \omega^2$ and $G'' \approx \omega$. On the other hand, as the SIS concentration increased, the jump of G' up to 1000 Pa at $\omega=100$ rad/s was observed. At the concentration of 15wt% and 17wt%, G' was higher than G'' . In other words, the interaction between polymer chains was strong enough to store the energy applied by external force. However, the solution began to show some brittleness. As for the SIS solution with DMF/toluene mixed solvent at DMF ratio of 0.5 (Figure 5.12), G' gradually increased as the SIS concentration increased, and G' was always higher than G'' . In other words, the interaction between polymer chains was moderately strong enough to store the energy applied by external force. G' was ~ 200 Pa at $\omega=100$ rad/s and lower than that of the solution with DMF/toluene mixed solvent at DMF ratio of 0.4.

These changes in rheological properties could be due to the network formation of micelles driven by the change in block solubility of tri-block copolymers. It is known that tri-block copolymers form micelles in solutions when the solvent has selective solubility to one block in the copolymer.⁹⁹⁻¹⁰⁵ At high polymer concentration, these micelles are densely packed and the solutions lose the fluidity.¹⁰⁶ However, when

the solubility of blocks becomes slightly poorer to the solvent, the micelles tend to form the self-assembly of micelles. This self-assembly heterogeneously exists in the solution and the solution still possesses the fluidity when the external forces were applied to the solution.

As mentioned before, the solubility parameters of the mixed solvent changed as the DMF ratio was increased in DMF/toluene mixed solvent. In detail, the mixed solvent became more compatible for polystyrene block as compared to polyisoprene block. This supported the formation of micelles with polyisoprene core and polystyrene shell. Further solubility change by increasing the DMF ratio led to the aggregation of these micelles due to the insolubility of polystyrene shell in the mixed solvent.

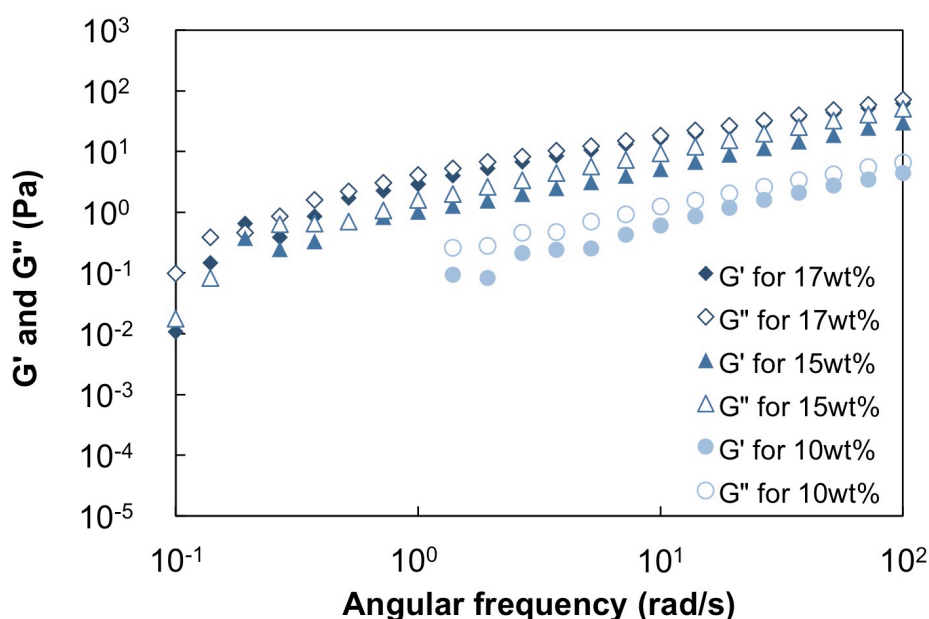


Figure 5. 10 DMA results for SIS solutions with DMF/toluene mixed solvent at DMF ratio of 0.2.

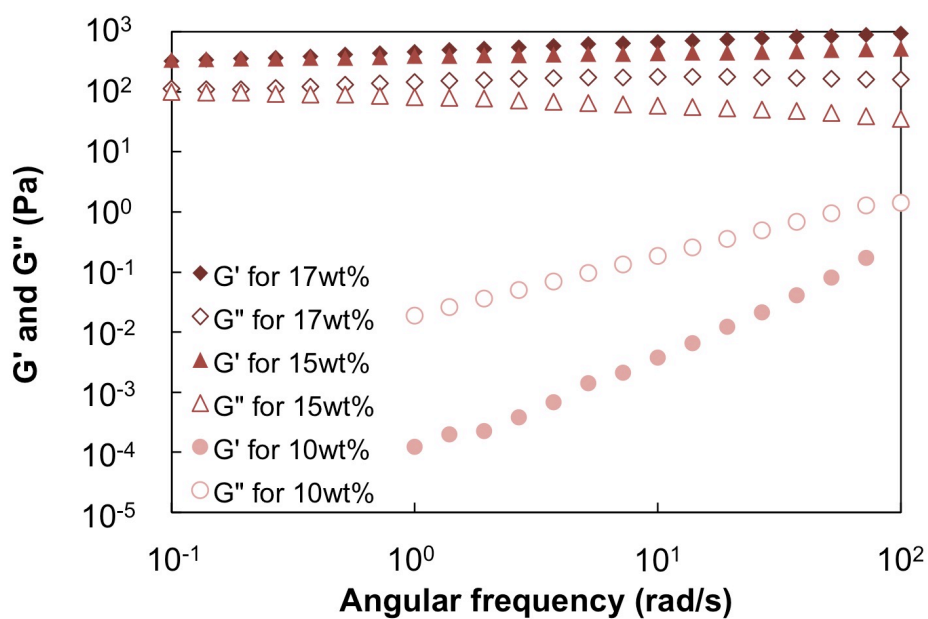


Figure 5. 11 DMA results for SIS solutions with DMF/toluene mixed solvent at DMF ratio of 0.4.

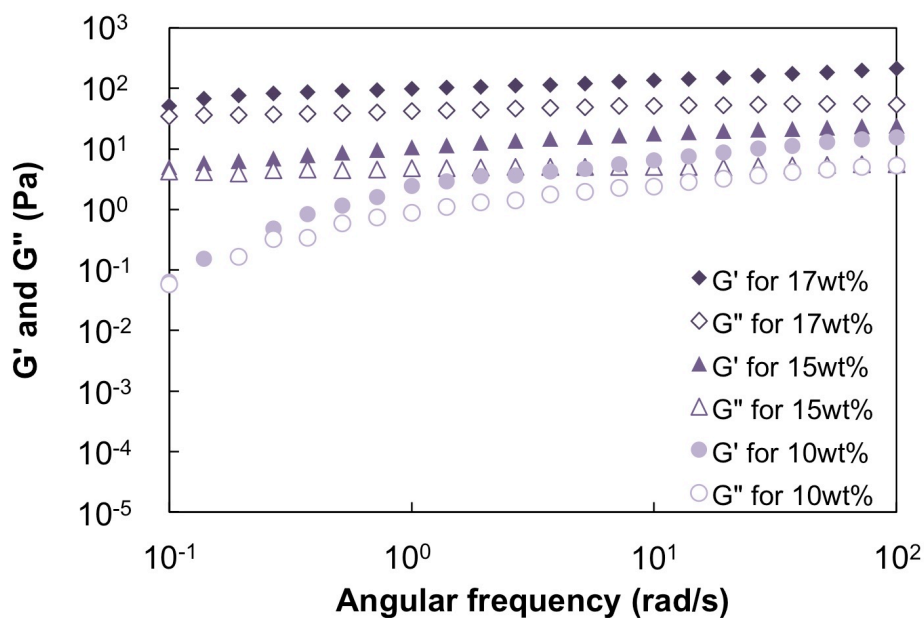


Figure 5. 12 DMA results for SIS solutions with DMF/toluene mixed solvent at DMF ratio of 0.5.

To summarize the results of rheological analysis, by measuring the viscosity of SIS solutions with pure toluene, the entanglement concentration c_e was determined to be ~6wt% and the concentration required for the formation of uniform fibers was determined to be in the range of 12–15wt%. However, nanofibers were not obtained from the SIS solution with pure toluene even at the concentration above 20wt%. This could be attributed to the fact that the interactions among polyisoprene chains of SIS were too weak, while the entanglement was enough to form fibers during electrospinning. On the other hand, nanofibers were obtained from the SIS solution with DMF/toluene mixed solvent at DMF ratio of 0.5. In the solution, the solubility of polyisoprene was poor and the micelles with polyisoprene core were formed. As a result, the interactions among the polyisoprene chains of SIS were enhanced. This led to the fiber formation at the concentration around 12–15wt%.

5.4. Summary of this chapter

Fabrication of SIS nanofibers by using DMF/toluene mixed solvent was systematically studied. SIS nanofibers with the average diameter of 350 nm were obtained by using the DMF/toluene mixed solvent and changing the DMF ratio in DMF/toluene mixed solvent. The addition of DMF enhanced the conductivity and dielectric constant, and lowered the volatility of solvent and made the solution suitable for electrospinning. At the same time, the addition of DMF enhanced the interactions among the SIS chains according to the results of rheological analysis. Therefore, it was found that as for tri-block copolymers the self-assembly of tri-block copolymers due to the change of solubility parameters could be useful for the nanofiber formation.

Chapter 6. Clay-sheet/PLGA-PEG-PLGA hydrogels

6.1. Background on PLGA-PEG-PLGA hydrogels

The aqueous solution of block copolymers based on poly (D,L-lactic acid-co-glycolic acid) (PLGA) and poly (ethylene glycol) (PEG) exhibits sol-gel transition in response to increasing temperature (i.e. thermo-responsive sol-gel transition) as well as biodegradability and biocompatibility, therefore the utilization of PLGA- and PEG-based block copolymers in biomedical fields is highly expected. After the original report on the synthesis of thermo-responsive hydrogels made from poly (L-lactic acid) (PLLA) and PEG for injectable drug-delivery systems by Jeong *et al.*,¹⁰⁷ Jeong *et al.* reported the synthesis and the thermo-responsive gelation of PEG-PLGA-PEG tri-block copolymers.¹⁰⁸⁻¹⁰⁹ They also reported the in situ gelation and the degradation behavior of PEG-PLGA-PEG aqueous solutions.¹¹⁰ On the other hand, PLGA-PEG-PLGA is a tri-block copolymer composed of hydrophilic PEG as a middle block and hydrophobic PLGA as endblocks. Zentner *et al.* firstly reported the synthesis of PLGA-PEG-PLGA called as ReGel[®] and presented the drug release from ReGel[®].³⁸ At the nearly same time, Lee *et al.* also reported the synthesis of PLGA-PEG-PLGA and the thermo-reversible gelation of PLGA-PEG-PLGA in aqueous solutions.¹¹¹⁻¹¹²

Since the success in the synthesis of PLGA-PEG-PLGA, the sol-gel transition temperature and the rheological property of PLGA-PEG-PLGA aqueous solutions were systematically investigated by changing the solution concentration and the compositions of PLGA-PEG-PLGA including molecular weight, PEG/PLGA block ratio, and LA/GA ratio. For example, in the case of PLGA-PEG-PLGA with PEG midblock ($M_n=1000$), as for the concentration required for the gelation (CGC), it was found that CGC increased as the PEG/PLGA ratio increased and PLGA-PEG-PLGA with PEG/PLGA ratio higher than ~ 0.56 did not form hydrogels due to the excess hydrophilicity. It was

also found that CGC gradually increased as the LA/GA ratio decreased. As for the gelation temperature (CGT), it was found that CGT decreased as the PEG/PLGA ratio and the LA/GA ratio increased. In order to have the gel-regions around the temperature of human body (37°C), the PEG/PLGA ratio should be lower than ~0.4 and the LA/GA ratio should be higher than 1.9 even when the concentration of PLGA-PEG-PLGA in water is over 10wt%.¹¹¹⁻¹¹² As for the molecular weight, it was also found that, in the case of PLGA-PEG-PLGA with same PEG/PLGA ratio and LA/GA ratio, the sol-gel transition temperature increased as the molecular weight of PEG increased and eventually the wider gel-regions around 37°C were obtained.¹¹² In addition to the basic studies on the gelation of PLGA-PEG-PLGA aqueous solutions, the drug-release tests from PLGA-PEG-PLGA hydrogels were also examined.¹¹³⁻¹¹⁵

In order to tune the CGC and the CGT, various approaches such as attaching end-capping group, blending different types of PLGA-PEG-PLGA, and changing the temperature of synthesis were reported. Yu *et al.* reported the preparation of PLGA-PEG-PLGA derivatives with end-capping groups and their sol-gel transition behavior. While PLGA-PEG-PLGA with hydroxyl end groups (i.e. virgin PLGA-PEG-PLGA with PEG/PLGA ratio of ~0.56) did not form hydrogels, PLGA-PEG-PLGA with acetate end groups and PLGA-PEG-PLGA with propionate end groups showed sol-gel transitions. However, PLGA-PEG-PLGA with butyrate end groups became precipitation in all temperature regions from 0°C to 50°C.¹¹⁶ Through the further studies, they concluded that the sol-gel transition was induced not only by the micelle formation but also the further hydrophobic aggregation of micelles leading to the large scale micelle network.¹¹⁷ As another method, Yu *et al.* reported mixing two types of PLGA-PEG-PLGA: PLGA-PEG-PLGA soluble in water as a sol in the experimental temperature region and PLGA-PEG-PLGA insoluble in water. By mixing

the two types of PLGA-PEG-PLGA at various ratios, the sol-gel transition on the temperature increase was observed. They concluded that the addition of hydrophilic PLGA-PEG-PLGA enhanced the solubility of less hydrophilic PLGA-PEG-PLGA and the elaborated balance induced the sol-gel transition.¹¹⁸ In addition to the studies on tuning CGC and CGT, Yu *et al.* also reported the biodegradability and biocompatibility of PLGA-PEG-PLGA hydrogels from mixing a sol and a precipitate.¹¹⁹ As for the temperature of synthesis, Yu *et al.* reported PLGA-PEG-PLGA synthesized at 130°C showed wider gel-region than PLGA-PEG-PLGA synthesized at 160°C. They concluded that PLGA-PEG-PLGA synthesized at 160°C possessed more random sequence in PLGA block than PLGA-PEG-PLGA synthesized at 130°C, and that the slight difference in the sequence structure led to the difference in the sol-gel transition temperature.¹²⁰

For the full utilization of high-biocompatible PEG, the CGC and CGT should also be tuned while remaining the PEG/PLGA block ratio high in PLGA-PEG-PLGA. Since PLGA-PEG-PLGA with PEG/PLGA block ratio higher than ~0.56 did not exhibit the thermo-responsive sol-gel transition as mentioned before, it is challenging to increase the PEG/PLGA ratio in PLGA-PEG-PLGA. Other than PLGA-PEG-PLGA, Li *et al.* reported an approach to prompt thermo-responsive sol-gel transition of poly (lactide)-*b*-poly (ethylene glycol)-*b*-poly (lactide) (PLA-PEG-PLA) using the formation of stereo-complex crystalline.¹²¹ However, there is no attempt to heighten the PEG/PLGA ratio for PLGA-PEG-PLGA hydrogels to the best of our knowledge.

Recently, our group developed a new type of PLGA-PEG-PLGA-based thermo-responsive hydrogels consisting of PLGA-PEG-PLGA with high PEG/PLGA ratio of ~0.83 (i.e. PLGA-PEG-PLGA without thermo-responsibility) and synthetic clay-sheet (Iaponite).³⁹ In the report, the aqueous system with 3.0wt% of

PLGA-PEG-PLGA (1.8k-3.0k-1.8k) (i.e. the PEG/PLGA ratio of ~ 0.83) and 0.9wt% of laponite was prepared. Laponite/PLGA-PEG-PLGA aqueous system immediately changed from sol to gel in response to the increase of temperature (from 10°C to 37°C). It should be noted that, interestingly, the thermo-responsive sol-gel transition at 37°C occurred at very low concentration of PLGA-PEG-PLGA and laponite.

Our co-workers also reported that the resultant laponite/PLGA-PEG-PLGA hydrogels showed excellent cell compatibility and excellent drug-release profiles of doxorubicin (DOX), an anthracycline antibiotic. In detail, Oyama *et al.* reported that L929 fibroblast cells cultured on laponite/PLGA-PEG-PLGA hydrogels were completely alive, while pure PLGA-PEG-PLGA hydrogels showed cytotoxicity.³⁹ Nagahama *et al.* reported that long-term release of DOX without initial burst from laponite/PLGA-PEG-PLGA hydrogels was achieved.¹²² In these works, although the preliminary study on gelation behavior and the usability of the resultant gels as injectable drug-delivery system were revealed, the molecular weight of PEG and the PEG/PLGA ratio were limited and the systematical understanding on gelation behavior has not yet been accomplished.

In this study, the thermo-responsive sol-gel transition behavior, the mechanical properties, and the microstructure of laponite/PLGA-PEG-PLGA aqueous systems were systematically studied as a function of the molecular weight of PLGA-PEG-PLGA and the laponite concentration in laponite/PLGA-PEG-PLGA aqueous systems. In detail, PLGA-PEG-PLGA with different PEG molecular weight (1.0k, 1.5k, and 3.0k) and PEG/PLGA block ratio (0.4 and 1.0) were synthesized. The sol-gel transition behavior of pure PLGA-PEG-PLGA aqueous solutions and laponite/PLGA-PEG-PLGA aqueous systems were investigated by tube inverting method. For the evaluation of the rheological properties, the dynamic mechanical

analysis (DMA) of the solutions was carried out. Moreover, for the microstructural observation, the cryogenic transmission electron microscopy (cryo-TEM) was conducted.

6.2. Experimental

6.2.1. Materials

Poly (ethylene glycol) with the molecular weight M_w of 1000, 1500, and 3000 g/mol, Glycolide, D, L-Lactide, and tin (II) 2-ethylhexanoate were purchased from Sigma-Aldrich Co. Iaponite was supplied by BYK Additives and Instruments. Ultrapure water was purchased from Kanto Chemical Co. Acetone was purchased from Wako Pure Chemical Industries, Ltd.

6.2.2. Synthesis of PLGA-PEG-PLGA

PLGA-PEG-PLGA triblock copolymers were synthesized by a ring-opening polymerization. PEG, D, L-lactide, and glycolide were dried under vacuum in a Schlenk flask for 24 h. After adding tin (II) 2-ethylhexanoate (0.2wt%) to the flask, the flask was sealed and purged with argon. Then, the flask was immersed in an oil bath and the reaction mixture was stirred and heated at 155°C for 6 h. The temperature of flask was subsequently reduced to 150°C and kept under vacuum for 30 min in order to remove the unreacted monomers. The products were dissolved into chloroform and precipitated in diethyl ether. The purified products were finally dried under vacuum at room temperature for 24 h.

6.2.3. Characterization of the synthesized PLGA-PEG-PLGA

$^1\text{H-NMR}$ measurements in CDCl_3 were performed using a 500 MHz NMR spectrometer (ECA-500, JEOL RESONANCE Inc.) in order to determine the molecular

weight and the composition of copolymers.

^1H NMR (CDCl_3): δ 1.55 (-OCH(**CH**₃)CO-), δ 3.60 (-O**CH**₂CH₂-), δ 4.30 (-OCH₂**CH**₂OCOCH₂O-), δ 4.80 (-O**CH**₂CO-), and δ 5.20 (-O**CH**(CH₃)CO-).

GPC measurements were performed using a high performance liquid chromatography (HPLC) (Prominence, SHIMADZU Co.) in order to determine the molecular weight and the molecular weight distribution. Chloroform was used as eluent at a flow rate of 1.0 mL/min at 25°C, and PEG standards (Agilent Technologies) were used as the calibration sample.

6.2.4. Aqueous system preparation

PLGA-PEG-PLGA was weighed and dissolved in acetone and pure water was added to the PLGA-PEG-PLGA/acetone solution. The acetone was completely evaporated by decompression in order to prepare homogeneous PLGA-PEG-PLGA aqueous solution. Laponite was weighed and dispersed into pure water in order to prepare laponite aqueous suspension. After laponite aqueous suspension was processed through autoclave treatment, PLGA-PEG-PLGA aqueous solution and laponite aqueous suspension were blended in order to prepare laponite/PLGA-PEG-PLGA aqueous solution.

The PLGA-PEG-PLGA aqueous solution was prepared at the concentrations of 2.0wt%, 4.0wt%, 6.0wt%, 8.0wt%, and 10wt%. The laponite aqueous solution was prepared at the concentrations of 1.0wt%, 1.5wt%, and 2.0wt%. With the mixture of the resultant solution and suspension in equal quantity, the concentrations of laponite/PLGA-PEG-PLGA aqueous system were set as follows: laponite (0.5wt% - 1.0wt%)/ PLGA-PEG-PLGA (1.0wt% - 5.0wt%).

6.2.5. Phase diagram measurement

The phase diagrams of aqueous PLGA-PEG-PLGA solutions with and without laponite were obtained by tube inverting method. Samples were prepared by varying the molecular weight of PLGA-PEG-PLGA and the concentration of laponite and PLGA-PEG-PLGA in laponite/PLGA-PEG-PLGA aqueous systems. The laponite/PLGA-PEG-PLGA system of 0.3 mL was sealed into 2 mL glass vials, and then the vials were immersed in a temperature-regulated water bath for 2 minutes at every temperature. The water bath temperature was controlled by a step of 1°C from 10 to 70°C. The system was determined as a gel if no visual liquid flow was observed in 30 s after a vial was inverted and as a precipitation state when excess water was excluded out of the gel. The sol-gel transition temperature and gel-precipitation transition temperature were both measured in heating process. The results were reproducible within $\pm 1^\circ\text{C}$.

6.2.6. Rheological analysis

The sol-gel transition temperatures were determined by dynamic mechanical analysis (DMA). DMA was conducted on a strain-controlled rheometer (ARES-G2, TA Instruments Inc.) using parallel plate geometry with the diameter of 25 mm. Samples were transferred from vials to Peltier system just before the measurement. The parallel plate-Peltier plate gap was kept constant at 1.00 mm. In the oscillatory frequency sweep test, the storage modulus G' and loss modulus G'' were collected as a function of temperature from 10 to 70°C with heating rate of 1.0°C/min. The oscillatory frequency was set at 10 rad/s. The shear strain amplitudes were set at suitable value determined by preliminary experiments to ensure the linearity of viscoelasticity depending on the temperature of each sample's transition (200% and 10% before and after sol-gel transition temperature, respectively). Samples were regarded as gel when storage

modulus G' exceeded loss modulus G'' .

6.2.7. Cryogenic-transmission electron microscopy (Cryo-TEM)

The microstructures of Iaponite/PLGA-PEG-PLGA systems with Iaponite (1.0wt%) and PLGA-PEG-PLGA (5.0wt%) in sol and gel state were analyzed by transmission electron microscopy (TEM), using TECNAI SPIRIT (FEI Company) with an accelerating voltage of 120 kV. The sample was adhered to carbon grids with grid pitch of 3 to 8 μm , and then the thickness of the sample attached to the grid was adjusted to 50 nm. Afterward, the grid was plunged into liquid propane slush for instantaneous freezing around -188°C , and then the observation was carried out keeping the temperature below -175°C .

6.3. Results and Discussion

6.3.1. Characterization of PLGA-PEG-PLGA triblock copolymers

Figure 6.1–Figure 6.6 shows the $^1\text{H-NMR}$ spectra of PLGA-PEG-PLGA copolymers. The signal appearing at 3.6 ppm is assigned to the methylene hydrogen of PEG, the signal appearing at 1.5 ppm is assigned to the methyl hydrogen of D,L -lactide (LA) units, the signal appearing at 5.2 ppm is assigned to the methane hydrogen of LA units, and the signal appearing at 4.8 ppm is assigned to methylene hydrogen of glycolide (GA) units. From these signals, the molecular weight, the PLGA/PEG ratio, and the LA/GA ratio of PLGA-PEG-PLGA were determined and summarized in Table 6.1.

Figure 6.7–Figure 6.9 shows the GPC curves of PLGA-PEG-PLGA copolymers. Since the curve gradually shifted to left and the increase in the width of curve was slight, it was indicated that the synthesis of PLGA-PEG-PLGA copolymers

were carried out well. From these curves, the molecular weight relative to PEG standards and the molecular weight distribution were determined and also summarized in Table 6.1. According to Table 6.1, it was confirmed that PLGA-PEG-PLGA with different PEG-midblock molecular weight of 1000, 1500, and 3000 g/mol, the PEG/PLGA ratio of ~ 0.4 , and ~ 1.0 , and the LA/GA ratio constant at ~ 2.4 were successfully synthesized as expected. The sample was named as follows: the number after P is the molecular weight of PEG-midblock in the unit of kg/mol and the next character represents the difference in PEG/PLGA ratio. The PEG/PLGA ratio of ~ 0.4 is assigned to “long” and the PEG/PLGA ratio of ~ 1.0 is assigned to “short”. For example, PLGA-PEG-PLGA with PEG-midblock molecular weight of 1000 and PEG/PLGA ratio of ~ 1.0 (i.e. PLGA-PEG-PLGA with relatively short PLGA block to PEG midblock) is called “P1.0-short”.

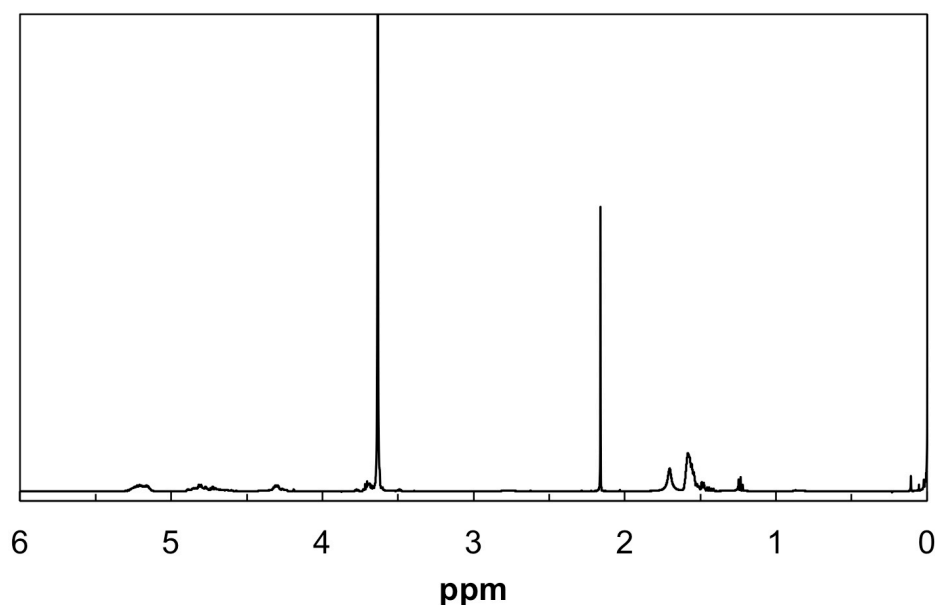


Figure 6. 1 $^1\text{H-NMR}$ spectrum of P1.0-short.

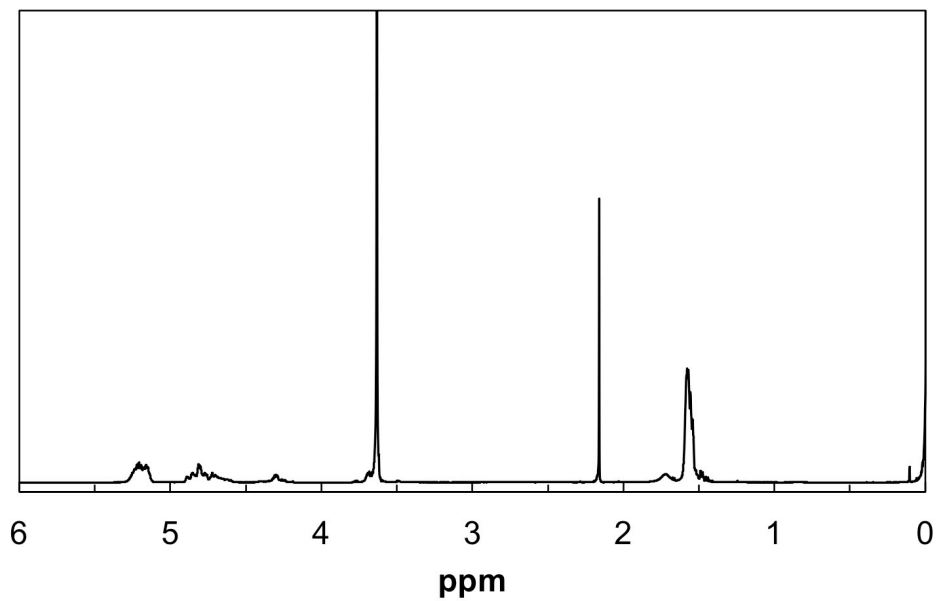


Figure 6. 2 ^1H -NMR spectrum of P1.0-long.

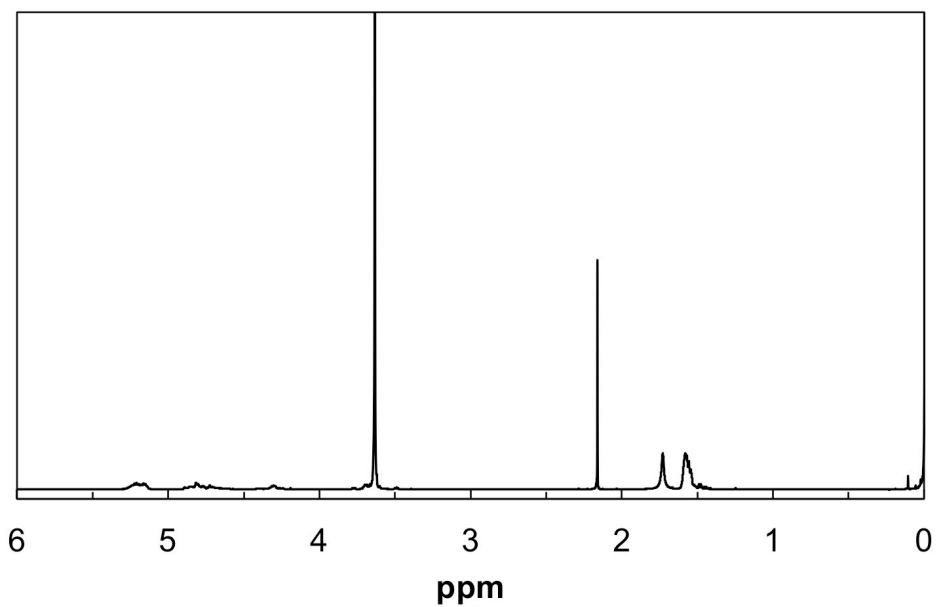


Figure 6. 3 ^1H -NMR spectrum of P1.5-short.

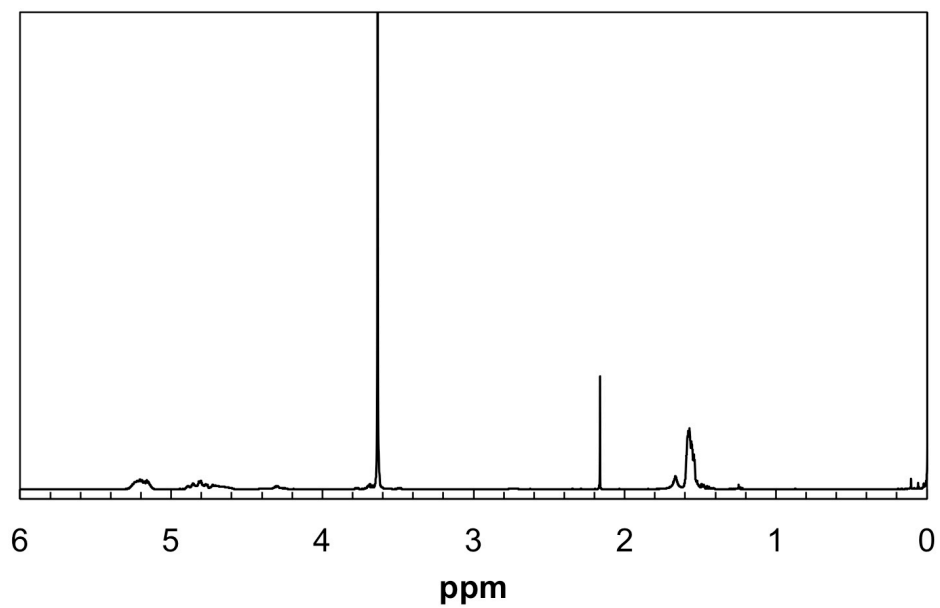


Figure 6. 4 ^1H -NMR spectrum of P1.5-long.

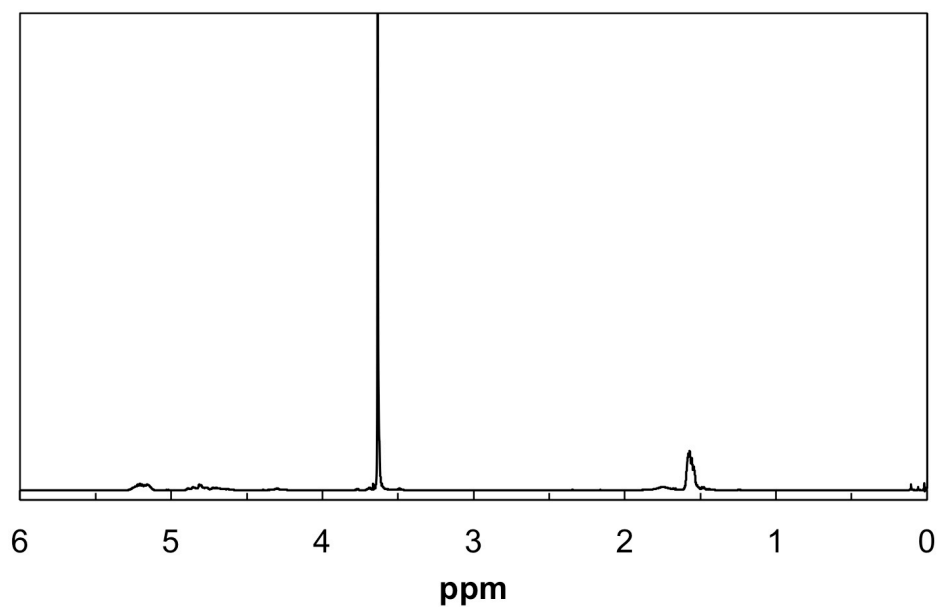


Figure 6. 5 ^1H -NMR spectrum of P3.0-short.

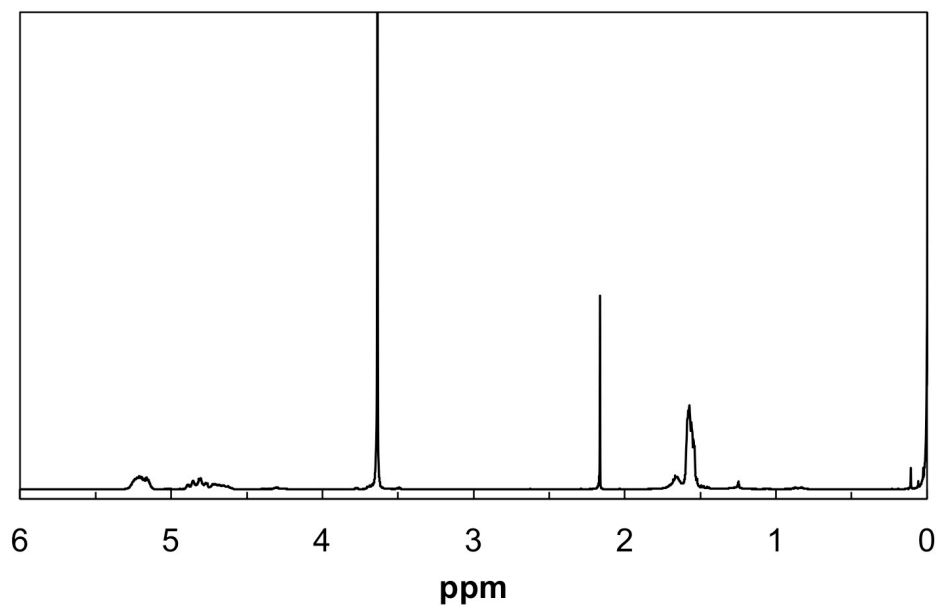


Figure 6. 6 $^1\text{H-NMR}$ spectrum of P3.0-long.

Table 6. 1 Molecular weight and composition of synthesized PLGA-PEG-PLGA.

Sample name	PLGA-PEG-PLGA Mn ^a	PLGA/PEG ^a	LA/GA ^a	Mw ^b	Mw/Mn ^b
P1.0-short	576-1000-576	1.0	2.2	1974	1.06
P1.0-long	1408-1000-1408	2.7	2.4	3005	1.14
P1.5-short	891-1500-891	1.2	2.4	2699	1.08
P1.5-long	1776-1500-1776	2.4	2.4	3684	1.12
P3.0-short	1886-3000-1886	1.3	2.5	4195	1.08
P3.0-long	3986-3000-3986	2.5	2.4	6241	1.14

^a calculated from $^1\text{H-NMR}$

^b measured by GPC (PEG standard)

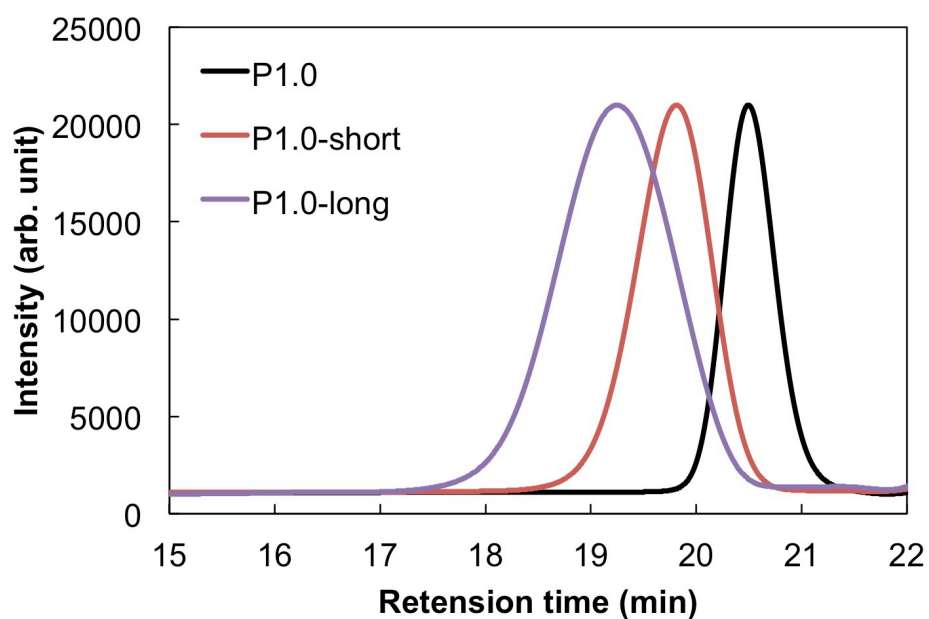


Figure 6. 7 GPC curves of PLGA-PEG-PLGA with PEG midblock of Mn=1000.

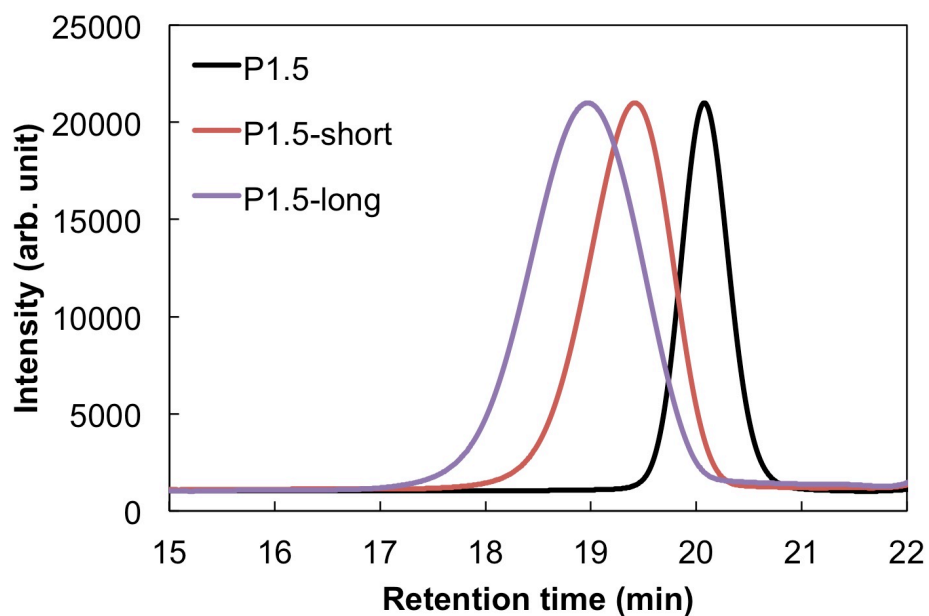


Figure 6. 8 GPC curves of PLGA-PEG-PLGA with PEG midblock of Mn=1500.

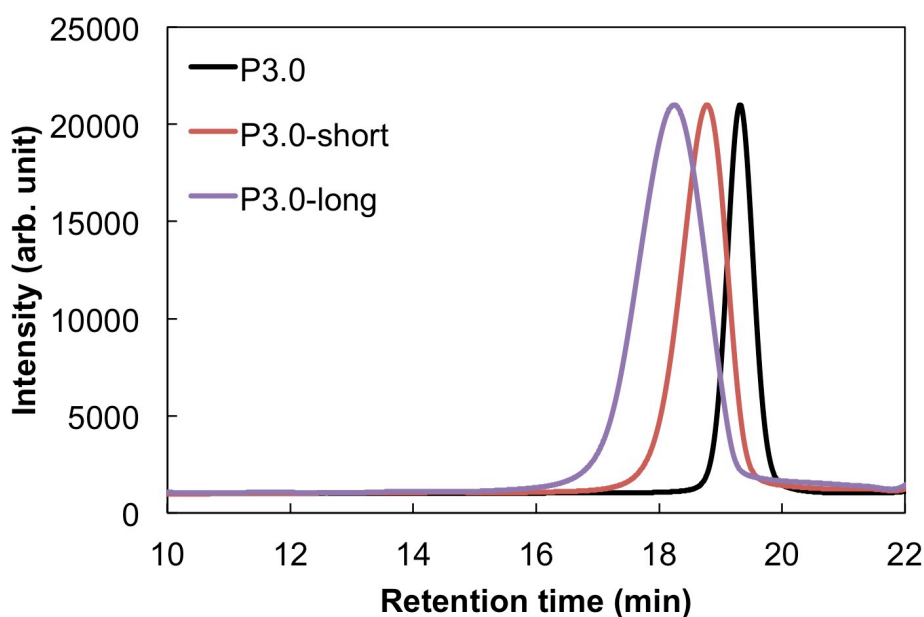


Figure 6. 9 GPC curves of PLGA-PEG-PLGA with PEG midblock of Mn=3000.

6.3.2. Thermo-responsive sol-gel transition behavior

Figure 6.10 shows the typical images of tube inverting test in order to confirm whether the laponite/PLGA-PEG-PLGA aqueous system is in sol-state or gel-state. Figure 6.10 (a) shows the image of pure P1.0-short solution (5.0wt%) and Figure 6.10 (b) shows the image of laponite/P1.0-short system (1.0wt%/5.0wt%). The aqueous solution of P1.0-short (i.e. pure PLGA-PEG-PLGA with short PLGA block) behaved as liquid both at 10°C and 37°C and did not form gel. After blending laponite into the solution, the laponite/P1.0-short system immediately became gel-state when heated at 37°C, while the system behaved as liquid when kept at low temperature (10°C). From these results, it was confirmed that pure PLGA-PEG-PLGA with short PLGA block like P1.0-short did not form gel and the phenomenon is in good agreement with the fact that PLGA-PEG-PLGAs with the PEG/PLGA block ratio of ~ 0.56 or higher do not form a gel as reported before.¹¹¹ Therefore, it was found that laponite supported the sol-gel

transitions of PLGA-PEG-PLGA with short PLGA block. In order to study the sol-gel transition of laponite/PLGA-PEG-PLGA system systematically, the tube inverting test was carried out for the laponite/PLGA-PEG-PLGA system with various laponite and PLGA-PEG-PLGA concentrations.

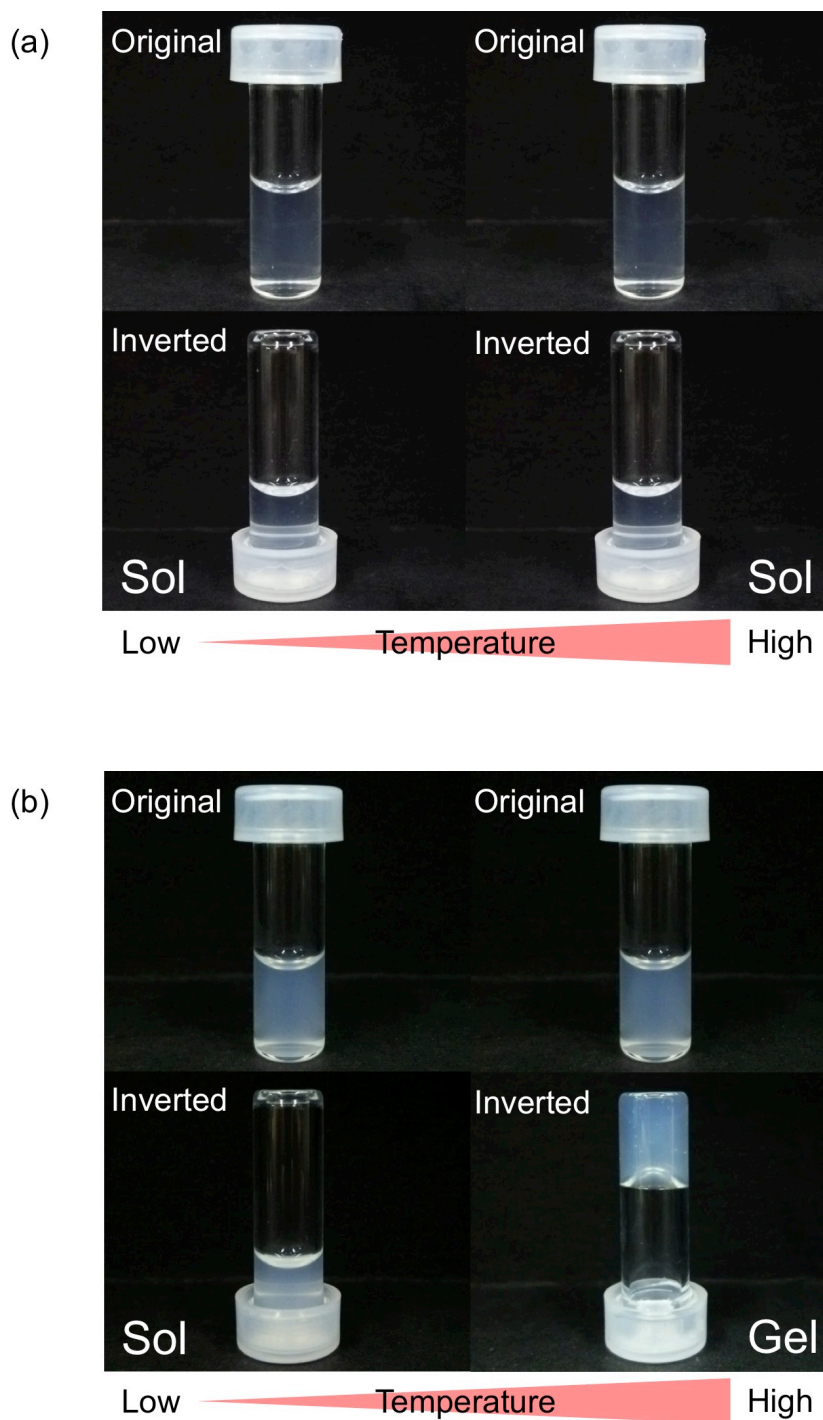
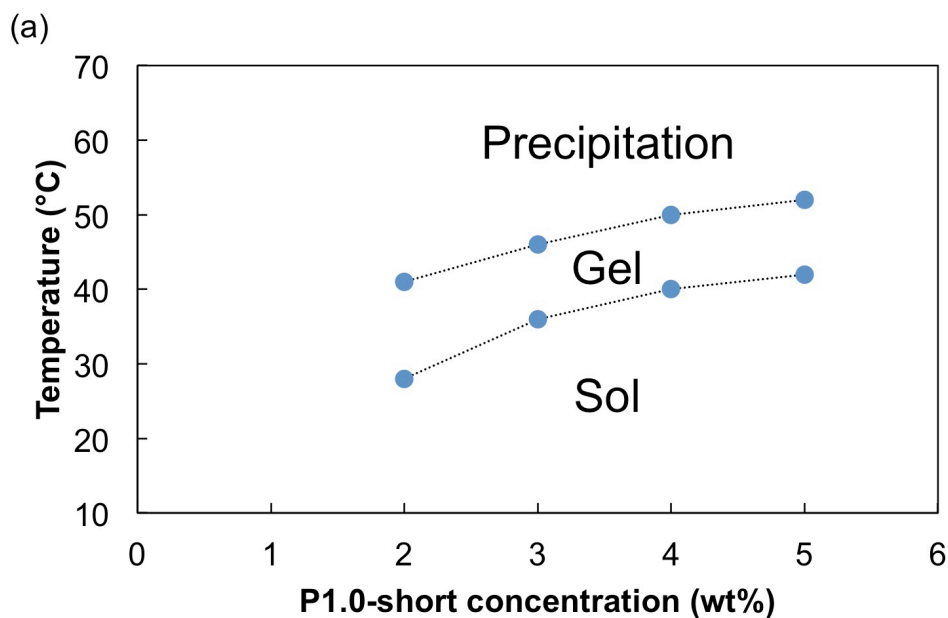


Figure 6. 10 Images of tube inverting test for solutions: (a) P1.0-short solution and (b) Iaponite/P1.0-short system (1.0wt%/5.0wt%).

Figure 6.11 shows the phase diagram of laponite/P1.0-short aqueous system determined by tube inverting method. P1.0-short is PLGA-PEG-PLGA with PEG-block molecular weight of 1000 g/mol and PEG/PLGA ratio of 1.0. The diagram consists of three regions indicating sol, gel, and precipitation. Figure 6.11 (a) is for the laponite/P1.0-short aqueous system with the laponite concentration of 0.75wt%. Figure 6.11 (b) is for the laponite/P1.0-short aqueous system with the laponite concentration of 1.0wt%. Figure 6.11 (c) is for the laponite/P1.0-short aqueous system with the laponite concentration of 1.5wt%. It was found that when the concentration of laponite became 0.75wt% or higher, the laponite/P1.0-short aqueous system formed gel. It was also found that the critical gelation polymer concentration (CGC) of laponite/P1.0-short aqueous system was 2.0wt%.



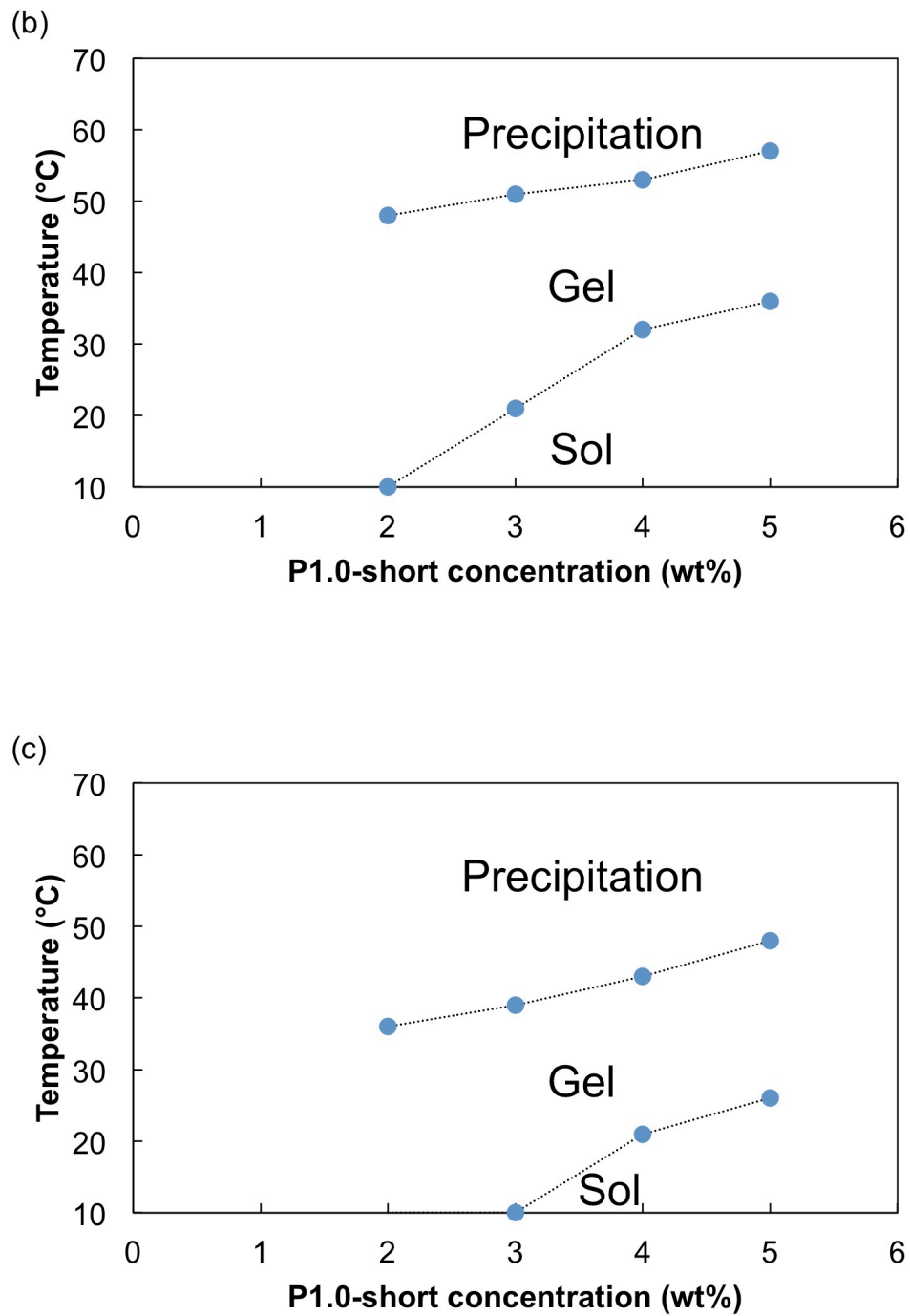


Figure 6. 11 Phase diagrams of laponite/P1.0-short aqueous systems with different laponite concentrations: (a) 0.75wt%, (b) 1.0wt%, and (c) 1.5wt%.

In terms of the sol-gel transition temperature ($T_{gelation}$), as shown in Figure 6.12, it was found that $T_{gelation}$ decreased as the concentration of laponite increased. This could be because the network formation of laponite was induced by the increase in the laponite concentration regardless of temperature and the gel-state became dominant at room temperature. It was also found that $T_{gelation}$ increased as the concentration of P1.0-short increased. This could be because the balance of hydrophobic/hydrophilic became more hydrophilic, and higher temperature was required for total aqueous system to become more hydrophobic. It is known that PLGA-PEG-PLGA with small PLGA block like P1.0-short does not form gel by itself due to the less hydrophobic aqueous system.¹¹⁶

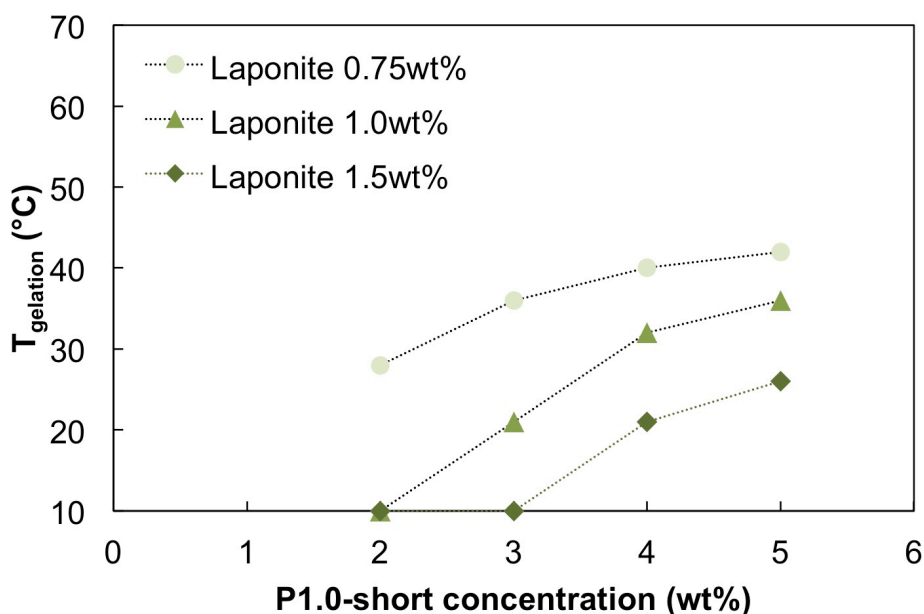


Figure 6. 12 Sol-gel transition temperatures of laponite/P1.0-short systems with different laponite concentrations.

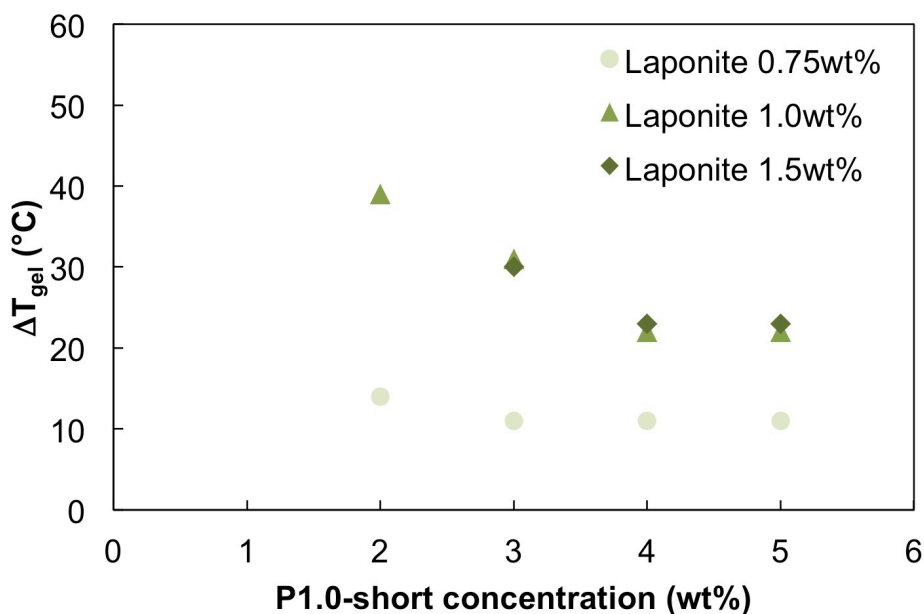
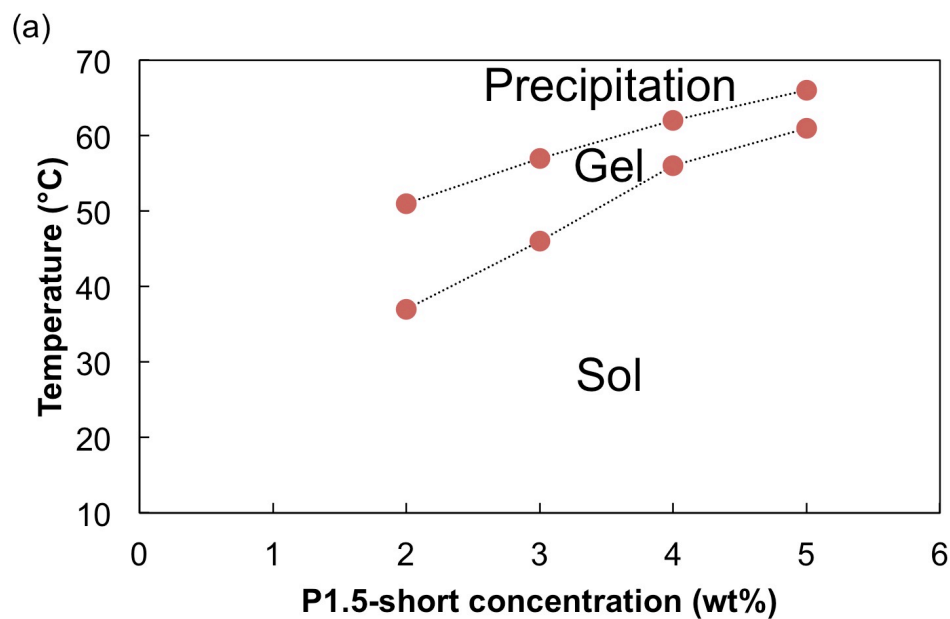


Figure 6. 13 Temperature range exhibiting gel for laponite/P1.0-short systems with different laponite concentrations.

As for the temperature range exhibiting gel-state ($\Delta T_{gel} = T_{precipitation}$ (gel-precipitation transition temperature) - $T_{gelation}$), as shown in Figure 6.13, ΔT_{gel} increased as the polymer concentration of P1.0-short decreased and the laponite concentration increased. This supported that the gel-state became dominant at room temperature due to the laponite network formation as mentioned before.

Figure 6.14 shows the phase diagram of laponite/P1.5-short aqueous systems determined by the tube inverting method. As well as the phase diagram of laponite/P1.0-short aqueous systems, the diagram consists of three regions indicating sol, gel, and precipitation. Figure 6.14 (a) is for the laponite/P1.5-short aqueous system with the laponite concentration of 0.75wt%, Figure 6.14 (b) is for the laponite/P1.5-short aqueous system with the laponite concentration of 1.0wt%, and Figure 6.14 (c) is for the laponite/P1.5-short aqueous system with the laponite

concentration of 1.5wt%. It was found that when the concentration of laponite became 0.75wt% or higher, the laponite/P1.5-short aqueous system formed gel. It was also found that the critical gelation polymer concentration (CGC) of laponite/P1.5-short aqueous system was 2.0wt%. In terms of $T_{gelation}$ and ΔT_{gel} , as shown in Figure 6.15 and Figure 6.16, the change of laponite/P1.5-short aqueous systems in $T_{gelation}$ and ΔT_{gel} according to the change in the concentration of laponite and PLGA-PEG-PLGA was in good agreement with that of laponite/P1.0-short aqueous systems.



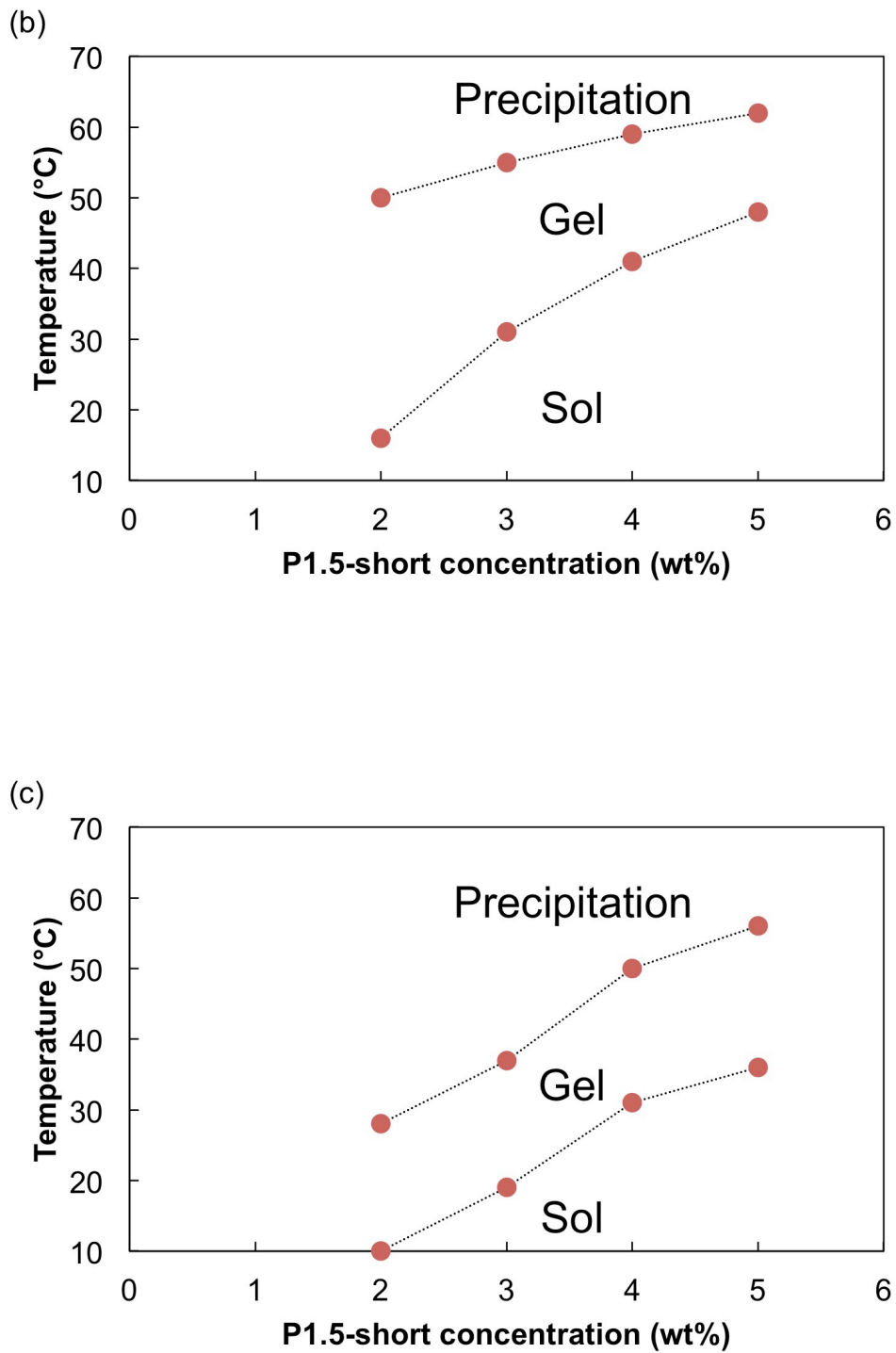


Figure 6. 14 Phase diagrams of Iaponite/P1.5-short aqueous systems with different Iaponite concentrations: (a) 0.75wt%, (b) 1.0wt%, and (c) 1.5wt%.

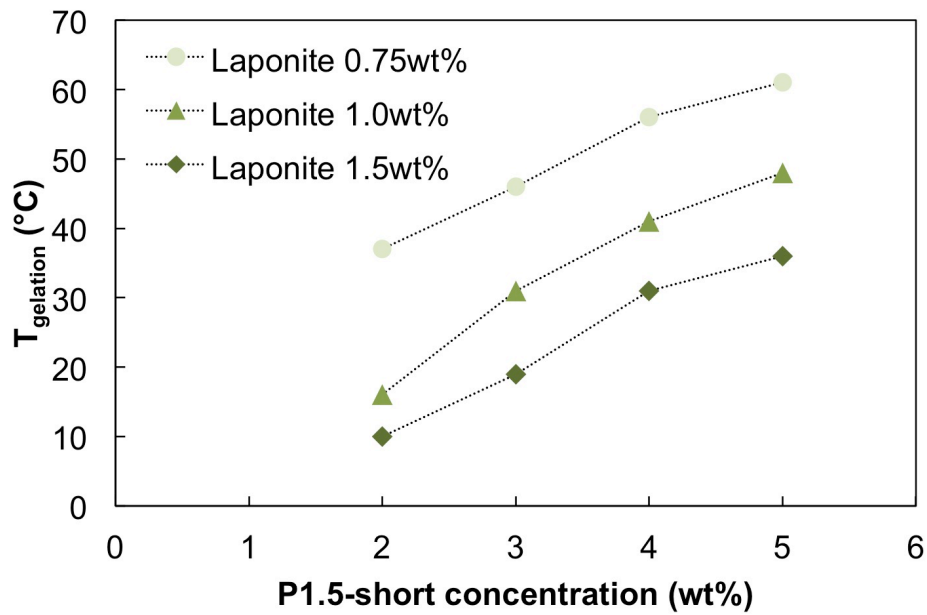


Figure 6. 15 Sol-gel transition temperatures of laponite/P1.5-short systems with different laponite concentrations.

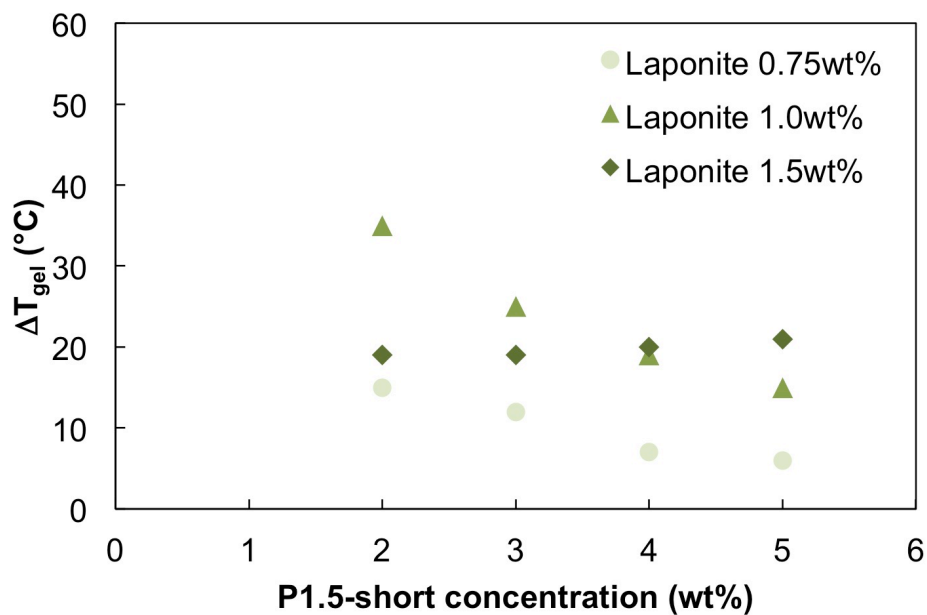
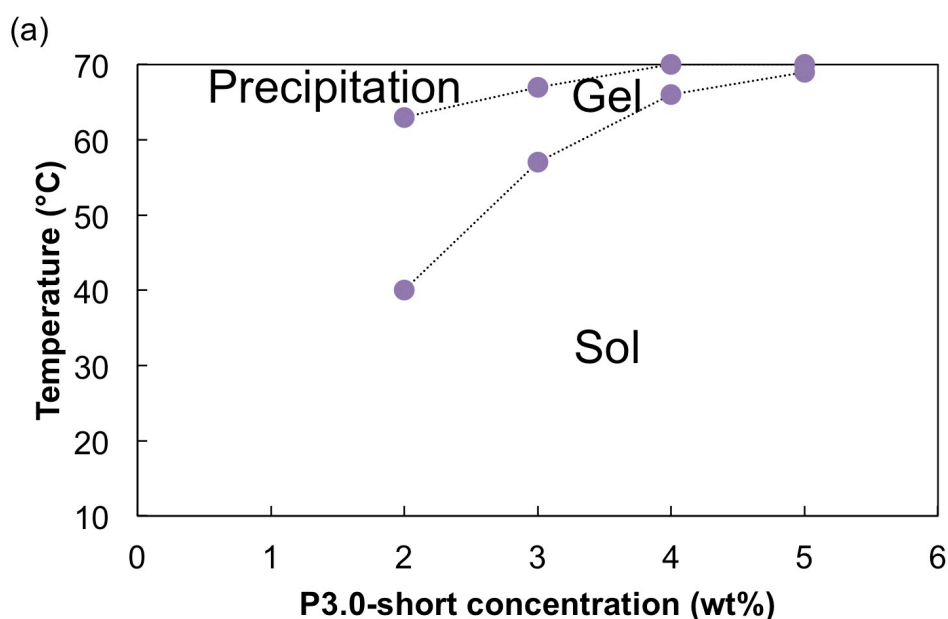


Figure 6. 16 Temperature range exhibiting gel for laponite/P1.5-short systems with different laponite concentrations.

Figure 6.17 shows the phase diagram of laponite/P3.0-short aqueous systems determined by the tube inverting method. As well as the phase diagram of laponite/P1.0-short aqueous systems, the diagram consists of three regions indicating sol, gel, and precipitation. Figure 6.17 (a) is for the laponite/P3.0-short aqueous system with the laponite concentration of 0.75wt%, Figure 6.17 (b) is for the laponite/P3.0-short aqueous system with the laponite concentration of 1.0wt%, and Figure 6.17 (c) is for the laponite/P3.0-short aqueous system with the laponite concentration of 1.5wt%. It was found that when the concentration of laponite became 0.5wt% or higher, the laponite/P3.0-short aqueous system formed gel. It was also found that the critical gelation polymer concentration (CGC) of laponite/P3.0-short aqueous system was 2.0wt%. In terms of $T_{gelation}$ and ΔT_{gel} , as shown in Figure 6.18 and Figure 6.19, the change of laponite/P3.0-short aqueous systems in $T_{gelation}$ and ΔT_{gel} according to the change in the concentration of laponite and PLGA-PEG-PLGA was in good agreement with that of laponite/P1.0-short aqueous systems.



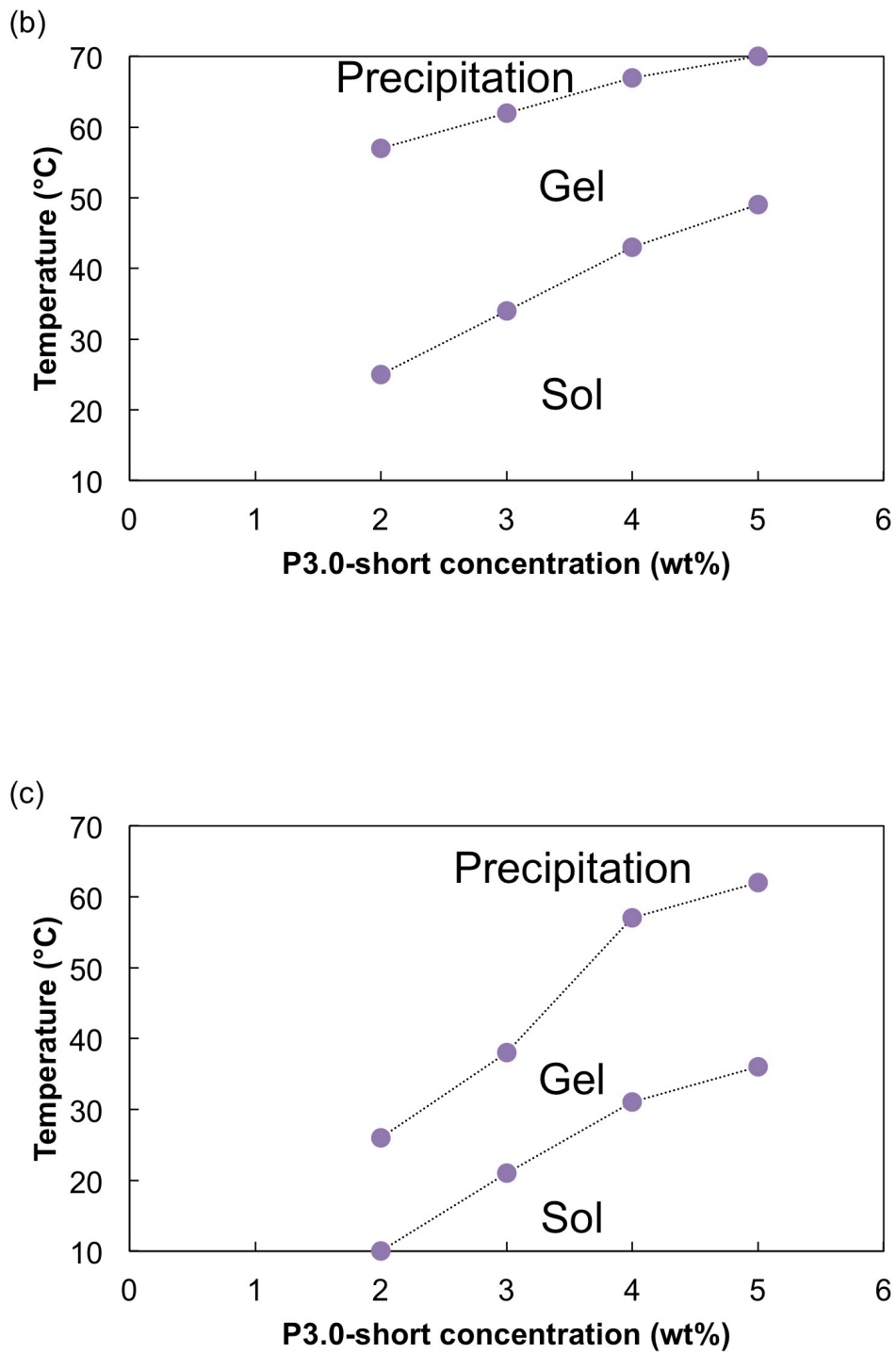


Figure 6. 17 Phase diagrams of Iaponite/P3.0-short aqueous systems with different Iaponite concentrations: (a) 0.75wt%, (b) 1.0wt%, and (c) 1.5wt%.

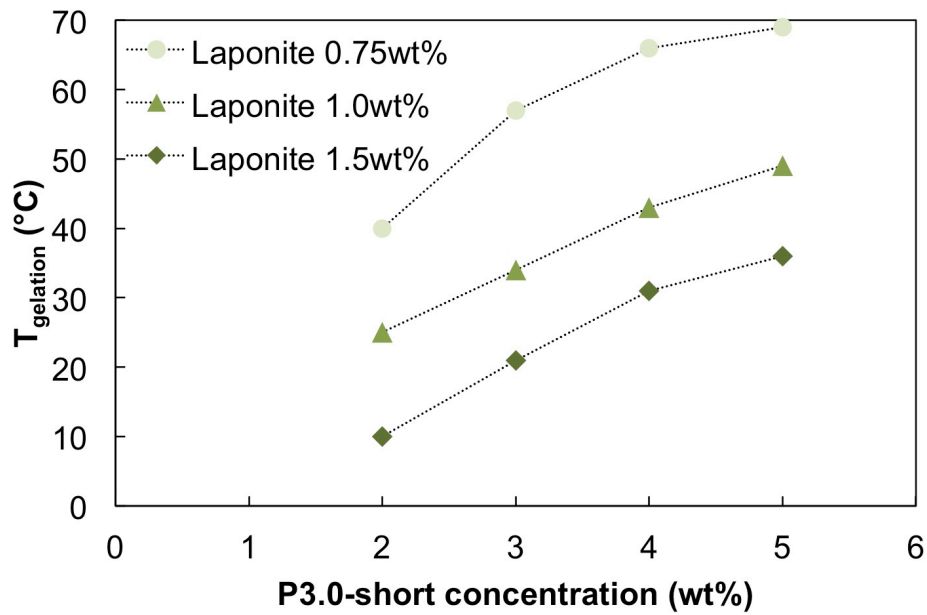


Figure 6. 18 Sol-gel transition temperatures of laponite/P3.0-short systems with different laponite concentrations.

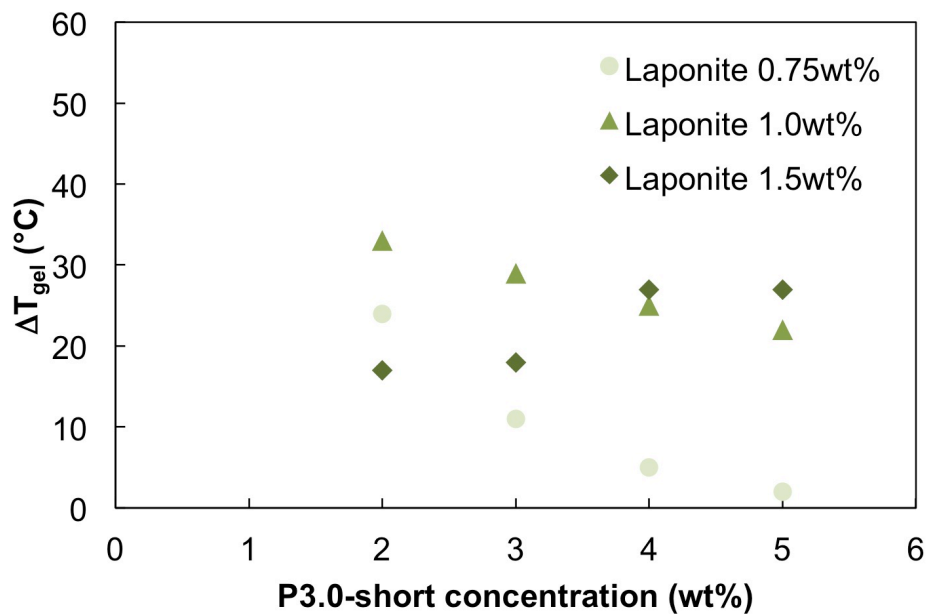


Figure 6. 19 Temperature range exhibiting gel for laponite/P3.0-short systems with different laponite concentrations.

In terms of the difference in the PEG-midblock molecular weights, it was found that $T_{gelation}$ increased as the PEG-midblock molecular weight of PLGA-PEG-PLGA increased as shown in Figure 6.20. This increase in $T_{gelation}$ according to the increase in the PEG-midblock molecular weight was also observed for pure PLGA-PEG-PLGA solution.¹¹²

In order to confirm the effect of molecular weight of PEG-midblock on the sol-gel transition temperature, phase diagram of pure PLGA-PEG-PLGAs with longer PLGA endblock (i.e. PLGA-PEG-PLGA able to form gels without laponite) was investigated as shown in Figure 6.21. From the phase diagram, the sol-gel transition temperatures were extracted and summarized in Figure 6.22. It was confirmed that the sol-gel transition temperature of PLGA-PEG-PLGA increased as the molecular weight of PEG-midblock increased. This tendency is in good agreement with the tendency observed in Figure 6.20.

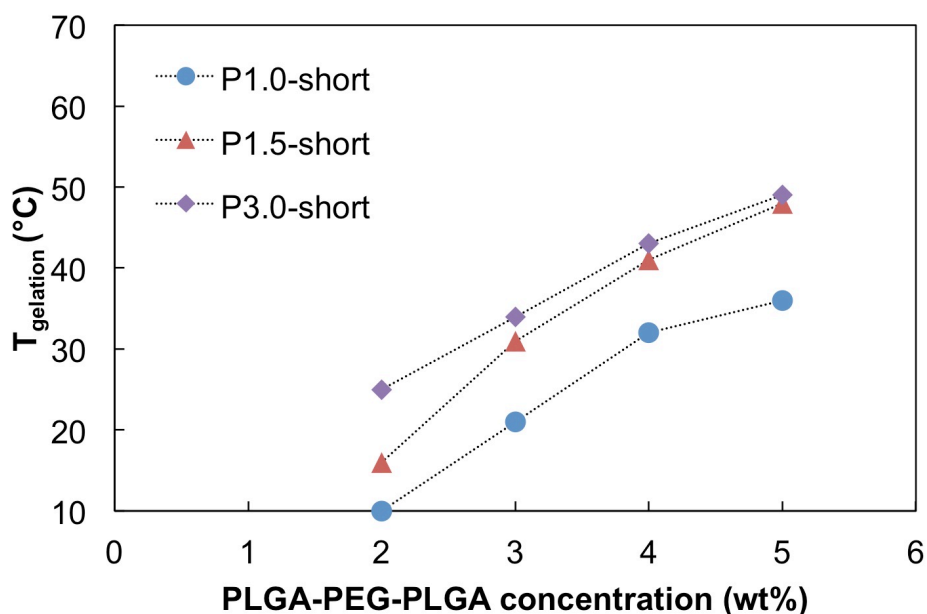


Figure 6. 20 Sol-gel transition temperature of laponite/PLGA-PEG-PLGA systems with different molecular weights of PEG midblock.

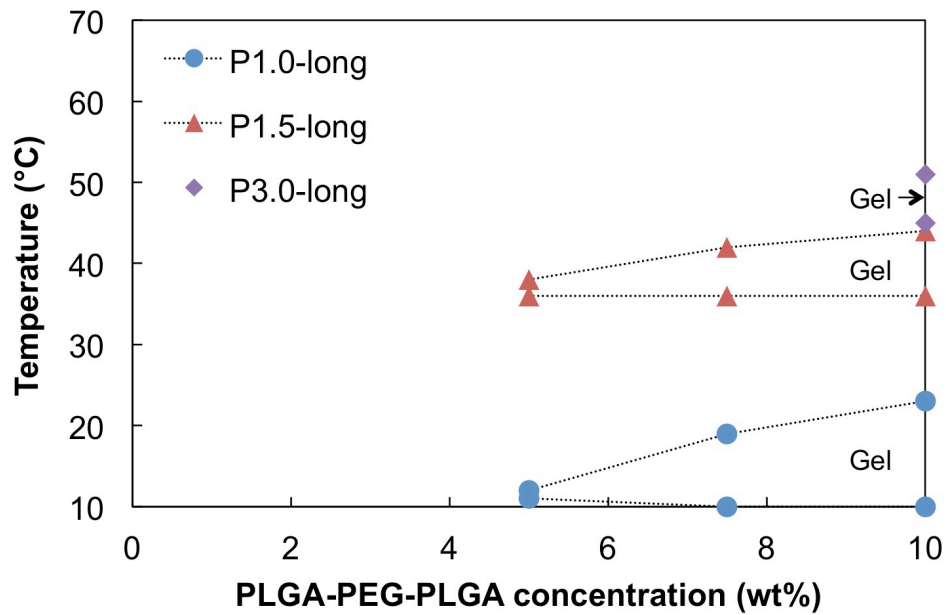


Figure 6. 21 Phase diagram of PLGA-PEG-PLGA aqueous solutions with long PLGA endblock.

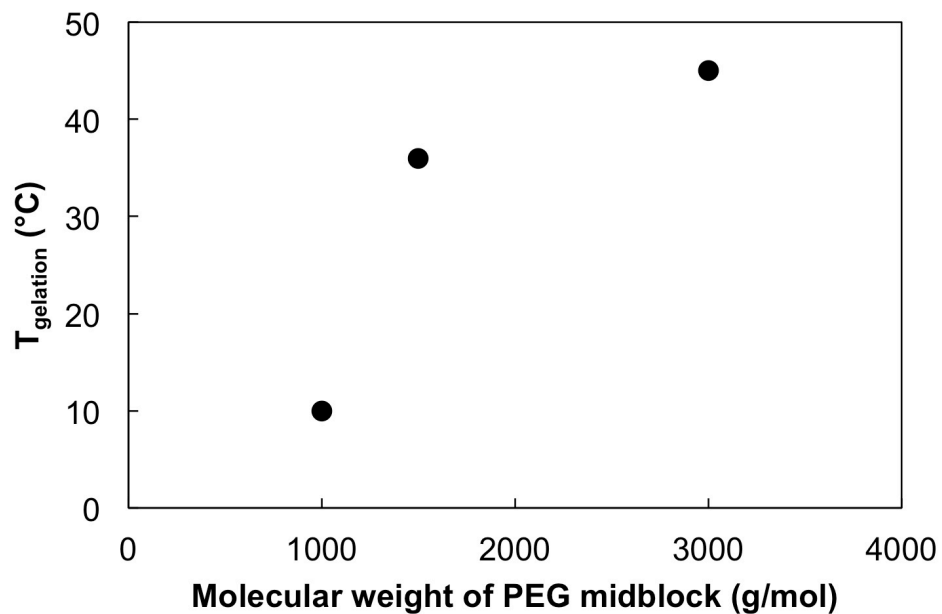


Figure 6. 22 Sol-gel transition temperatures of PLGA-PEG-PLGA aqueous solutions with long PLGA endblock.

Therefore, it was concluded that the nature of PLGA-PEG-PLGA (i.e. the nature of PEG midblock molecular weight affecting $T_{gelation}$) affects the $T_{gelation}$ of laponite/PLGA-PEG-PLGA solutions.

To summarize these results, $T_{gelation}$ change in laponite/PLGA-PEG-PLGA aqueous system is as follows. The larger the laponite concentration is, the lower the transition temperature becomes. The larger the PLGA-PEG-PLGA concentration is, the higher the transition temperature becomes. The larger the PEG midblock molecular weight is, the higher the transition temperature becomes.

Incidentally, the sol-gel transition of pure laponite aqueous suspensions was also confirmed. The pure laponite aqueous solutions did not indicate thermo-responsive sol-gel transition and the gelation occurred at the concentration equal to 2.0wt% or higher. Considering these facts, it was indicated that both laponite and PLGA-PEG-PLGA were the necessity for thermo-responsive gelation of laponite/PLGA-PEG-PLGA systems. It was also inferred that as $T_{gelation}$ lowered with the increase of laponite concentration, the laponite network was working as the main network of the hydrogel.

6.3.3. Rheological properties of laponite/PLGA-PEG-PLGA systems

The rheological properties of laponite/PLGA-PEG-PLGA aqueous systems were analyzed by DMA. The storage modulus G' and loss modulus G'' reflect the energy stored and dissipated, respectively. The sample is defined as gel when G' eclipses G'' . Figure 6.23 shows the storage modulus G' and the loss modulus G'' of laponite/P1.0-short system (1.0wt%/3.0wt%) as a function of temperature. At the temperature below $T_{gelation}$, G'' was much larger than G' exhibiting a typical liquid behavior. Around $T_{gelation}$, both G' and G'' abruptly increased and eventually G' exceeded G'' . This crossover point denotes $T_{gelation}$ in DMA. Above $T_{gelation}$, G' and G'' reached the maximum values, and then they eventually decreased with a trend to become precipitation. $T_{gelation}$ was determined about 20.4°C for laponite/P1.0-short system. This was quite close to $T_{gelation}$ of 21°C determined by the tube inverting method. The maximum value of G' of the laponite /P1.0-short system was 83.7 Pa around 28°C.

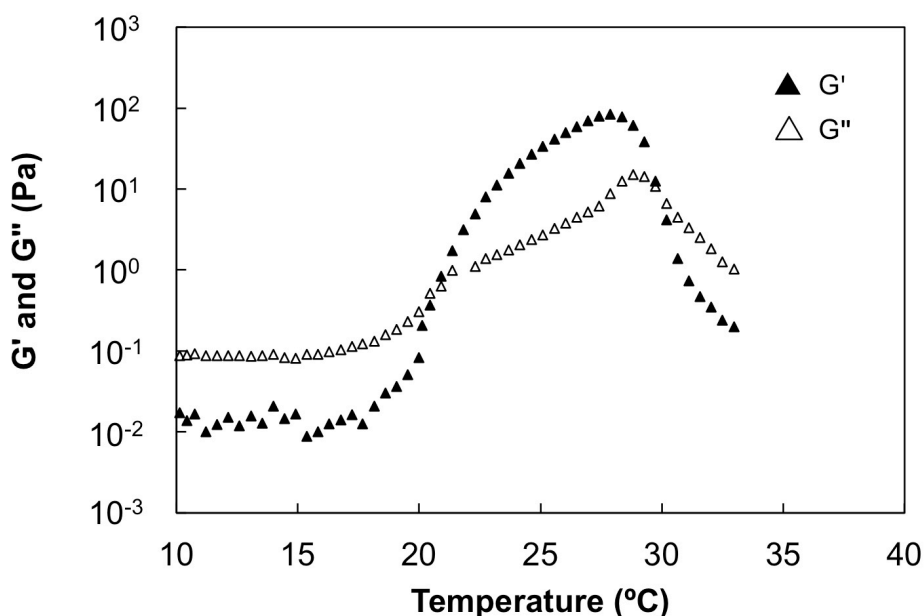


Figure 6. 23 DMA results as a function of temperature for laponite/P1.0-short systems (1.0wt%/5.0wt%).

Figure 6.24 shows G' and G'' of laponite/P1.0-short systems with different concentrations of P1.0-short. Storage modulus G' and loss modulus G'' are presented in Figure 6.24 (a) and Figure 6.24 (b) separately for visual lucidity. It was found that $T_{gelation}$ increased as the concentration of P1.0-short increased. This tendency is in good agreement with the results obtained from the tube inverting method. In detail, $T_{gelation}$ of laponite/P1.0-short system was 14.3°C at the P1.0-short concentration of 2.0wt%, 20.4°C at the P1.0-short concentration of 3.0wt%, 28.9°C at the P1.0-short concentration of 4.0wt%, and 33.1°C at the P1.0-short concentration of 5.0wt%. Some of $T_{gelation}$ traced the results obtained from the tube inverting method, and some of $T_{gelation}$ indicated lower temperature than that determined by the tube inverting method. Even though there are some quantitative gaps between the DMA results and the results from tube inverting method, the tube inverting method is yet of great utility in order to determine $T_{gelation}$ because the method shows the exact temperature at which the solution macroscopically forms gel as it is actually used as thermo-responsive material.

As for the maximum values of storage modulus G' and loss modulus G'' , G' was almost stable or slightly decreased, while G'' rapidly increased as the P1.0-short concentration increased. It was indicated that the viscous component in the system was enhanced by the increase in P1.0-short concentration. In other words, the rheological properties could be controlled finely by tuning the concentration of P1.0-short. It is inferred that laponite was working as the main network of the hydrogel and PLGA-PEG-PLGA supported the network of laponite.

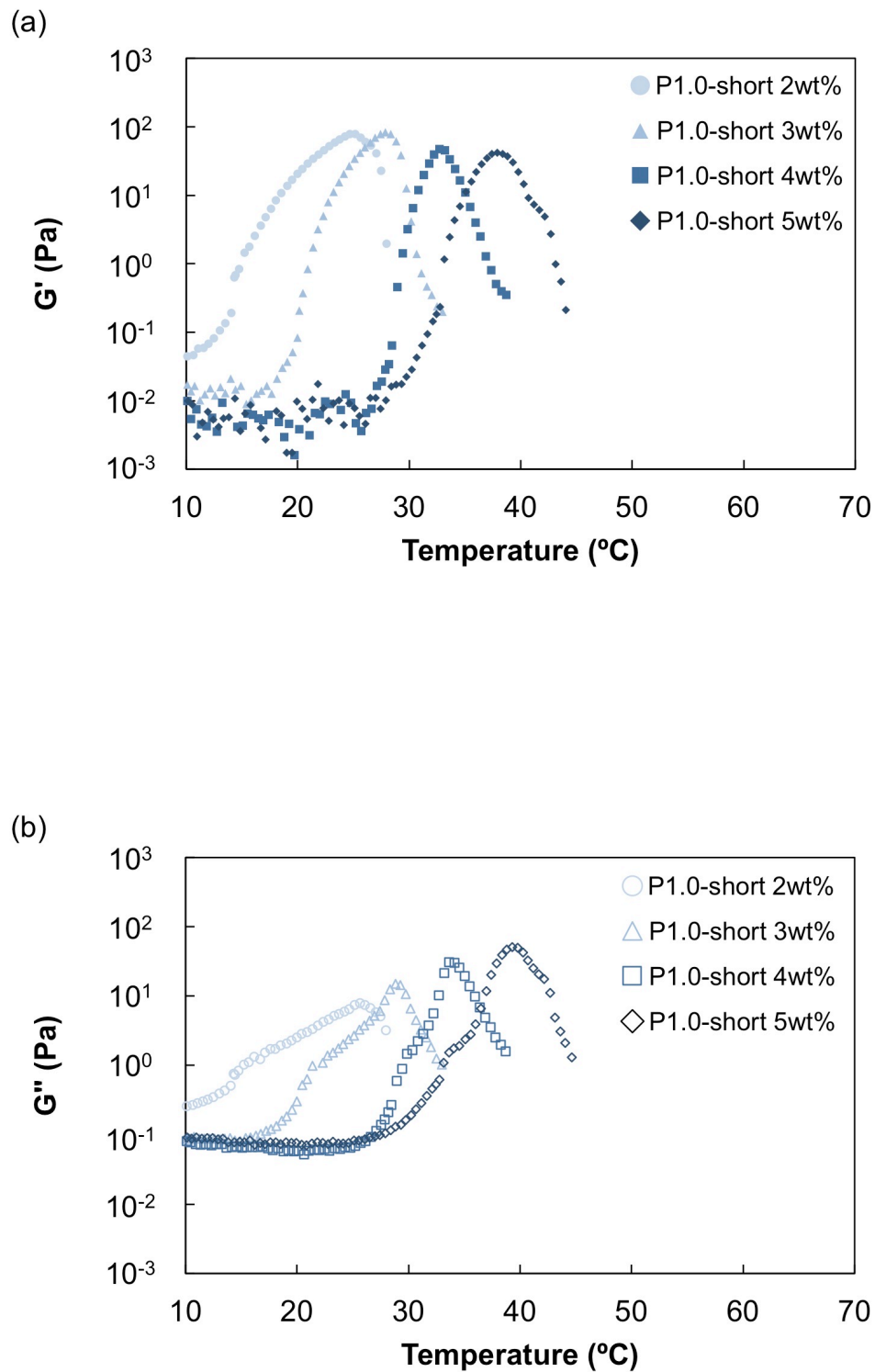


Figure 6. 24 DMA results as a function of temperature for laponite/P1.0-short systems with 1.0wt% of laponite and with different P1.0-short concentrations: (a) G' and (b) G'' .

Figure 6.25 shows storage modulus G' and loss modulus G'' of laponite/P1.5-short aqueous systems. As well as the laponite/P1.0-short systems, $T_{gelation}$ shifted to higher temperatures as the concentration of P1.5-short increased. In detail, $T_{gelation}$ of laponite/P1.5-short system was 16.6°C at the P1.5-short concentration of 2.0wt%, 27.6°C at the P1.5-short concentration of 3.0wt%, 34.6°C at the P1.5-short concentration of 4.0wt%, and 36.7°C at the P1.5-short concentration of 5.0wt%. Furthermore, $T_{gelation}$ of laponite/P1.5-short systems was higher than that of laponite/P1.0-short, respectively, regardless of PLGA-PEG-PLGA concentration. This was also in good agreement with the results obtained from the tube inverting method.

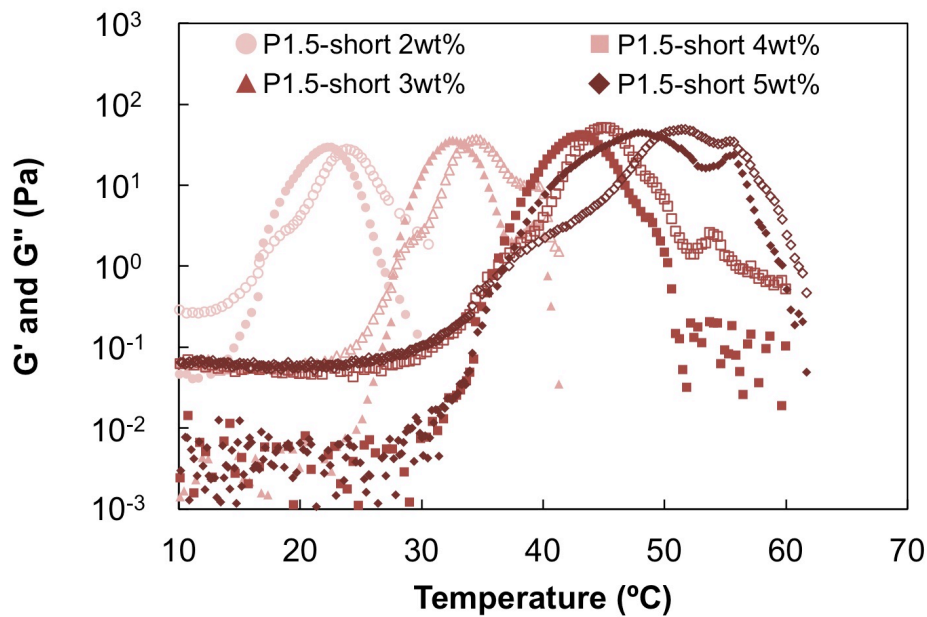


Figure 6. 25 DMA results as a function of temperature for laponite/P1.5-short systems with 1.0wt% of laponite and with different P1.5-short concentrations: solid for G' and hollow for G'' .

6.3.4. Microstructural analysis of laponite/PLGA-PEG-PLGA systems

Figure 6.26 and Figure 6.27 shows the cryo-TEM images of laponite/P1.0-short systems (1.0wt%/5.0wt%). Figure 6.26 shows the sol-state laponite/P1.0-short system and Figure 6.27 shows the gel-state laponite/P1.0-short system. In sol-state, the network of laponite could be clearly seen and the spherical micelle structures were dispersed homogenously. On the other hand, in gel-state, the network of laponite could hardly be seen and the heterogeneous dark part possibly due to the aggregation of micelles was observed.

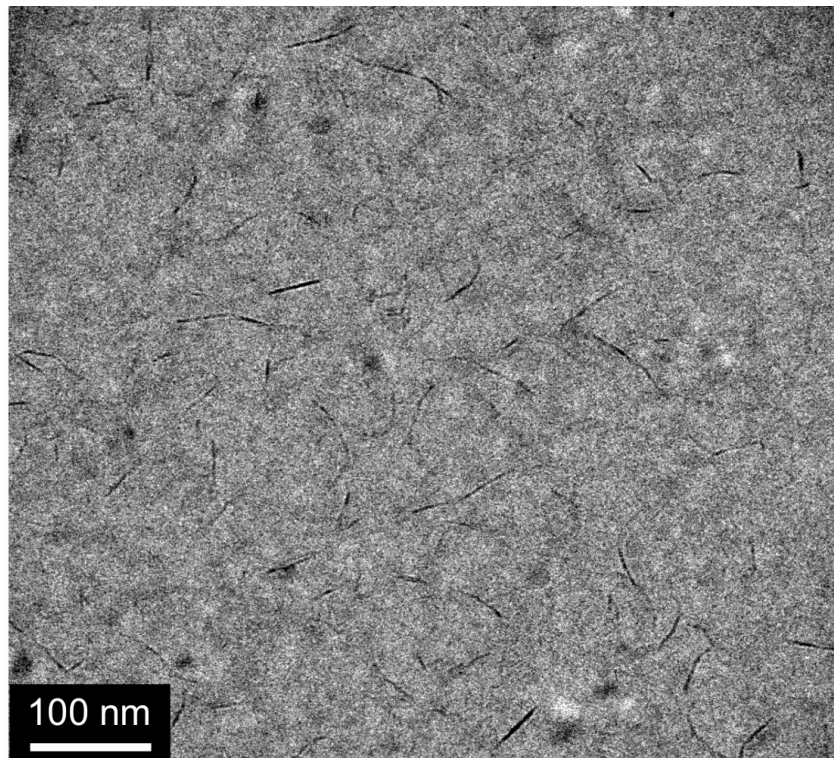


Figure 6. 26 Cryo-TEM images of laponite/P1.0-short system (1wt%/5wt%) in sol state.

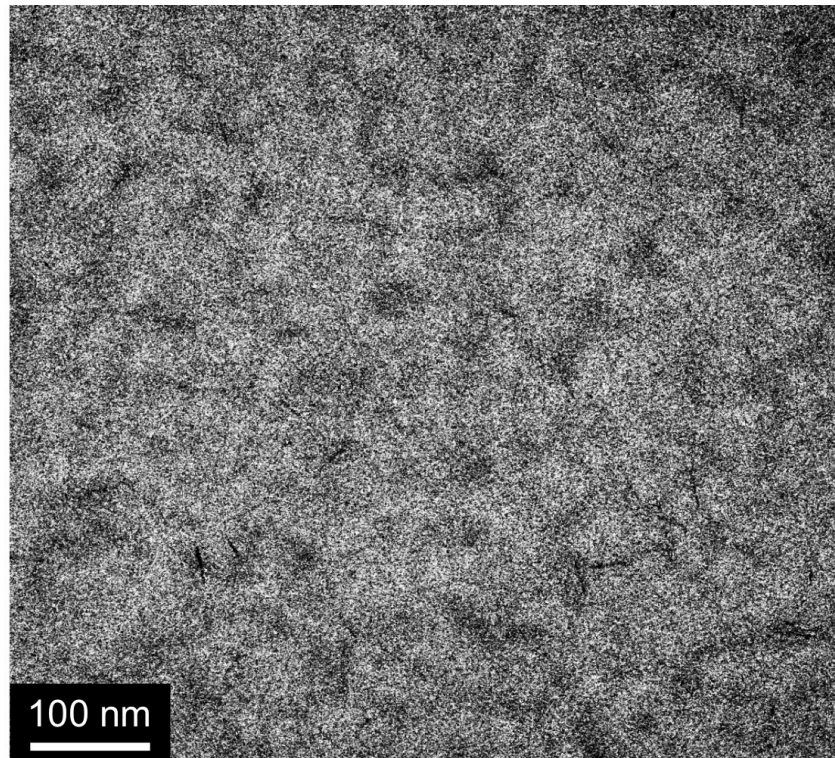


Figure 6. 27 Cryo-TEM images of laponite/P1.0-short system (1wt%/5wt%) in gel state.

From these results, the assumed mechanism of gelation for laponite/PLGA-PEG-PLGA was summarized in Figure 6.28 and described as follows. At the temperature well below $T_{gelation}$, unimers, individual micelles, and aggregated micelles of PLGA-PEG-PLGA coexist in the sol state. At the same time, laponite gradually forms short network structures by self-assembly as shown in Figure 6.28 (a). As increasing the temperature, the fraction of unimers decreased and the size of aggregated micelles rapidly increased. Due to the further increase in temperature, micelles were percolated and the macroscopic self-assembly of micelles was induced involving the preformed laponite network by hydrophobic interaction as shown in Figure 6.28 (b). Thus, the laponite/PLGA-PEG-PLGA system becomes opaque gels.

When the temperature was raised furthermore, the PEG midblock in PLGA-PEG-PLGA undergoes dehydration. Eventually, the strong hydrophobic interactions among micelles and laponite networks induce the large-scale aggregation and the laponite/PLGA-PEG-PLGA system becomes precipitate.

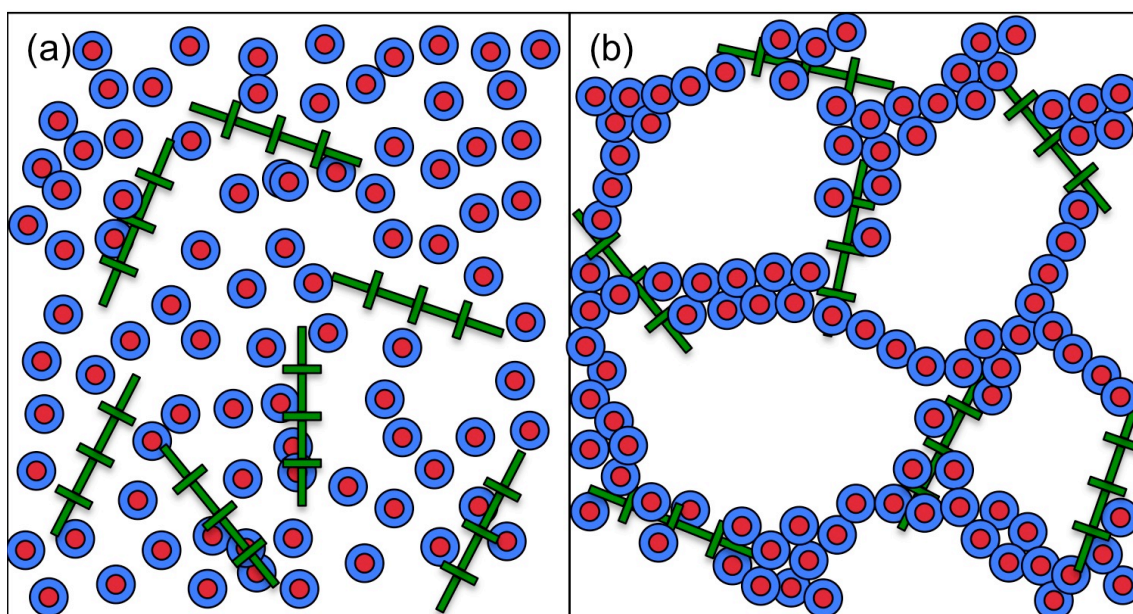


Figure 6. 28 Schematic images of gelation for laponite/PLGA-PEG-PLGA systems: (a) in sol state and (b) in gel state.

6.4. Summary of this chapter

The systematical analysis on thermo-responsive sol-gel transition behavior of laponite/PLGA-PEG-PLGA aqueous system was carried out as well as the rheological and microstructural analysis. For the purpose, the molecular weight, the PEG/PLGA block ratio of PLGA-PEG-PLGA and the concentration of PLGA-PEG-PLGA and laponite were systematically changed. It was found that laponite/PLGA-PEG-PLGA aqueous system with PLGA-PEG-PLGA with PEG/PLGA ratio of ~ 1.0 formed gels, while the pure PLGA-PEG-PLGA aqueous solutions with PEG/PLGA ratio of ~ 1.0 did not form gels regardless of concentration. This PEG/PLGA ratio of ~ 1.0 was highest ratio among the PLGA-PEG-PLGA hydrogels reported previously. It was also found that the sol-gel transition temperatures depended largely on the concentrations of laponite and PLGA-PEG-PLGA and the molecular weight of PEG midblock. In detail, the transition temperatures increased as the PLGA-PEG-PLGA concentration increased, and decreased as the laponite concentration increased. Also, by changing the concentrations of laponite and PLGA-PEG-PLGA, the rheological properties were tuned finely. From the rheological analysis by tube inverting test and DMA and the microstructural analysis by cryo-TEM, the gelation may be attributed to the large-scale self-assembly of micelles with laponite network due to the balance of hydrophobic/hydrophilic accommodated by over-hydrophilic PLGA-PEG-PLGA and laponite with slightly hydrophobic surfaces.

Chapter 7. Summary

In order to enhance the functionality of nanofiber-sheets and hydrogels, the fabrication of thinner nanofibers from crystalline polymers and copolymers with strong polymer interactions, and the fabrication of hydrogels with low amount of copolymers with weak polymer interactions were examined. The results were summarized as follows:

7.1. Summary on nanofiber fabrication

In order to develop thinner nanofiber-sheets from materials other than amorphous homopolymers, the fabrication conditions were systematically studied using three different types of polymers. As for crystalline polymers with strong polymer interactions, sPP nanofibers with the average diameter of 230 nm were successfully fabricated by using methyl-cyclohexane as a solvent. It was found that for the fabrication of nanofibers with crystalline polymers, it is crucial to consider the entanglement of the molecules and hence to choose the moderate gelation speed and the lower specific viscosity of the crystalline polymer solution at $\sim k_f C_e$. As for random copolymers, MPC nanofibers with the average diameter of ~ 160 nm were successfully produced by electrospinning using ethanol as a solvent. It was found that for random copolymer, the viscosity of solutions should be considered for the fiber fabrication as well as amorphous homo-polymers. As for triblock copolymer, SIS nanofibers with the average diameter of 350 nm were obtained by using the DMF/toluene mixed solvents. It was found that for triblock copolymers, tuning the self-assembly of triblock copolymer by changing the solubility parameters of solvents could be useful for the nanofiber formation. Therefore, nanofibers from polymers with strong polymer interactions could be obtained by the careful selection of solvents to weaken the polymer interactions.

7.2. Summary on hydrogel fabrication

In order to develop thermo-responsive hydrogels with low amount of copolymers with weak polymer interactions, the new types of hydrogels made from PLGA-PEG-PLGA copolymers with less hydrophobic interactions and clay sheets (laponite) were developed and systematically studied. The laponite/PLGA-PEG-PLGA aqueous solution with PLGA-PEG-PLGA at PEG/PLGA ratio of ~ 1.0 formed gels at the minimum concentration of 2.75wt%. It was found that the sol-gel transition temperatures depended largely on the concentrations of laponite, PLGA-PEG-PLGA, and the molecular weight of PEG midblock. It was also found that by changing the concentrations of laponite and PLGA-PEG-PLGA, the rheological properties were tuned finely. The mechanism of gelation could be attributed to the large-scale self-assembly of micelles supported by the laponite network. This is due to the balance of hydrophobic/hydrophilic from too hydrophilic PLGA-PEG-PLGA and laponite with slightly hydrophobic surfaces.

List of publications

Chapter 3:

- T. Maeda, K. Takaesu, A. Hotta, “Syndiotactic polypropylene nanofibers obtained from solution electrospinning process at ambient temperature”, Journal of Applied Polymer Science, in press.

Chapter 4:

- T. Maeda, K. Hagiwara, S. Yoshida, T. Hasebe, A. Hotta, “Preparation and characterization of 2-methacryloyloxyethyl phosphorylcholine polymer nanofibers prepared via electrospinning for biomedical materials”, Journal of Applied Polymer Science, Vol. 131, 40606 (2014).

Works not covered in chapters:

- N. Oyama, H. Minami, D. Kawano, M. Miyazaki, T. Maeda, K. Toma, A. Hotta, K. Nagahama, “A nanocomposite approach to develop biodegradable thermogels exhibiting excellent cell-compatibility for injectable cell delivery”, Biomaterials Science, Vol. 2, pp.1057-1062 (2014).
- T. Otsuka, T. Maeda, A. Hotta, “Effects of salt concentrations of the aqueous peptide-amphiphile solutions on the sol-gel transitions, the gelation speed, and the gel characteristics”, The Journal of Physical Chemistry Part B, Vol. 118 (39), pp.11537-11545 (2014).
- K. Bito, T. Maeda, K. Hagiwara, S. Yoshida, T. Hasebe, A. Hotta, “Poly (2-methacryloyloxyethyl phosphorylcholine) (MPC) nanofibers coated with micro-patterned diamond-like carbon (DLC) for the controlled drug release”, Journal of Biorheology, Vol. 29, pp. 51-55 (2015).

- S. Mizuno, T. Maeda, C. Kanemura, A. Hotta, “Biodegradability, reprocessability, and mechanical properties of polybutylene succinate (PBS) photografted by hydrophilic or hydrophobic membranes”, *Polymer Degradation and Stability*, Vol. 117, pp. 58-65 (2015).

Acknowledgement

This work was conducted under the supervision of Professor Atsushi Hotta. First of all, I would like to express my sincere appreciation to my supervisor, Professor Atsushi Hotta for the continuous support for this Ph.D. work and the related work I have done in his group. He showed me the attitude as a researcher and gave advices both on research and career path.

Besides my supervisor, I would like to greatly appreciate Professor Tetsuya Suzuki, and Professor Hiroaki Onoe, and Professor Satoko Fujioka giving me an opportunity for fruitful discussion and reviewing my Ph.D. thesis.

I also would like to express my great appreciation to faculty members in Department of Mechanical Engineering. I learned a lot on education and the attitude as a faculty member.

My appreciation also goes to the member of Hotta group: Ms. Rena Asakawa, Mr. Yoshinori Orimo, Mr. Takato Shiraishi, Mr. Masaaki Mori, Mr. Masaki Akiyama, Mr. Tetsu Ouchi, Ms. Chiharu Kanemura, Mr. Daisei Tanaka, Mr. Atsushi Nakano, Ms. Jun Fujii, and Mr. Norihiro Matsumoto, Mr. Takahiro Otsuka, Ms. Natsumi Kobayashi, Mr. Koji Nakamura, Mr. Katsuya Hagiwara, Mr. Yuta Yamagishi, Mr. Kohei Iwase, Ms. Yukako Oishi, Mr. Ryohei Mizukami, Ms. Sawako Mizuno, Ms. Ayana Murano, Mr. Shun Yagi, Mr. Joto Yasuda, Mr. Fuyuaki Endo, Mr. Ryusuke Okoshi, Mr. Naruki Kurokawa, Ms. Yui Kurokawa, Mr. Kazuhisa Tsuji, Mr. Kenta Bito, Mr. Makoto Miyazaki, Mr. Taku Aoki, Mr. Shunta Kimura, Mr. Satoshi Shirahata, Ms. Megumi Nakadoi, Mr. Kenji Hirashima, Mr. Masashi Yamamoto, Mr. Yuya Ishii, Ms. Saya Kamitabira, Mr. Takashi Kikuchi, Mr. Shunsuke Tazawa, Ms. Narumi Nozawa, and Mr. Ryosuke Yamazaki. Especially, I would like to express my thanks to my fellow

lab-mates: Mr. Akihiro Aso, Ms. Alice Gros, Mr. Keita Takaesu, Mr. Hiroki Tashiro, Mr. Akihito Mori, Mr. Soki Yoshida, and Mr. Kentaro Watanabe. I also appreciate Dr. Jun Takahashi showing the attitude as a Ph.D. student.

My appreciation also goes to the member of Suzuki group. I spent plenty of quality time with them through the summer school and the daily research activities.

I also appreciate “Global environmental system leaders (GESL) program”. This work was supported in part by the MEXT Grant-in-Aid for the Program for Leading Graduate Schools. Through the activities of GESL program, I learned a lot on environmental issues and politics as well as technology.

I also really appreciate the people I met in University of California, Santa Barbara during the international training of GESL program. First of all, I appreciate Professor Craig J. Hawker giving me an opportunity to visit his group and learn the synthesis of polymers. There, Mr. Jeffery Gopez taught me the basis of polymer synthesis. Fortunately, I could meet many brilliant researchers of Japanese industrial companies. I really appreciate Mr. Kazuhiko Tsurui, Mr. Takuya Murakami, and Mr. Takashi Kawamori. And I also appreciate Ms. Colleen Kerry who supported my stay in Santa Barbara.

I also appreciate Mr. Masaki Nakaya working for KIRIN Co. Ltd. giving me an opportunity to work collaboratively and to learn the industrial point of view.

Last but not the least, I would like to express my sincere appreciation to my parents. They agreed with my opinion to go on to Ph.D. course and supported me. Moreover, since I left home to enter Keio University, they have cared a lot about my activities.

References

1. Reneker, D. H.; Yarin, A. L.; Zussman, E.; Xu, H., Electrospinning of nanofibers from polymer solutions and melts. *Advances in Applied Mechanics* **2007**, *41*, 43-195.
2. Agarwal, S.; Wendorff, J. H.; Greiner, A., Use of electrospinning technique for biomedical applications. *Polymer* **2008**, *49* (26), 5603-5621.
3. Thavasi, V.; Singh, G.; Ramakrishna, S., Electrospun nanofibers in energy and environmental applications. *Energy & Environmental Science* **2008**, *1* (2), 205-221.
4. Cavaliere, S.; Subianto, S.; Savych, I.; Jones, D. J.; Roziere, J., Electrospinning: designed architectures for energy conversion and storage devices. *Energy & Environmental Science* **2011**, *4* (12), 4761-4785.
5. Jang, J., Conducting polymer nanomaterials and their applications. In *Emissive Materials Nanomaterials*, Springer Berlin Heidelberg: 2006; pp 189-260.
6. Ding, B.; Wang, M. R.; Yu, J. Y.; Sun, G., Gas sensors based on electrospun nanofibers. *Sensors* **2009**, *9* (3), 1609-1624.
7. Teo, W. E.; Ramakrishna, S., Electrospun nanofibers as a platform for multifunctional, hierarchically organized nanocomposite. *Composites Science and Technology* **2009**, *69* (11-12), 1804-1817.
8. Chronakis, I. S., Novel nanocomposites and nanoceramics based on polymer nanofibers using electrospinning process - A review. *Journal of Materials Processing Technology* **2005**, *167* (2-3), 283-293.
9. Zucchelli, A.; Focarete, M. L.; Gualandi, C.; Ramakrishna, S., Electrospun nanofibers for enhancing structural performance of composite materials. *Polymers for Advanced Technologies* **2011**, *22* (3), 339-349.
10. Wu, X. F.; Yarin, A. L., Recent progress in interfacial toughening and damage self-healing of polymer composites based on electrospun and solution-blown nanofibers: An overview. *Journal of Applied Polymer Science* **2013**, *130* (4), 2225-2237.

11. Mohammadzadehmoghadam, S.; Dong, Y.; Davies, I. J., Recent progress in electrospun nanofibers: reinforcement effect and mechanical performance. *Journal of Polymer Science Part B-Polymer Physics* **2015**, *53* (17), 1171-1212.
12. Barnes, C. P.; Sell, S. A.; Boland, E. D.; Simpson, D. G.; Bowlin, G. L., Nanofiber technology: Designing the next generation of tissue engineering scaffolds. *Advanced Drug Delivery Reviews* **2007**, *59* (14), 1413-1433.
13. Yoo, H. S.; Kim, T. G.; Park, T. G., Surface-functionalized electrospun nanofibers for tissue engineering and drug delivery. *Advanced Drug Delivery Reviews* **2009**, *61* (12), 1033-1042.
14. Jang, J. H.; Castano, O.; Kim, H. W., Electrospun materials as potential platforms for bone tissue engineering. *Advanced Drug Delivery Reviews* **2009**, *61* (12), 1065-1083.
15. Peppas, N. A.; Hilt, J. Z.; Khademhosseini, A.; Langer, R., Hydrogels in biology and medicine: From molecular principles to bionanotechnology. *Advanced Materials* **2006**, *18* (11), 1345-1360.
16. Hoare, T. R.; Kohane, D. S., Hydrogels in drug delivery: Progress and challenges. *Polymer* **2008**, *49* (8), 1993-2007.
17. Yu, L.; Ding, J. D., Injectable hydrogels as unique biomedical materials. *Chemical Society Reviews* **2008**, *37* (8), 1473-1481.
18. Jeong, B.; Kim, S. W.; Bae, Y. H., Thermosensitive sol-gel reversible hydrogels. *Advanced Drug Delivery Reviews* **2012**, *64*, 154-162.
19. Alexander, A.; Ajazuddin; Khan, J.; Saraf, S.; Saraf, S., Poly(ethylene glycol)-poly(lactic-co-glycolic acid) based thermosensitive injectable hydrogels for biomedical applications. *Journal of Controlled Release* **2013**, *172* (3), 715-729.
20. Radhakrishnan, J.; Krishnan, U. M.; Sethuraman, S., Hydrogel based injectable scaffolds for cardiac tissue regeneration. *Biotechnology Advances* **2014**, *32* (2), 449-461.
21. Matanovic, M. R.; Kristl, J.; Grabnar, P. A., Thermoresponsive polymers: Insights into decisive hydrogel characteristics, mechanisms of gelation, and promising biomedical applications. *International Journal of Pharmaceutics* **2014**, *472* (1-2),

- 262-275.
22. Dou, Q. Q.; Liow, S. S.; Ye, E. Y.; Lakshminarayanan, R.; Loh, X. J., Biodegradable thermogelling polymers: working towards clinical applications. *Advanced Healthcare Materials* **2014**, *3* (7), 977-988.
 23. Sill, T. J.; von Recum, H. A., Electrospinning: Applications in drug delivery and tissue engineering. *Biomaterials* **2008**, *29* (13), 1989-2006.
 24. Hynes, R. O., The extracellular matrix: Not just pretty fibrils. *Science* **2009**, *326* (5957), 1216-1219.
 25. Nakano, A.; Miki, N.; Hishida, K.; Hotta, A., Solution parameters for the fabrication of thinner silicone fibers by electrospinning. *Physical Review E* **2012**, *86* (1).
 26. Kwon, I. K.; Kidoaki, S.; Matsuda, T., Electrospun nano- to microfiber fabrics made of biodegradable copolyesters: structural characteristics, mechanical properties and cell adhesion potential. *Biomaterials* **2005**, *26* (18), 3929-3939.
 27. Aghdam, R. M.; Najarian, S.; Shakhesi, S.; Khanlari, S.; Shaabani, K.; Sharifi, S., Investigating the effect of PGA on physical and mechanical properties of electrospun PCL/PGA blend nanofibers. *Journal of Applied Polymer Science* **2012**, *124* (1), 123-131.
 28. Spearman, S. S.; Rivero, I. V.; Abidi, N., Influence of polycaprolactone/polyglycolide blended electrospun fibers on the morphology and mechanical properties of polycaprolactone. *Journal of Applied Polymer Science* **2014**, *131* (9).
 29. Zhang, Z. Y.; Liu, S.; Jing, X. B.; Huang, Y. B., Electrospun PLA/MWCNT composite nanofibers for combined chemo- and photothermal therapy with near-infrared radiation. *Journal of Controlled Release* **2015**, *213*, E149-E150.
 30. Pant, H. R.; Pokharel, P.; Joshi, M. K.; Adhikari, S.; Kim, H. J.; Park, C. H.; Kim, C. S., Processing and characterization of electrospun graphene oxide/polyurethane composite nanofibers for stent coating. *Chemical Engineering Journal* **2015**, *270*, 336-342.
 31. Liu, Z. Y.; Yan, J. J.; Miao, Y. E.; Huang, Y. P.; Liu, T. X., Catalytic and antibacterial activities of green-synthesized silver nanoparticles on electrospun

- polystyrene nanofiber membranes using tea polyphenols. *Composites Part B-Engineering* **2015**, *79*, 217-223.
32. Farooq, A.; Yar, M.; Khan, A. S.; Shahzadi, L.; Siddiqi, S. A.; Mahmood, N.; Rauf, A.; Qureshi, Z. U.; Manzoor, F.; Chaudhry, A. A.; Rehman, I. U., Synthesis of piroxicam loaded novel electrospun biodegradable nanocomposite scaffolds for periodontal regeneration. *Materials Science & Engineering C-Materials for Biological Applications* **2015**, *56*, 104-113.
33. Gu, H. Q.; Hou, Y. J.; Xu, F.; Wang, S. H., Electrospinning preparation, thermal, and luminescence properties of Eu-2(BTP)3(Phen)2 complex doped in PMMA. *Colloid and Polymer Science* **2015**, *293* (8), 2201-2208.
34. Pham, Q. P.; Sharma, U.; Mikos, A. G., Electrospinning of polymeric nanofibers for tissue engineering applications: A review. *Tissue Engineering* **2006**, *12* (5), 1197-1211.
35. Slaughter, B. V.; Khurshid, S. S.; Fisher, O. Z.; Khademhosseini, A.; Peppas, N. A., Hydrogels in Regenerative Medicine. *Advanced Materials* **2009**, *21* (32-33), 3307-3329.
36. Mano, J. F., Stimuli-responsive polymeric systems for biomedical applications. *Advanced Engineering Materials* **2008**, *10* (6), 515-527.
37. Kabanov, A. V.; Batrakova, E. V.; Alakhov, V. Y., Pluronic block copolymers as novel polymer therapeutics for drug and gene delivery. *Journal of Controlled Release* **2002**, *82* (2-3), 189-212.
38. Zentner, G. M.; Rathi, R.; Shih, C.; McRea, J. C.; Seo, M. H.; Oh, H.; Rhee, B. G.; Mestecky, J.; Moldoveanu, Z.; Morgan, M.; Weitman, S., Biodegradable block copolymers for delivery of proteins and water-insoluble drugs. *Journal of Controlled Release* **2001**, *72* (1-3), 203-215.
39. Oyama, N.; Minami, H.; Kawano, D.; Miyazaki, M.; Maeda, T.; Toma, K.; Hotta, A.; Nagahama, K., A nanocomposite approach to develop biodegradable thermogels exhibiting excellent cell-compatibility for injectable cell delivery. *Biomaterials Science* **2014**, *2* (8), 1057-1062.
40. Hildebrand, J. H.; Scott, R. L., *The Solubility of Nonelectrolytes*. 3rd ed.; Reinhold:

- New York, 1950; p 488.
41. Small, P. A., SOME FACTORS AFFECTING THE SOLUBILITY OF POLYMERS. *Journal of Applied Chemistry* **1953**, 3 (2), 71-80.
 42. Hansen, C. M., *Hansen solubility parameters : a user's handbook*. CRC Press: Boca Raton, 2007; p 519.
 43. Shin, Y. M.; Hohman, M. M.; Brenner, M. P.; Rutledge, G. C., Electrospinning: A whipping fluid jet generates submicron polymer fibers. *Applied Physics Letters* **2001**, 78 (8), 1149-1151.
 44. Reneker, D. H.; Yarin, A. L., Electrospinning jets and polymer nanofibers. *Polymer* **2008**, 49 (10), 2387-2425.
 45. Bhardwaj, N.; Kundu, S. C., Electrospinning: A fascinating fiber fabrication technique. *Biotechnology Advances* **2010**, 28 (3), 325-347.
 46. Deitzel, J. M.; Kleinmeyer, J.; Harris, D.; Tan, N. C. B., The effect of processing variables on the morphology of electrospun nanofibers and textiles. *Polymer* **2001**, 42 (1), 261-272.
 47. Geng, X. Y.; Kwon, O. H.; Jang, J. H., Electrospinning of chitosan dissolved in concentrated acetic acid solution. *Biomaterials* **2005**, 26 (27), 5427-5432.
 48. Ki, C. S.; Baek, D. H.; Gang, K. D.; Lee, K. H.; Um, I. C.; Park, Y. H., Characterization of gelatin nanofiber prepared from gelatin-formic acid solution. *Polymer* **2005**, 46 (14), 5094-5102.
 49. Zhang, C. X.; Yuan, X. Y.; Wu, L. L.; Han, Y.; Sheng, J., Study on morphology of electrospun poly(vinyl alcohol) mats. *European Polymer Journal* **2005**, 41 (3), 423-432.
 50. Zong, X. H.; Kim, K.; Fang, D. F.; Ran, S. F.; Hsiao, B. S.; Chu, B., Structure and process relationship of electrospun bioabsorbable nanofiber membranes. *Polymer* **2002**, 43 (16), 4403-4412.
 51. Yuan, X. Y.; Zhang, Y. Y.; Dong, C. H.; Sheng, J., Morphology of ultrafine polysulfone fibers prepared by electrospinning. *Polymer International* **2004**, 53 (11), 1704-1710.
 52. Wannatong, L.; Sirivat, A.; Supaphol, P., Effects of solvents on electrospun

-
- polymeric fibers: preliminary study on polystyrene. *Polymer International* **2004**, 53 (11), 1851-1859.
53. Zhao, Z. Z.; Li, J. Q.; Yuan, X. Y.; Li, X.; Zhang, Y. Y.; Sheng, J., Preparation and properties of electrospun poly(vinylidene fluoride) membranes. *Journal of Applied Polymer Science* **2005**, 97 (2), 466-474.
54. Sirignano, W. A.; Mehring, C., Review of theory of distortion and disintegration of liquid streams. *Progress in Energy and Combustion Science* **2000**, 26 (4-6), 609-655.
55. Barber, P. S.; Griggs, C. S.; Bonner, J. R.; Rogers, R. D., Electrospinning of chitin nanofibers directly from an ionic liquid extract of shrimp shells. *Green Chemistry* **2013**, 15 (3), 601-607.
56. Luo, C. J.; Stride, E.; Edirisinghe, M., Mapping the influence of solubility and dielectric constant on electrospinning polycaprolactone solutions. *Macromolecules* **2012**, 45 (11), 4669-4680.
57. He, Y. Y.; Boswell, P. G.; Buhlmann, P.; Lodge, T. P., Ion gels by self-assembly of a triblock copolymer in an ionic liquid. *Journal of Physical Chemistry B* **2007**, 111 (18), 4645-4652.
58. Cheng, Y. W.; Lu, H. A.; Wang, Y. C.; Thierry, A.; Lotz, B.; Wang, C., Syndiotactic polystyrene nanofibers obtained from high-temperature solution electrospinning process. *Macromolecules* **2010**, 43 (5), 2371-2376.
59. Wang, C.; Chu, Y. L.; Wu, Y. J., Electrospun isotactic polystyrene nanofibers as a novel beta-nucleating agent for isotactic polypropylene. *Polymer* **2012**, 53 (23), 5404-5412.
60. Nakaoki, T.; Inaji, Y., Molecular structure of isotactic polypropylene formed from homogeneous solution. Gelation and crystallization. *Polymer Journal* **2002**, 34 (7), 539-543.
61. Crne, M.; Park, J. O.; Srinivasarao, M., Electrospinning physical gels: the case of stereocomplex PMMA. *Macromolecules* **2009**, 42 (13), 4353-4355.
62. Watanabe, K.; Kim, B. S.; Kim, I. S., Development of polypropylene nanofiber production system. *Polymer Reviews* **2011**, 51 (3), 288-308.
-

-
63. Wang, C.; Hsieh, T. C.; Cheng, Y. W., Solution-electrospun isotactic polypropylene fibers: Processing and microstructure development during stepwise annealing. *Macromolecules* **2010**, *43* (21), 9022-9029.
 64. Cho, D.; Zhou, H. J.; Cho, Y.; Audus, D.; Joo, Y. L., Structural properties and superhydrophobicity of electrospun polypropylene fibers from solution and melt. *Polymer* **2010**, *51* (25), 6005-6012.
 65. Lee, K. H.; Ohsawa, O.; Watanabe, K.; Kim, I. S.; Givens, S. R.; Chase, B.; Rabolt, J. F., Electrospinning of syndiotactic polypropylene from a polymer solution at ambient temperatures. *Macromolecules* **2009**, *42* (14), 5215-5218.
 66. Watanabe, K.; Nakamura, T.; Kim, B. S.; Kim, I. S., Effect of organic solvent on morphology and mechanical properties of electrospun syndiotactic polypropylene nanofibers. *Polymer Bulletin* **2011**, *67* (9), 2025-2033.
 67. Jao, C. S.; Wang, Y.; Wang, C., Novel elastic nanofibers of syndiotactic polypropylene obtained from electrospinning. *European Polymer Journal* **2014**, *54*, 181-189.
 68. Suzuki, A.; Arino, K., Polypropylene nanofiber sheets prepared by CO₂ laser supersonic multi-drawing. *European Polymer Journal* **2012**, *48* (7), 1169-1176.
 69. Takahashi, N.; Kanaya, T.; Nishida, K.; Kaji, K., Effects of cononsolvency on gelation of poly(vinyl alcohol) in mixed solvents of dimethyl sulfoxide and water. *Polymer* **2003**, *44* (15), 4075-4078.
 70. Ohkura, M.; Kanaya, T.; Kaji, K., Gelation rates of poly(vinyl alcohol) solution. *Polymer* **1992**, *33* (23), 5044-5048.
 71. Mochizuki, J.; Sano, T.; Tokami, T.; Itagaki, H., Decisive properties of solvent able to form gels with syndiotactic polystyrene. *Polymer* **2015**, *67*, 118-127.
 72. Barton, A. F. M., *Handbook of polymer-liquid interaction parameters and solubility parameters*. CRC Press: 1990; p 768.
 73. McKee, M. G.; Wilkes, G. L.; Colby, R. H.; Long, T. E., Correlations of solution rheology with electrospun fiber formation of linear and branched polyesters. *Macromolecules* **2004**, *37* (5), 1760-1767.
 74. Fetters, L. J.; Lohse, D. J.; Milner, S. T.; Graessley, W. W., Packing length
-

- influence in linear polymer melts on the entanglement, critical, and reptation molecular weights. *Macromolecules* **1999**, *32* (20), 6847-6851.
75. Liu, C. Y.; Yu, J.; He, J. S.; Liu, W.; Sun, C. Y.; Jing, Z. H., A reexamination of GN0 and Me of syndiotactic polypropylenes with metallocene catalysts. *Macromolecules* **2004**, *37* (24), 9279-9282.
76. Tripatanasuwan, S.; Zhong, Z. X.; Reneker, D. H., Effect of evaporation and solidification of the charged jet in electrospinning of poly(ethylene oxide) aqueous solution. *Polymer* **2007**, *48* (19), 5742-5746.
77. Colby, R. H.; Fetters, L. J.; Funk, W. G.; Graessley, W. W., Effects of concentration and thermodynamic interaction on the viscoelastic properties of polymer solutions. *Macromolecules* **1991**, *24* (13), 3873-3882.
78. Nakai, S.; Nakaya, T.; Imoto, M., Polymeric phospholipid analog, .10. Synthesis and polymerization of 2-(methacryloyloxy)ethyl 2-aminoethyl hydrogen phosphate. *Makromolekulare Chemie-Macromolecular Chemistry and Physics* **1977**, *178* (10), 2963-2967.
79. Kadoma, Y.; Nakabayashi, N.; Masuhara, E.; Yamauchi, J., Synthesis and hemolysis test of polymer containing phosphorylcholine groups. *Kobunshi Ronbunshu* **1978**, *35* (7), 423-427.
80. Ishihara, K.; Ueda, T.; Nakabayashi, N., Preparation of phospholipid polymers and their properties as polymer hydrogel membranes. *Polymer Journal* **1990**, *22* (5), 355-360.
81. Ueda, T.; Oshida, H.; Kurita, K.; Ishihara, K.; Nakabayashi, N., Preparation of 2-methacryloyloxyethyl phosphorylcholine copolymers with alkyl methacrylates and their blood compatibility. *Polymer Journal* **1992**, *24* (11), 1259-1269.
82. Kojima, M.; Ishihara, K.; Watanabe, A.; Nakabayashi, N., Interaction between phospholipids and biocompatible polymers containing a phosphorylcholine moiety. *Biomaterials* **1991**, *12* (2), 121-124.
83. Fukushima, S.; Kadoma, Y.; Nakabayashi, N., Interaction between the polymer containing phosphorylcholine group and cells. *Kobunshi Ronbunshu* **1983**, *40* (12), 785-793.

-
84. Ishihara, K.; Aragaki, R.; Ueda, T.; Watanabe, A.; Nakabayashi, N., Reduced thrombogenicity of polymers having phospholipid polar groups. *Journal of Biomedical Materials Research* **1990**, *24* (8), 1069-1077.
 85. Ishihara, K.; Ziats, N. P.; Tierney, B. P.; Nakabayashi, N.; Anderson, J. M., Protein adsorption from human plasma is reduced on phospholipid polymers. *Journal of Biomedical Materials Research* **1991**, *25* (11), 1397-1407.
 86. Ishihara, K.; Oshida, H.; Endo, Y.; Ueda, T.; Watanabe, A.; Nakabayashi, N., Hemocompatibility of human whole-blood on polymers with a phospholipid polar group and its mechanism. *Journal of Biomedical Materials Research* **1992**, *26* (12), 1543-1552.
 87. Koombhongse, S.; Liu, W. X.; Reneker, D. H., Flat polymer ribbons and other shapes by electrospinning. *Journal of Polymer Science Part B-Polymer Physics* **2001**, *39* (21), 2598-2606.
 88. Donth, E.; Beiner, M.; Reissig, S.; Korus, J.; Garwe, F.; Vieweg, S.; Kahle, S.; Hempel, E.; Schroter, K., Fine structure of the main transition in amorphous polymers: Entanglement spacing and characteristic length of the glass transition. Discussion of examples. *Macromolecules* **1996**, *29* (20), 6589-6600.
 89. Higuchi, T., Mechanism of sustained-action medication. Theoretical analysis of rate of release of solid drugs dispersed in solid matrices. *Journal of Pharmaceutical Sciences* **1963**, *52* (12), 1145-1149.
 90. Chuangchote, S.; Sirivat, A.; Supaphol, P., Electrospinning of styrene-isoprene copolymeric thermoplastic elastomers. *Polymer Journal* **2006**, *38* (9), 961-969.
 91. Feng, S. Q.; Shen, X. Y.; Fu, Z. Y.; Ji, Y. L., Studies on the electrospun submicron fibers of SiS and its mechanical properties. *Journal of Applied Polymer Science* **2009**, *114* (3), 1580-1586.
 92. Feng, S. Q.; Shen, X. Y., Electrospinning and mechanical properties of polystyrene and styrene-isoprene-styrene block copolymer blend nanofibres. *Journal of Macromolecular Science Part B-Physics* **2010**, *49* (2), 345-354.
 93. Fong, H.; Reneker, D. H., Elastomeric nanofibers of styrene-butadiene-styrene triblock copolymer. *Journal of Polymer Science Part B-Polymer Physics* **1999**, *37*
-

- (24), 3488-3493.
94. Feng, S. Q.; Shen, X. Y.; Ji, Y. L., Submicron ion-exchange fibers of polystyrene and styrene-butadiene-styrene copolymer blends. *Journal of Macromolecular Science Part B-Physics* **2011**, *50* (9), 1673-1681.
95. Lim, G. T.; Puskas, J. E.; Reneker, D. H.; Jakli, A.; Horton, W. E., Highly hydrophobic electrospun fiber mats from polyisobutylene-based thermoplastic elastomers. *Biomacromolecules* **2011**, *12* (5), 1795-1799.
96. Monge, S.; Joly-Duhamel, C.; Boyer, C.; Robin, J. J., Synthesis and characterisation of organogels from ABA triblock copolymers. *Macromolecular Chemistry and Physics* **2007**, *208* (3), 262-270.
97. Barton, A. F. M., Solubility Parameters. *Chemical Reviews* **1975**, *75* (6), 731-753.
98. Kong, L. Y.; Ziegler, G. R., Role of molecular entanglements in starch fiber formation by electrospinning. *Biomacromolecules* **2012**, *13* (8), 2247-2253.
99. Zhang, Q. L.; Tsui, O. K. C.; Du, B. Y.; Zhang, F. J.; Tang, T.; He, T. B., Observation of inverted phases in poly(styrene-b-butadiene-b-styrene) triblock copolymer by solvent-induced order-disorder phase transition. *Macromolecules* **2000**, *33* (26), 9561-9567.
100. Laurer, J. H.; Khan, S. A.; Spontak, R. J.; Satkowski, M. M.; Grothaus, J. T.; Smith, S. D.; Lin, J. S., Morphology and rheology of SIS and SEPS triblock copolymers in the presence of a midblock-selective solvent. *Langmuir* **1999**, *15* (23), 7947-7955.
101. Iatrou, H.; Hadjichristidis, N.; Meier, G.; Frielinghaus, H.; Monkenbusch, M., Synthesis and characterization of model cyclic block copolymers of styrene and butadiene. Comparison of the aggregation phenomena in selective solvents with linear diblock and triblock analogues. *Macromolecules* **2002**, *35* (14), 5426-5437.
102. Sato, T.; Watanabe, H.; Osaki, K., Rheological and dielectric behavior of a styrene-isoprene-styrene triblock copolymer in n-tetradecane .1. Rubbery-plastic-viscous transition. *Macromolecules* **1996**, *29* (19), 6231-6239.
103. Vega, D. A.; Sebastian, J. M.; Loo, Y. L.; Register, R. A., Phase behavior and viscoelastic properties of entangled block copolymer gels. *Journal of Polymer*

-
- Science Part B-Polymer Physics* **2001**, *39* (18), 2183-2197.
104. Sato, T.; Watanabe, H.; Osaki, K., Thermoreversible physical gelation of block copolymers in a selective solvent. *Macromolecules* **2000**, *33* (5), 1686-1691.
105. Durrschmidt, T.; Hoffmann, H., Organogels from ABA triblock copolymers. *Colloid and Polymer Science* **2001**, *279* (10), 1005-1012.
106. Watanabe, H.; Sato, T.; Osaki, K.; Yao, M. L.; Yamagishi, A., Rheological and dielectric behavior of a styrene-isoprene-styrene triblock copolymer in selective solvents .2. Contribution of loop-type middle blocks to elasticity and plasticity. *Macromolecules* **1997**, *30* (19), 5877-5892.
107. Jeong, B.; Bae, Y. H.; Lee, D. S.; Kim, S. W., Biodegradable block copolymers as injectable drug-delivery systems. *Nature* **1997**, *388* (6645), 860-862.
108. Jeong, B.; Bae, Y. H.; Kim, S. W., Thermoreversible gelation of PEG-PLGA-PEG triblock copolymer aqueous solutions. *Macromolecules* **1999**, *32* (21), 7064-7069.
109. Jeong, B.; Bae, Y. H.; Kim, S. W., Biodegradable thermosensitive micelles of PEG-PLGA-PEG triblock copolymers. *Colloids and Surfaces B-Biointerfaces* **1999**, *16* (1-4), 185-193.
110. Jeong, B.; Bae, Y. H.; Kim, S. W., In situ gelation of PEG-PLGA-PEG triblock copolymer aqueous solutions and degradation thereof. *Journal of Biomedical Materials Research* **2000**, *50* (2), 171-177.
111. Lee, D. S.; Shim, M. S.; Kim, S. W.; Lee, H.; Park, I.; Chang, T. Y., Novel thermoreversible gelation of biodegradable PLGA-block-PEO-block-PLGA triblock copolymers in aqueous solution. *Macromolecular Rapid Communications* **2001**, *22* (8), 587-592.
112. Shim, M. S.; Lee, H. T.; Shim, W. S.; Park, I.; Lee, H.; Chang, T.; Kim, S. W.; Lee, D. S., Poly(D,L-lactic acid-co-glycolic acid)-b-poly(ethylene glycol)-b-poly(D,L-lactic acid-co-glycolic acid) triblock copolymer and thermoreversible phase transition in water. *Journal of Biomedical Materials Research* **2002**, *61* (2), 188-196.
113. Qiao, M. X.; Chen, D. W.; Ma, X. C.; Liu, Y. J., Injectable biodegradable temperature-responsive PLGA-PEG-PLGA copolymers: Synthesis and effect of
-

- copolymer composition on the drug release from the copolymer-based hydrogels. *International Journal of Pharmaceutics* **2005**, *294* (1-2), 103-112.
114. Qiao, M. X.; Chen, D. W.; Ma, X. C.; Hu, H. Y., Sustained release of bee venom peptide from biodegradable thermosensitive PLGA-PEG-PLGA triblock copolymer-based hydrogels in vitro. *Pharmazie* **2006**, *61* (3), 199-202.
115. Yu, L.; Chang, G. T.; Zhang, H.; Ding, J. D., Injectable block copolymer hydrogels for sustained release of a PEGylated drug. *International Journal of Pharmaceutics* **2008**, *348* (1-2), 95-106.
116. Yu, L.; Zhang, H.; Ding, J. D., A subtle end-group effect on macroscopic physical gelation of triblock copolymer aqueous solutions. *Angewandte Chemie-International Edition* **2006**, *45* (14), 2232-2235.
117. Yu, L.; Chang, G. T.; Zhang, H.; Ding, J. D., Temperature-induced spontaneous sol-gel transitions of poly(D,L-lactic acid-co-glycolic acid)-b-poly(ethylene glycol)-b-poly(D,L-lactic acid-co-glycolic acid) triblock copolymers and their end-capped derivatives in water. *Journal of Polymer Science Part a-Polymer Chemistry* **2007**, *45* (6), 1122-1133.
118. Yu, L.; Zhang, Z.; Zhang, H.; Ding, J. D., Mixing a sol and a precipitate of block copolymers with different block ratios leads to an injectable hydrogel. *Biomacromolecules* **2009**, *10* (6), 1547-1553.
119. Yu, L.; Zhang, Z.; Zhang, H. A.; Ding, J. D., Biodegradability and biocompatibility of thermoreversible hydrogels formed from mixing a sol and a precipitate of block copolymers in water. *Biomacromolecules* **2010**, *11* (8), 2169-2178.
120. Yu, L.; Zhang, Z.; Ding, J. D., In vitro degradation and protein release of transparent and opaque physical hydrogels of block copolymers at body temperature. *Macromolecular Research* **2012**, *20* (3), 234-243.
121. Li, S. M.; Vert, M., Synthesis, characterization, and stereocomplex-induced gelation of block copolymers prepared by ring-opening polymerization of L(D)-lactide in the presence of poly(ethylene glycol). *Macromolecules* **2003**, *36* (21), 8008-8014.

122. Nagahama, K.; Kawano, D.; Oyama, N.; Takemoto, A.; Kumano, T.; Kawakami, J., Self-assembling polymer micelle/clay nanodisk/doxorubicin hybrid injectable gels for safe and efficient focal treatment of cancer. *Biomacromolecules* **2015**, *16* (3), 880-889.